Distribution Category:
Biology and Medicine
(UC-48)

ANL-82-65
Part I

ANL--82-65-Pt.1

DE84 009127

ARGONNE NATIONAL LABORATORY
9700 South Cass Avenue
Argonne, Illinois 60439

RADIOLOGICAL AND ENVIRONMENTAL RESEARCH DIVISION ANNUAL REPORT

Fundamental Molecular Physics and Chemistry

October 1981 - December 1982

A. F. Stehney, Acting Division Director
Mitio Inokuti, Section Head

December 1983

Preceding Report

ANL-81-85 Part I, October 1980-September 1981

FOREWORD

This document is the twelfth Annual Report of our Fundamental Molecular Physics and Chemistry Program. Scientifically, the work of the Program deals with aspects of the physics and chemistry of molecules related to their interactions with photons, electrons, and other external agents. We chose these areas of study in view of our programmatic goals; that is to say, we chose them so that the eventual outcome of our work meets some of the needs of the U.S. Department of Energy (DOE) and of other government agencies that support our research.

First, we endeavor to determine theoretically and experimentally cross sections for electron and photon interactions with molecules, because those cross sections are indispensable for detailed microscopic analyses of the earliest processes of radiation action on any molecular substance, including biological materials. Those analyses in turn provide a sound basis for radiology and radiation dosimetry. Second, we study the spectroscopy of certain molecules and of small clusters of molecules because this topic is fundamental to the full understanding of atmospheric-pollutant chemistry. Work in these areas constitutes a main part of our program, and is supported by the Office of Health and Environmental Research, DOE.

Part of our work is concerned with the generation of atomic data needed in fusion-plasma research. These data are related to energy levels of stripped atomic ions, their transition probabilities, and collision cross sections for various elementary processes. Work in this area was supported by the Office of Magnetic Fusion, DOE.

Another part of our work concerns high-resolution spectroscopy of molecules by use of lasers and synchrotron radiations, and is aimed at elucidating a hitherto poorly explored scientific topic, i.e., the detailed dynamics of electronically excited states, often interacting strongly with nuclear motion. Work in this area is supported in part by the Office of Naval Research, Department of Defense, and is conducted in part in collaboration with the National Bureau of Standards, Department of Commerce.

The articles in the present report are loosely arranged according to the subject matters they treat. Papers 1 through 14 treat photoionization dynamics, as studied by photoelectron analysis, mass spectrometry of

photoions, or theory. Papers 15 through 18 concern electronic properties of molecular clusters. Papers 19-21 deal with multiple-photon resonance ionization spectroscopy. Papers 22 through 30 report various aspects of our extensive activities in research on electron collisions with atoms, molecules, and ions. Papers 31 through 33 represent our immediate contributions to radiation physics. Finally, papers 36 through 40 deal with atomic ion spectra pertinent to fusion plasmas and other topics in theoretical atomic physics.

In conclusion, we point out our extensive interactions with various institutions outside the Laboratory. First of all, many of the co-authors of the articles in this report belong to other institutions. I thank them deeply for their contributions to our program. Second, we played hosts for two major meetings: Workshop on the Interface between Radiation Chemistry and Physics, 9-10 September, and the Symposium in Honor of Ugo Fano, 11-12 November 1983. Third, P. M. Dehmer serves as Secretary-Treasurer of the Division of Electronic and Atomic Physics, The American Physical Society, and also as a member of the Publication Committee of the same society. Finally, I continue to work for the International Commission on Radiation Units and Measurements, as Vice-Chairman of the Report Committe on Stopping Power. (The Committee's initial report, on stopping powers for electrons and positrons, will be issued soon as ICRU Report No. 37.)

Mitio Inokuti
Section Head

TABLE OF CONTENTS

1. PHOTOIONIZATION DYNAMICS OF SMALL MOLECULES*

J. L. Dehmer, Dan Dill,† and A. C. Parr‡

Photoionization dynamics of small molecules are discussed, with emphasis on shape and autoionizing resonances. These resonant processes are important probes of photoionization for various reasons, the most obvious being that they are usually displayed prominently against nonresonant behavior in such observables as the total photoionization cross section, photoionization branching ratios, and photoelectron angular distributions. More importantly, the study of resonant features has repeatedly led to a deeper physical insight into the mechanisms of excitation, resonant trapping of the photoelectron, and decay of the excited complex that occur during the photoionization process. Of particular interest in this context are the uniquely molecular aspects resulting from the anisotropy of molecular fields and from the interplay among rovibronic modes. We review the fundamental aspects of both types of resonant processes and discuss recent progress and prospects for future work from both experimental and theoretical points of view. Finally, a brief overview of various approaches not covered in the main discussion is presented to stress the variety and complementarity of alternative probes of molecular photoionization dynamics.

---

*Abstract of a book chapter to appear in Photophysics and Photochemistry in the Vacuum Ultraviolet, eds. S. McGlynn, G. Findley, and R. Huebner (D. Reidel Publ., Dordrecht, 1983).

†Department of Chemistry, Boston University, Boston, MA 02215.

‡National Bureau of Standards, Washington, DC 20234.

2. CONSTANT PHOTOELECTRON ENERGY SPECTROSCOPY OF ACETYLENE*

D. M. P. Holland,† J. B. West,† A. C. Parr,‡ D. L. Ederer,‡
R. Stockbauer,‡ R. D. Buff,‡ and J. L. Dehmer

Constant-photoelectron-energy spectra of acetylene are reported for electron kinetic energies of 0, 0.1, 0.5, and 1.0 eV in the spectral range 11 eV < hν < 22 eV. This form of photoelectron spectroscopy involves measuring the intensity of photoelectrons with a particular kinetic energy as a function of the wavelength of the incident radiation. Such measurements may be carried out using small wavelength increments and can be used to distinguish between direct and indirect, e.g., autoionization, photoionization processes. Autoionization features in the range 12.5 eV < hν < 16 eV are observed. These populate high vibrational levels of the ground state far beyond the Franck-Condon region. The data discussed in this paper are plotted in Figure 1.

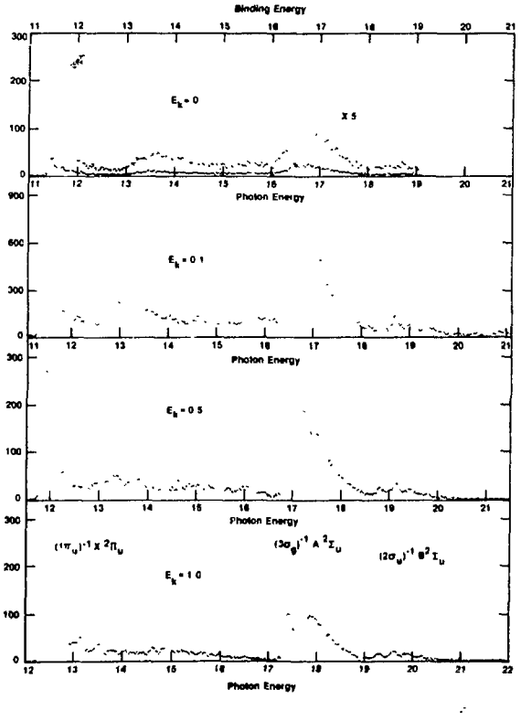

Fig. 1. Constant-photoelectron-energy spectra of acetylene at four electron kinetic energies; E_k = 0, 0.1, 0.5, and 1.0 eV. All spectra are aligned on a common binding energy, $E_I = E_{ph} - E_k$, scale, shown at the top of the figure. The photon energy scale consequently shifts for each E_k, and is indicated on the abcissa of each frame. The threshold electron spectrum, E_k = 0, is plotted x1 and x5 above 12 eV.

---

*Abstract of a paper published in J. Chem. Phys. 78, 124 (1983).
†Daresbury Laboratory, Daresbury, Warrington, WA4 4AD, England.
‡National Bureau of Standards, Washington, DC 20234.

3. VALENCE-SHELL PHOTOABSORPTION BY CO_2 AND ITS CONNECTIONS WITH ELECTRON-CO_2 SCATTERING*

P. M. Dittman,† Dan Dill,† and J. L. Dehmer

Photoabsorption cross sections and photoelectron asymmetry parameters, calculated with the multiple-scattering model (MSM) are reported for the $4\sigma_g$, $3\sigma_u$, $1\pi_u$, and $1\pi_g$ valence levels of CO_2. The results are discussed in the context of photoabsorption and electron energy loss measurements and other theoretical calculations. Further comparisons are made with previously reported MSM calculations of elastic electron-CO_2 scattering. The close connection between the sets of shape resonances in the electron-scattering and photoabsorption by CO_2 is emphasized with plots of continuum eigenchannel wavefunctions for shape-resonant and non-resonant eigenchannels of σ_u symmetry. Selected results from this study are shown in Figure 1.

---

*Abstract and sample results from a paper published in Chem. Phys. 78, 405 (1983).

†Department of Chemistry, Boston University, Boston, MA 02215.

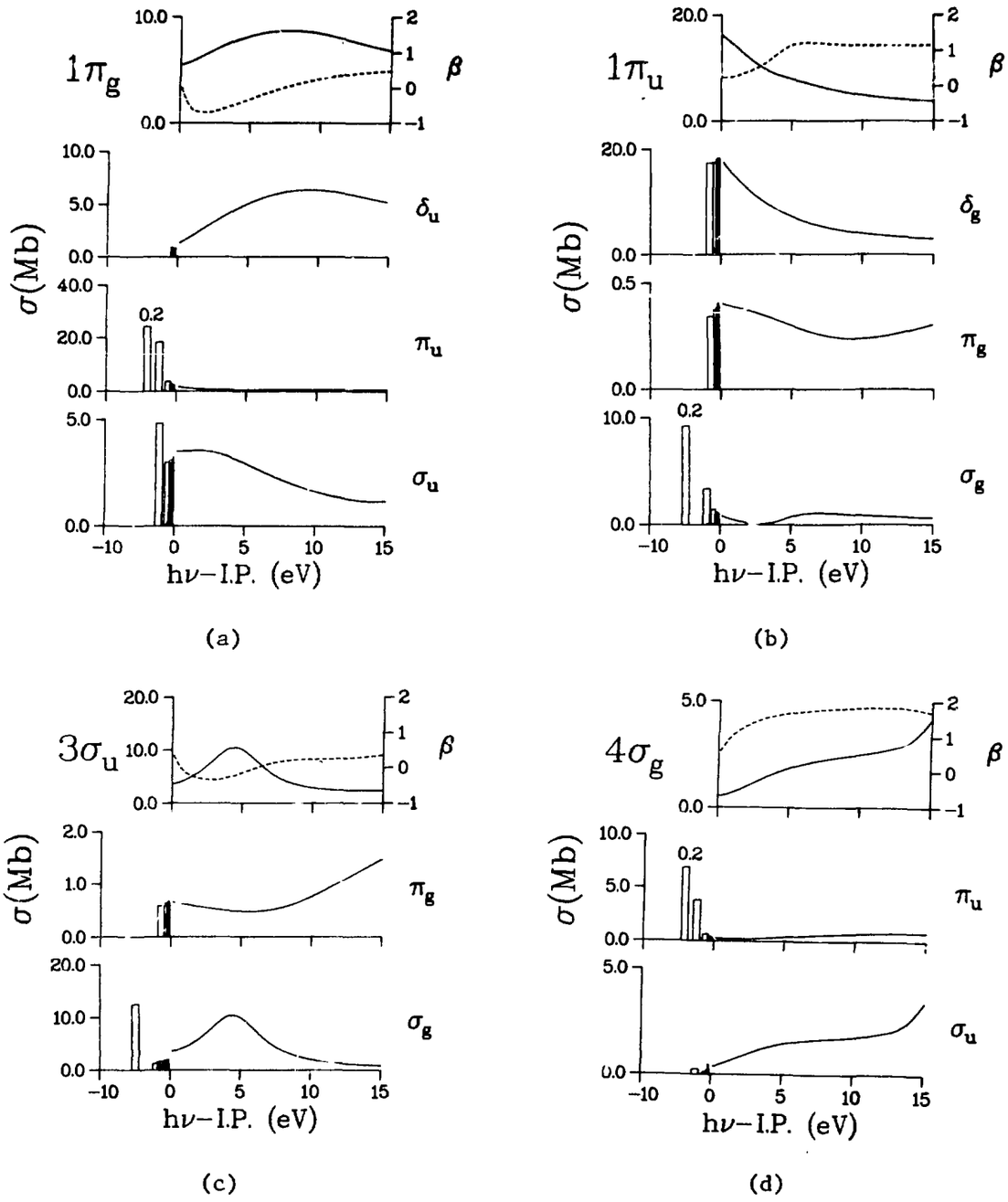

Fig. 1. Photoabsorption spectra for the (a) $1\pi_g$ valence level, (b) $1\pi_u$ valence level, (c) $3\sigma_u$ valence level, and (d) $4\sigma_g$ valence level of CO_2. The lower subplots display partial cross sections for the dipole-allowed channels; the uppermost subplot shows the total cross section (solid line - left scale) and asymmetry parameter (dashed line - right scale) as a function of excitation energy.

4. PHOTOELECTRON SPECTROMETER FOR HIGH RESOLUTION ANGULAR RESOLVED STUDIES*

A. C. Parr,† S. H. Southworth,† J. L. Dehmer, and
D. M. P. Holland‡

We report on a new electron spectrometer system designed for use on storage-ring light sources. The system features a large (76 cm dia. × 92 cm long), triply magnetically shielded vacuum chamber and two 10.2 cm mean radius hemispherical electron energy analyzers. One of the analyzers is fixed and the other is rotatable through about 150°. The chamber is pumped by a combination of a cryopump and a turbomolecular pump to allow investigators to conduct experiments with a variety of gases under different conditions. The light-detection system includes both a direct-beam monitor and a polarization analyzer. Electron detection is accomplished either with a continuous channel electron multiplier or with multichannel arrays used as area detectors. A schematic diagram of the system is shown in Figure 1.

---

*Summary of an article published in Nucl. Instr. Meth. 208, 767 (1983).
†National Bureau of Standards, Washington, DC 20234.
‡Daresbury Laboratory, Daresbury, Warrington, WA4 4AD, England.

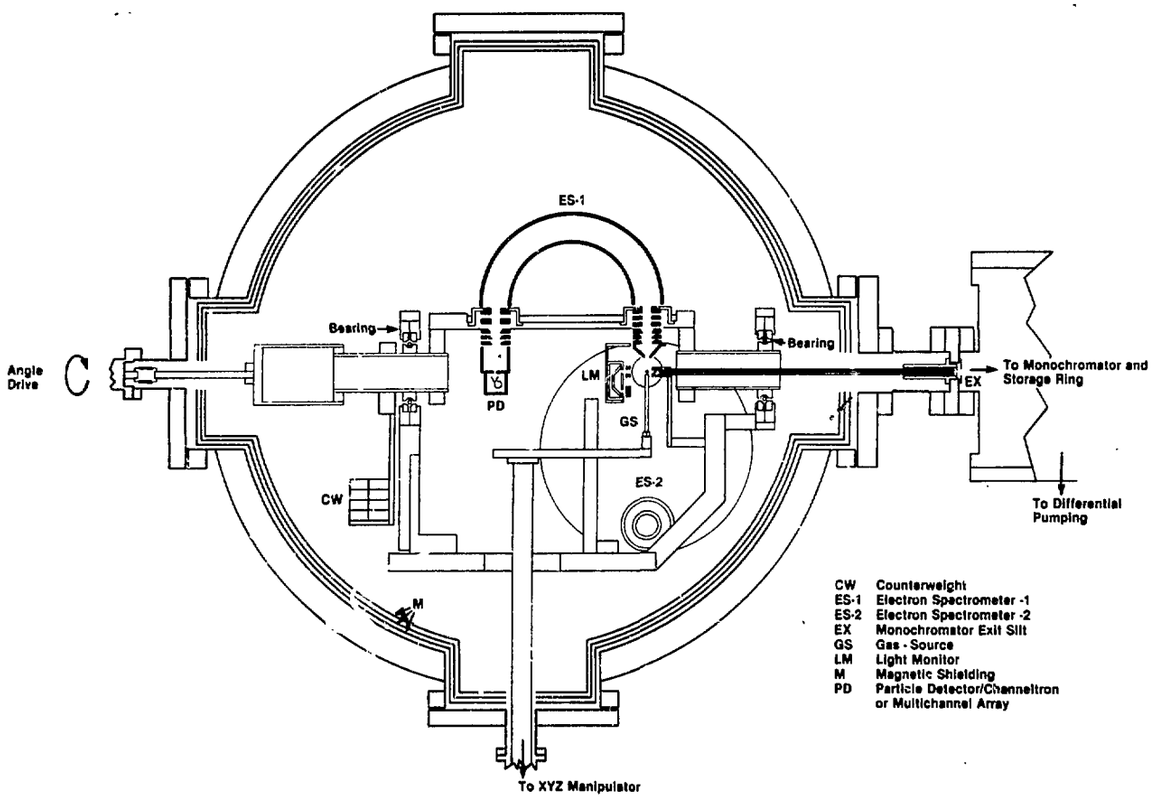

Fig. 1. Schematic representation of the electron spectrometer system. Only major components of the apparatus are identified.

5. TRIPLY DIFFERENTIAL PHOTOELECTRON STUDIES OF THE FOUR OUTERMOST VALENCE ORBITALS OF CYANOGEN*

D. M. P. Holland,† A. C. Parr,‡ D. L. Ederer,‡ J. B. West,† and J. L. Dehmer

---

Synchrotron radiation has been used to perform photoelectron measurements (differential in incident wavelength, photoelectron energy, and photoelectron ejection angle), on cyanogen, C_2N_2, from threshold to $h\nu$ = 24 eV. The results are presented in the form of photoionization branching ratios and photoelectron angular distributions, including vibrationally resolved results for the outermost orbital $1\pi_g$. Some evidence for resonant processes is observed, and this evidence is discussed within the framework of recent work with related molecules. However, reliable assignments require further theoretical guidance in regard to the location and identities of possible shape resonances and autoionizing intravalence transitions in the C_2N_2 spectrum.

---

*Abstract of an article published in Int. J. Mass. Spect. and Ion Phys. 52, 195 (1983).

†Daresbury Laboratory, Daresbury, Warrington, WA4 4AD, England.
‡National Bureau of Standards, Washington, DC 20234.

6. PHOTOELECTRON ASYMMETRY PARAMETERS AND BRANCHING RATIOS FOR SULPHUR DIOXIDE IN THE PHOTON ENERGY RANGE 14 TO 25 eV*

D. M. P. Holland,† A. C. Parr,‡ and J. L. Dehmer

Triply differential photoelectron spectroscopy has been performed on sulphur dioxide in the photon energy range 14 to 25 eV. The results are presented in the form of electronic branching ratios and asymmetry parameters and are discussed briefly in the context of similar data for CO_2 and inner-shell spectra of sulphur dioxide.

---

*Abstract of an article to be published in J. Electron Spectrosc.

†Daresbury Laboratory, Daresbury, Warrington, WA4 4AD, England.
‡National Bureau of Standards, Washington, DC 20234.

7. FLUORESCENCE POLARIZATION AS A PROBE OF MOLECULAR AUTOIONIZATION*

E. D. Poliakoff,† J. L. Dehmer, A. C. Parr,‡ and G. E. Leroi§

Extensive effort in VUV spectroscopy has gone into developing an understanding of the spectroscopy and dynamics of autoionizing Rydberg states.[1,2] We use initial results on CO_2 autoionization to show that the polarization of fluorescence from excited-state molecular photoions can be a significant tool in ascertaining both the symmetry signatures and dynamical properties of autoionizing resonances. The process studied in this work is:

$$\begin{array}{l} \xrightarrow{-3\sigma_u} CO_2^*(R) \\ CO_2(X^1\Sigma_g^+) + h\nu \\ \xrightarrow{-1\pi_u} CO_2^+(A^2\Pi_u) + e^-(\varepsilon\sigma_g, \varepsilon\pi_g, \varepsilon\delta_g) \\ \qquad\qquad \downarrow \\ \qquad\qquad CO_2^+(X^2\Pi_g) + h\nu' \ , \end{array}$$

where R denotes a Rydberg state, $-3\sigma_u$ and $-1\pi_u$ indicate which electron is excited, and ε denotes a continuum electron. The experiment is carried out by scanning the excitation photon energy, $h\nu$, and measuring the polarization of the undispersed CO_2^+ $A^2\Pi_u \rightarrow X^2\Pi_g$ fluorescence, $h\nu'$.

The fluorescence polarization from molecular photoions reflects the degree of alignment of the molecular ion in the laboratory-fixed frame which is, in turn, determined by the relative dipole strengths for degenerate photoionization channels that have different symmetries in the molecule-fixed frame. This basic framework is used to infer, from fluorescence polarization measurements, the symmetry properties of autoionizing resonances that are superimposed on a nonresonant background of known symmetry.

---

*Summary of a paper published in J. Chem. Phys. 77, 5243 (1982).
†Department of Chemistry, Boston University, Boston, MA 02215.
‡National Bureau of Standards, Washington, DC 20234.
§Department of Chemistry, Michigan State University, East Lansing, MI 48824.

Results are plotted in Figure 1. The excitation spectrum shows extensive autoionization structure, and the fluorescence polarization data exhibit features analogous to the structure in the excitation spectrum. The physical basis for the structure in this fluorescence polarization spectrum is the movement of the absorption transition dipole into the plane of molecular rotation as the resonance pathway becomes enhanced. This leads to a greater degree of alignment between the absorption and fluorescence transition dipoles than in the case of nonresonant ionization. The key point is that the degree of alignment of the molecular ion in the laboratory frame is dependent on the dipole strengths for the ionization channels populating the excited ionic state. These results underscore the conclusion that this method serves as a direct probe of symmetry information on autoionizing Rydberg states.

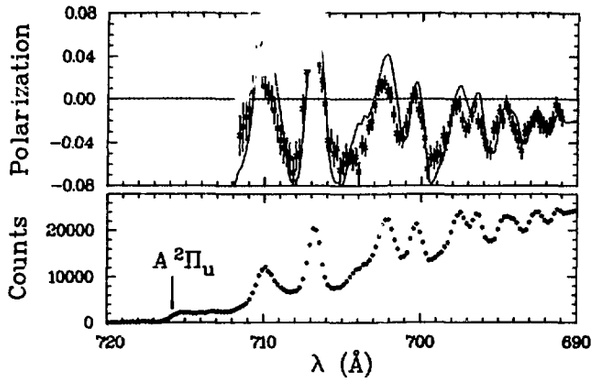

Fig. 1. Excitation spectrum (bottom) and fluorescence polarization spectrum (top). The solid line is the prediction of a simple mixing model.

References

1. U. Fano, J. Opt. Soc. Am. 65, 979 (1975).
2. M. Raoult and Ch. Jungen, J. Chem. Phys. 74, 3388 (1981).

8. KINEMATIC ANALYSIS OF PHOTOELECTRONS FROM POLARIZED TARGETS WITH J = 1/2*

K.-N. Huang

Photoionization is conceptually the simplest way of studying atoms and molecules via impact processes. Considerable information can be obtained about the atomic or molecular structure by measuring the angular distribution and spin polarization of photoelectrons. In atomic photoionization processes, a complete measurement of photoelectrons from a certain subshell can, in principle, yield as many as 17 independent dynamical quantities for the electric dipole transitions.[1,2] Comparison of these 17 quantities with corresponding theoretical predictions would provide the most rigorous test of atomic dynamical theories, including correlation and relativistic effects. Photoionization experiments with unpolarized targets can, in principle, test five dynamical quantities.[3]

In most photoionization experiments, unpolarized targets have been used, and only the cross section and angular distribution of photoelectrons have been measured; therefore, at most, two dynamical quantities can be extracted from these experiments. In recent years, two additional dynamical quantities involving the spin polarization of photoelectrons have been measured, and the agreement of these measurements with theoretical predictions are good. Recently, convenient sources of polarized atoms have become available,[4,5] and polarized atomic sources may be produced by laser excitations or by applying magnetic fields. Therefore, it is timely to undertake kinematic analysis of photoelectrons from polarized targets. This kind of analysis will assist experimentalists in designing apparatus and in analyzing data, and eventually will lead to the experimental testing of all 17 dynamical quantities concerning detailed correlation and relativistic effects in atoms.

In this paper I give a complete kinematic analysis of photoelectrons from polarized targets with total angular momentum J = 1/2. The angular distribution and spin polarization of photoelectrons are given in concise formulas in terms of dynamical parameters in the electric dipole approximation. De-

*Summary of a letter published in Phys. Rev. Lett. 48, 1811 (1982).

tailed derivation and explicit expressions of the dynamical parameters will be given in a separate paper.

References

1. K.-N. Huang, Bull. Am. Phys. Soc. 26, 1301 (1981).
2. K.-N. Huang, Bull. Am. Phys. Soc. 27, 40 (1982).
3. K.-N. Huang, Phys. Rev. A 22, 223 (1980).
4. D. Hils, W. Jitschin, and H. Kleinpoppen, Appl. Phys. 25, 39 (1981).
5. D. Kleppner, Massachusetts Institute of Technology, private communication.

9. ANGULAR DISTRIBUTION AND SPIN POLARIZATION OF AUGER ELECTRONS FOLLOWING PHOTOIONIZATION AND PHOTOEXCITATION*

Keh-Ning Huang

Through collision processes, an atom can be ionized or excited such that the ion or atom is left in an excited state. In the deexcitation of the ion or atom, the transition energy can be carried off by the emission of photons (fluorescence radiation) and/or by the ejection of electrons (called Auger electrons, or autoionizing electrons in specific cases). Auger transitions in are more sensitive to detailed atomic structure than many other measurable atomic quantities.[1-3] To obtain a complete analysis of the Auger electron, we must measure its energy or momentum, angular distribution, and spin polarization and compare those values with theoretical predictions.

Cleff and Mehlhorn[4] have derived angular distribution of Auger electrons following impact ionization by unpolarized projectiles in terms of the relative population of magnetic substates (or equivalently the state multipoles defined by Fano[5]). The quantum-beat phenomena and the effect of hyperfine interactions in the angular distribution have been treated by Mehlhorn and Taulbjerg[6] and by Bruch and Klar.[7] Spin polarization of Auger electrons has been analyzed by Klar[8] in terms of the state multipoles; however, no convenient expressions were given. By considering a special case, Kabachnik[9] has obtained slightly improved expressions similar to those of Klar.[8] Nevertheless, none of those authors has provided expressions relating the angular distribution and spin polarization of Auger electrons to the initial excitation processes.

In the present study we provide concise general expressions for the angular distribution and spin polarization of Auger electrons following photoionization or photoexcitation, including the quantum-beat phenomena and the effect of hyperfine interactions with the nucleus. These expressions have exactly the same form as expressions for photoelectrons when the initial atom is excited or ionized in the electric dipole transition. This striking simi-

---

*Summary of a paper published in Phys. Rev. 26, 2274 (1982).

larity enables one to apply kinematic properties known for photoelectrons[10] in analyzing Auger electrons. By kinematic properties, we mean properties such as the ranges of dynamical parameters, functional forms of measured quantities in terms of dynamical parameters, functional relationships between measured quantities, and transformation properties.

References

1. W. B. Bambynek, B. Crasemann, R. W. Fink, H. U. Freund, H. Mark, C. D. Swift, R. E. Price, and P. V. Rao, Rev. Mod. Phys. 44, 716 (1972).
2. E. J. McGuire, in Atomic Inner-Shell Processes, edited by B. Crasemann (Academic, New York, 1975), Vol. I, p. 293.
3. M. O. Krause, in Atomic Inner-Shell Processes, edited by B. Crasemann (Academic New York, 1975), Vol. II, p. 33.
4. B. Cleff and W. Mehlhorn, J. Phys. B 7, 593 (1974).
5. U. Fano, Phys. Rev. 90, 577 (1953).
6. W. Mehlhorn and K. Taulbjerg, J. Phys. B 13, 445 (1980).
7. R. Bruch and H. Klar, J. Phys. B 13, 1363, 2885 (1980).
8. H. Klar, J. Phys. B 13, 4741 (1980).
9. N. M. Kabachnik, J. Phys. B 14, L337 (1981).
10. K.-N. Huang, Phys. Rev. A 22, 223 (1980).

10. ADDENDUM TO "THEORY OF ANGULAR DISTRIBUTION AND SPIN POLARIZATION OF PHOTOELECTRONS"*

Keh-Ning Huang

The angular distribution and spin polarization of photoelectrons, including all multipole transitions have been given in Eqs. (4.20) through (4.23) of Reference 1. They can be cast in more convenient form as:

$$\frac{d\sigma(\theta,\phi)}{d\Omega} = \frac{\sigma}{4\pi} F(\theta,\phi) \ , \tag{1}$$

where the angular distribution function is:

$$F(\theta,\phi) = 1 + \sum_{\ell\geq 1} \beta_{0\ell} d^{\ell}_{00} + (S_X \cos 2\phi + S_Y \sin 2\phi) \sum_{\ell\geq 2} \beta_{1\ell} d^{\ell}_{20} \ , \tag{2}$$

and

$$P_x(\theta,\phi)F(\theta,\phi) = S_Z \sum_{\ell\geq 1} \xi_{3\ell} d^{\ell}_{01} + (S_X \sin 2\phi - S_Y \cos 2\phi) \sum_{\ell\geq 2} (\xi_{2\ell} d^{\ell}_{21} + \eta_{2\ell} d^{\ell}_{2-1}), \tag{3}$$

$$P_y(\theta,\phi)F(\theta,\phi) = \sum_{\ell\geq 1} \eta_{0\ell} d^{\ell}_{01} + (S_X \cos 2\phi + S_Y \sin 2\phi) \sum_{\ell\geq 2} (\xi_{2\ell} d^{\ell}_{21} - \eta_{2\ell} d^{\ell}_{2-1}), \tag{4}$$

$$P_z(\theta,\phi)F(\theta,\phi) = S_Z \sum_{\ell\geq 0} \zeta_{3\ell} d^{\ell}_{00} + (S_X \sin 2\phi - S_Y \cos 2\phi) \sum_{\ell\geq 2} \zeta_{2\ell} d^{\ell}_{20} \ . \tag{5}$$

Here $d^{\ell}_{mn}(\theta)$ are the standard d functions of the rotation matrices, and $d^{\ell}_{00}(\theta) = P_{\ell}(\cos\theta)$, the Legendre polynomial. Equations (1) through (5) are similar to those for the fluorescence radiation[2] and the Auger electron[3] in the deexcitation of the residual ion. Besides the total cross section σ there are, in general, eight kinds of dynamical parameters: $\beta_{0\ell}$, $\beta_{1\ell}$, $\xi_{2\ell}$, $\xi_{3\ell}$, $\eta_{0\ell}$, $\eta_{2\ell}$, $\zeta_{2\ell}$, and $\zeta_{3\ell}$. We note that maximum information on the photoelectron from an unpolarized target can be obtained at any azimuthal orientation ϕ. Therefore it is sufficient to consider the angular distribution and spin polarization at $\phi=0$.

References

1. K.-N. Huang, Phys. Rev. A 22, 223 (1980).
2. K.-N. Huang, Phys. Rev. A 25, 3438 (1982).
3. K.-N. Huang, Phys. Rev. A 26, 2274, (1982).

---

*Summary of a paper published in Phys. Rev. A 26, 3676 (1982).

11. COHERENT FLUORESCENCE RADIATION FOLLOWING PHOTOEXCITATION AND PHOTOIONIZATION*

K.-N. Huang

Measurement of impact-induced coherent radiation has become a very useful tool in high-resolution spectroscopy. Among the coherence effects, the quantum-beat phenomena are conceptually the simplest and the most basic. Optically induced quantum-beat phenomena have been reviewed and certain specific cases worked out. Nevertheless, no general expressions have been given for the fluorescence radiation including all multipole transitions. Concise general formulas will help experimentalists in designing apparatus and in analyzing data in terms of a minimum number of dynamical parameters under arbitrary experimental conditions. In addition, high-multipole transitions, which depend both on the photon energy and on the extent of the overlap of electron wave functions, may become important when we consider high Rydberg or molecular orbitals whose radial sizes are extremely large, or when we consider cases where inner-shell electrons of heavy atoms are excited or ionized, such that the usual electric dipole approximation fails. Furthermore, when the electric dipole transition is forbidden by the parity selection rule, we have to consider the magnetic dipole and higher-multipole transitions. In this paper we present concise general formulas for the angular distribution and polarization of the coherent fluorescence radiation following photoexcitation and photoionization, including all multipole transitions.

---

*Summary of a Rapid Communication published in Phys. Rev. A 25, 3438 (1982).

12. DISSOCIATION IN SMALL MOLECULES*

P. M. Dehmer

The study of molecular dissociation processes is one of the most interesting areas of modern spectroscopy because of the challenges presented by even the simplest of diatomic molecules. In this paper we review the commonly used descriptions of molecular dissociation processes for diatomic molecules, the selection rules for predissociation, and a few of the principles to be remembered when one is forced to speculate about dissociation mechanisms in a new molecule.

Mechanisms for molecular dissociation resulting either from excitation out of the ground state or from the decay of a valence or Rydberg state can be classified as follows:[1]

(1) Direct dissociation. The most important case of dissociation continua in absorption is that in which a transition occurs from a stable lower state to a repulsive upper state or to the continuous portion of a stable upper state. The energy dependence of the continuum intensity is governed (to a first approximation) by the Franck-Condon principle, i.e., the most probable transition in absorption is that going vertically upward from the minimum of the lower potential energy curve.

(2) Radiative decay. Molecular dissociation results when a molecule in a stable excited state radiatively decays to a lower repulsive state. This is a common phenomenon and the resulting continuous radiation is often used for laboratory light sources.

(3) Nonradiative decay. When a discrete level overlaps an energetically accessible dissociation continuum, the possibility exists that the

---

*Summary of a paper that appeared in Desorption Induced by Electronic Transitions, edited by N. H. Tolk, M. M. Traum, J. C. Tully, and T. E. Madey (Springer-Verlag, Berlin, 1983), p. 164.

state will decay without the emission of radiation. Such a state normally has a very short lifetime (much shorter than typical radiative lifetimes), and as a result, the discrete level may appear broadened in absorption. Furthermore, there may be an absence or weakening of molecular emission, since only those molecules that do not decompose may radiate. This process, which is termed predissociation, occurs in diatomic molecules by the conversion of electronic or rotational energy and in polyatomic molecules by these mechanisms, as well as by the conversion of vibrational energy. Another nonradiative decay process that is analogous to predissociation and that is important in the dissociative ionization process in O_2 and other molecules is preionization. In this process, a discrete level overlaps an energetically accessible ionization continuum and decays via the ejection of an electron. The resulting parent ion may then predissociate to form a fragment ion.

Predissocation and preionization are special cases of perturbations, and therefore are subject to the same selection rules as perturbations. For diatomic molecules in any coupling scheme,[1] $\Delta J = 0, + \not\leftrightarrow -$, and $s \not\leftrightarrow a$; in Hund's case (a) and (b), $\Delta S = 0$ and $\Delta\Lambda = 0, \pm 1$. If both states belong to case (a), $\Delta\Sigma = 0$; if both states belong to case (b), $\Delta K = 0$; and if both states belong to case (c), $\Delta\Omega = 0, \pm 1$ (rather than $\Delta S = 0$ and $\Delta\Lambda = 0, \pm 1$). Similar considerations apply to preionization; however, the quantum numbers and symmetry properties in the continuous range of energy levels now refer to the system of molecular ion plus electron.

The selection rules for predissociation and preionization of triatomic and larger polyatomic molecules may be considerably more complex because of the interaction of electronic and vibrational angular momenta. Gelbart[2] has discussed the photodissociation of polyatomic molecules in detail in a recent review article, as has Okabe[3] in a recent book.

In addition to the energy, symmetry, and angular momentum restrictions imposed on predissociation and preionization processes, the Franck-Condon overlap of the potential energy curves of the interacting states imposes a further constraint that determines which of the allowed predissociations and preionizations will actually occur. It must be remembered that the Franck-

Condon principle governs radiationless as well as radiative transitions. In general, a transition is possible if the relevant potential energy curves intersect or at least closely approach one another.

References

1. G. Herzberg, Spectra of Diatomic Molecules (Van Nostrand, Princeton, 1950).
2. W. M. Gelbart, Ann. Rev. Phys. Chem. 28, 323 (1977).
3. H. Okabe, Photochemistry of Small Molecules (Wiley, New York, 1978).

13. PHOTOABSORPTION AND PHOTOIONIZATION OF HD*

P. M. Dehmer and W. A. Chupka†

Relative photoabsorption and photoionization cross sections have been measured for HD at a temperature of 78°K in the wavelength region of 735 to 805 Å. The wavelength resolution of 0.016 Å represents an improvement of more than two orders of magnitude over that of previous photoionization studies of this molecule. Bands of the $3p\pi\ D\ ^1\Pi_u \leftarrow X\ ^1\Sigma_g^+$ system are observed to nearly the dissociation limit, and ionization efficiencies were determined for a number of Rydberg states of low principal quantum number. As in the case of H_2, the ionization efficiency is close to unity for Rydberg states that can autoionize with $\Delta v = -1$, but drops to zero for states that can autoionize only with a large change in vibrational quantum number and that are significantly predissociated (such as the $3p\pi\ D\ ^1\Pi_u$ state). The accurate line intensities and line profiles obtained in the present experiment complement the accurate line positions obtained using photographic techniques. These data may be used together with the results of current theory to gain further insight into the dynamics of the nonradiative decay processes of molecular Rydberg states. To date, H_2 is the only example of a molecular system for which a quantitative quantum mechanical account of both autoionization and predissociation has been achieved, and the present data on the unsymmetric isotope HD should provide further information on the nonadiabatic effects, especially on the effects of (g, u) mixing.

*Summary of an article published in J. Chem. Phys. 79, 1569 (1983).
†Department of Chemistry, Yale University, New Haven, Connecticut 06511.

14. DECAY OF RYDBERG STATES VIA AUTOIONIZATION AND PREDISSOCIATION*

P. M. Dehmer

Details of the interaction between Rydberg states and ionization and dissociation continua traditionally have been obtained from the measurement of line shapes and line widths in absorption cross sections. However, the direct observation of one or more of the decay products as a function of excitation energy often is preferable, since this gives detailed information on the partial cross sections and on the competition among the various decay channels. A line shape often may change dramatically when observed in different decay channels, thus providing information on the interaction of a discrete level with several specific continua. A number of examples of autoionization and predissociation phenomena obtained by the observation of charged particles (ions or electrons) or fluorescent photons demonstrate this.

---

*Abstract of an invited talk presented at the XIV Annual Meeting of the Division of Electron and Atomic Physics, American Physical Society, 23-25 May 1983.

15. PHOTOIONIZATION OF CO_2 CLUSTERS

P. M. Dehmer and S. T. Pratt

Relative photoionization cross sections have been determined for $(CO_2)_2$ and $(CO_2)_3$ under experimental conditions such that fragmentation of heavier clusters does not contribute to the observations. In addition, the thresholds for formation of $(CO_2)_n^+$ (where n = 1 - 5) have been determined. The results of these measurements are given in Figures 1 and 2. A complete analysis of the results will be given in a forthcoming publication.

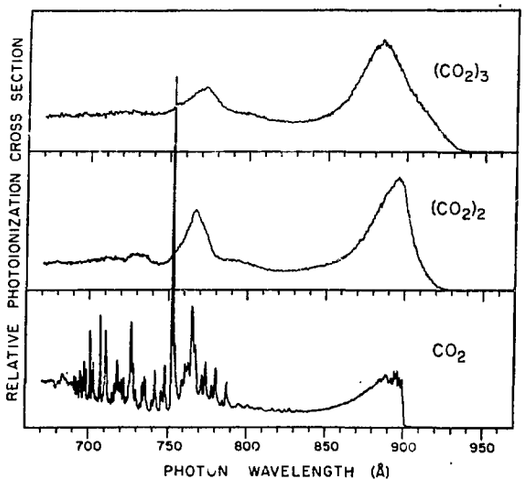

Fig. 1. Relative photoionization cross sections for CO_2, $(CO_2)_2$, and $(CO_2)_3$ taken under conditions such that fragmentation of heavier clusters does not contribute to the observed signal.

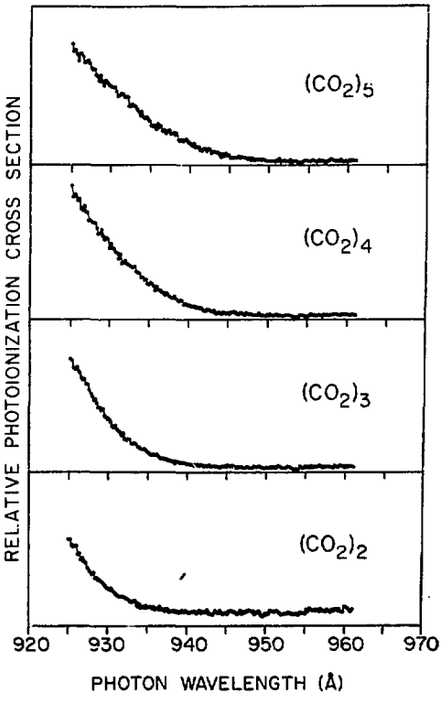

Fig. 2. Relative photoionization cross sections for $(CO_2)_n$ (n = 2 - 5) in the region of the appearance potential of the parent ion.

16. ON THE DISSOCIATION ENERGY OF $ArCO_2^+$*

S. T. Pratt and P. M. Dehmer

In a recent paper,[1] we presented a summary of the bond dissociation energies of the homonuclear and heteronuclear rare gas dimer ions determined from measurements of the ion appearance potentials using the technique of photoionization mass spectrometry. In this note, we present an extension of those studies to the determination of the bond dissociation energy of $ArCO_2^+$. The $ArCO_2$ was produced by expanding a premixed 10 to 1 sample of Ar and CO_2 through a 12.5-μm jet using a stagnation pressure of 7.8 atm. The appearance potential of $ArCO_2^+$ is 13.53 ± 0.03 eV.

Assuming that the appearance potential is identical to the adiabatic ionization potential, we can calculate the $Ar-CO_2^+$ bond dissociation energy using the relation $D_0(ArCO_2^+) = I.P.(CO_2) + D_0(ArCO_2) - I.P.(ArCO_2)$. If values of 13.773 ± 0.002 eV for the ionization potential[2] of CO_2 and 0.020 ± 0.010 eV for the dissociation energy[3-5] of $Ar-CO_2$ are used, the dissociation energy of the ground state of $ArCO_2^+$ is 0.26 ± 0.04 eV. As expected,[6,7] this is significantly lower than the dissociation energies of the homonuclear dimers Ar_2^+ (1.269 ± 0.017 eV)[8] and $(CO_2)_2^+$ (values of 0.51 ± 0.02 eV[9] and 0.50 ± 0.03 eV[10] have been obtained from photoionization studies).

It is of interest to compare the bond dissociation energies of $ArCO_2^+$ and $ArKr^+$ to assess the effects of the delocalized positive charge. It is expected that delocalization will have a considerable effect, since electrostatic forces play a major role in the bonding in the excited states and the ions of heteronuclear van der Waals molecules.[6] The dissociation energy of a molecular system AB^+ may be estimated[11] $D_0 \simeq (H_{AB})^2/(H_{AA}-H_{BB})$, where H_{ij} are the usual Hamiltonian integrals $\int \phi_i H \phi_j \, dr$, and ϕ_i and ϕ_j are the atomic orbitals. H_{AA} and H_{BB} frequently are approximated by the ionization potentials of the species A and B,[11] and H_{AB} is termed the interaction energy. Although the ionization potentials of Kr (14.000 eV)[12] and CO_2 (13.773 eV) are approximately equal, the bond energy of $ArKr^+$ (0.528 eV)[1] is twice that of $ArCO_2^+$ (0.26 eV).

*Summary of an article published in J. Chem. Phys. 78, 6336 (1983).

Using the ionization potentials of Ar, Kr, and CO_2 and the dissociation energies of $ArKr^+$ and $ArCO_2^+$, the interaction energies are 0.96 and 0.73 eV for $ArKr^+$ and $ArCO_2^+$, respectively. Thus, the delocalized nature of the unfilled molecular orbital appears to reduce significantly the interaction energy and the bond energy in $ArCO_2^+$. A similar effect occurs in the homonuclear dimer ions Kr_2^+ and $(CO_2)_2^+$. Even though Kr and CO_2 have nearly identical values of average polarizability[13-15] and of ionization potential, the dissociation energy of Kr_2^+ (1.150 eV)[1] is twice that of $(CO_2)_2^+$ (0.51 to 0.59 eV), suggesting that charge delocalization also influences the bonding in $(CO_2)_2^+$.

References

1. P. M. Dehmer and S. T. Pratt, J. Chem. Phys. 77, 4804 (1982), and references therein.
2. K. E. McCulloh, J. Chem. Phys. 59, 4250 (1973).
3. G. A. Parker, R. L. Snow, and R. T. Pack, J. Chem. Phys. 64, 1668 (1976).
4. H. J. Loesch, Chem. Phys. 18, 431 (1976).
5. The zero-point energy of the $ArCO_2$ stretch is approximately 0.002 eV and has been ignored in the calculation of the dissociation energy of $ArCO_2^+$. See J. M. Steed, T. A. Dixon, and W. Klemperer, J. Chem. Phys. 70, 4095 (1979).
6. H. Margenau, Rev. Mod. Phys. 11, 1 (1939).
7. R. S. Mulliken, Phys. Rev. 130, 1674 (1960).
8. P. M. Dehmer and S. T. Pratt, J. Chem. Phys. 76, 843 (1982).
9. S. H. Linn and C. Y. Ng, J. Chem. Phys. 75, 4921 (1981).
10. S. T. Pratt and P. M. Dehmer (unpublished).
11. J. N. Murrell, S. F. A. Kettle, and J. M. Tedder, The Chemical Bond (Wiley, New York, 1978), pp. 82-85, 91, and 168.
12. K. Yoshino and Y. Tanaka, J. Opt. Soc. Am. 69, 159 (1979).
13. A. Dalgarno and A. E. Kingston, Proc. R. Soc. London Ser. A 259, 424 (1960).
14. A. Dalgarno and A. E. Kingston, Proc. Phys. Soc. London 78, 607 (1961).
15. J. O. Hirschfelder, C. F. Curtiss, and R. B. Bird, Molecular Theory of Gases and Liquids (Wiley, New York, 1954), p. 950.

17. VUV SPECTROSCOPY OF VAN DER WAALS DIMERS AND HEAVIER CLUSTERS*

P. M. Dehmer

It is well known that forces between rare-gas atoms are repulsive, except for van der Waals forces, which cause weak molecular binding in all of the homonuclear and heteronuclear dimers except possibly He_2.[1] Removal of the outermost electron, which is antibonding in character, leads to a stable ground ionic state for all of the dimers. Several of the excited ionic states are bound as well, although, in general, the dissociation energies of the excited states are much smaller than that of the ground state. The addition of an electron in a Rydberg orbital to an ion in one of the bound states may result in a bound Rydberg state. However, little is known about the stable excited states of the neutral rare-gas dimers, except for those molecular states that arise from the lowest atomic resonance states (i.e., the molecular excimer states). A notable exception is the detailed multichannel quantum defect theory analysis of the Rydberg states in He_2 presented recently by Ginter and Ginter.[2]

With this in mind, we have undertaken a systematic study of the photoionization spectra of the homonuclear and heteronuclear rare-gas dimers in order to examine the nature of the bonding in the Rydberg states and ions of these molecules. We have obtained results for Ar_2,[3,4] Kr_2,[5] Xe_2,[6] NeAr, NeKr, NeXe,[7] ArKr, ArXe, and KrXe.[8] Of the remaining dimer species (Ne_2 and the He rare-gas dimers), only Ne_2 has been studied using photoionization mass spectrometry.[9]

The results of the present series of experiments provide information both on the excited states of the neutral dimers and on the ground and excited states of the dimer ions. Using the data obtained in these measurements, we are able to compile for the first time a nearly complete list of ground-state

---

*Summary of an invited talk presented at the NATO Advanced Study Institute on Photophysics and Photochemistry in the Vacuum Ultraviolet, Lake Geneva, Wisconsin, August 19, 1982, and a paper to be published in Photophysics and Photochemistry in the Vacuum Ultraviolet, edited by S. P. McGlynn, G. L. Findley, and R. H. Huebner, (D. Reidel Publishing Co., Dordrecht, Holland, 1983), p. xxx.

dissociation energies for the homonuclear and heteronuclear rare-gas dimer ions. Somewhat less extensive results are obtained for the excited states of these species. The observed trends in binding energy provide an excellent example of the systematic changes that occur as a result of changes in atomic orbital energies, polarizability, and internuclear distance, and these trends can be explained qualitatively in terms of simple molecular orbital theory.

References

1. R. S. Mulliken, J. Chem. Phys. 52, 5170 (1970).
2. D. S. Ginter and M. L. Ginter, J. Mol. Spectrosc. 82, 152 (1980) and references therein.
3. P. M. Dehmer and E. D. Poliakoff, Chem. Phys. Lett. 77, 326 (1981).
4. P. M. Dehmer, J. Chem. Phys. 76, 1263 (1982).
5. S. T. Pratt and P. M. Dehmer, Chem. Phys. Lett. 87, 533 (1982).
6. P. M. Dehmer and S. T. Pratt, J. Chem. Phys. 75, 5265 (1981).
7. S. T. Pratt and P. M. Dehmer, J. Chem. Phys. 76, 3433 (1982).
8. P. M. Dehmer and S. T. Pratt, J. Chem. Phys. (submitted).
9. D. J. Trevor, Ph.D. thesis, University of California, Berkeley, 1980.

18. RYDBERG STATES OF VAN DER WAALS MOLECULES -- A COMPARISON WITH RYDBERG STATES OF ATOMS AND OF CHEMICALLY BONDED SPECIES*

P. M. Dehmer

Since the ground states of van der Waals molecules are very weakly bound, it is of interest to ask if the Rydberg states of these species can be described as perturbed atomic Rydberg states, or, alternatively, if the bonding forces must be described as chemical. This question has no simple answer, since the appearance of the electronic spectra of van der Waals molecules may vary from quite complex (as, for example, in some regions of rare-gas dimer spectra) to remarkably similar to the monomer spectrum (as, for example, in spectra of He-molecule complexes). It is perhaps safe to say that states in a specific Rydberg series in a van der Waals molecule can be described as perturbed atomic states when the series converges to a weakly bound ionic limit and there are no perturbers of the Rydberg series. This only applies to regions of the spectrum in which the energy separation between adjacent molecular Rydberg states is much greater than the Rydberg-state dissociation energy. Unfortunately, these criteria are fulfilled in only a very few cases, and therefore the analogy between atomic and molecular spectra is of limited use in the detailed interpretation of molecular van der Waals spectra.

In general, the Rydberg spectra of van der Waals molecules may suffer from all of the complexities that affect the Rydberg spectra of chemically bonded molecules, namely diffuseness due to predissociation and autoionization and perturbations from other Rydberg and valence states. Furthermore, an apparent similarity between spectra features in atomic and molecular spectra does not guarantee a simple or straightforward analysis for either van der Waals or chemically bonded molecules.

*Summary of a paper that appeared in Comments At. Mol. Phys. 13, 205 (1983).

19. MULTIPHOTON IONIZATION AS A PROBE OF MOLECULAR PHOTOIONIZATION DYNAMICS*

J. L. Dehmer, P. M. Dehmer, and S. T. Pratt

The last decade has witnessed remarkable progress in the characterization of dynamical aspects of molecular photoionization in the VUV and X-ray energy ranges (see, e.g., Ref. 1). The general challenge has been to gain insight into the processes occurring during photoexcitation and the subsequent escape of the photoelectron through the anisotropic molecular field in terms of various physical observables, such as total and partial photoionization cross sections and photoelectron angular distributions. Much of this work has focussed on the prominent effects resulting from photoionization via shape and autoionizing resonances.

Recently, pulsed dye lasers have been combined with mass and electron energy analysis to form a new and complementary source of information on molecular photoionization dynamics.[2-7] In particular, it is now possible to excite well-defined multiphoton ionization processes in small molecules and to observe photoelectron branching ratios and angular distributions -- the standard dynamical observables used to study single-photon processes. In the multiphoton case, however, we are probing excited states of the neutral molecule which are resonant or quasiresonant at an intermediate stage of the multiphoton process. The high resolution of laser probes permits the excitation of particular vibrational and rotational quantum states of the excited molecule. Moreover, the currently available wavelength ranges and peak powers permit the study of small diatomic molecules of fundamental interest.

Although the main prototype system for this type of study[2-5] has been NO (partly due to its low ionization potential), we discuss recent studies[6,7] on CO and H_2, which serve to demonstrate the broad applicability of this approach. As an example, we cite the multiphoton ionization of CO involving a three-photon resonance to the v = 2 level of the CO A $^1\Pi$ state followed by the absorption of three additional photons to reach the ionization continuum.

*Extended abstract of an invited talk presented at the First U.S.-Japan Seminar on Electron Molecule Collisions and Molecular Photoionization, 26-29 October 1982, California Institute of Technology.

Figure 1 shows a schematic of the apparatus, which consists of a hemispherical electron spectrometer and a time-of-flight mass spectrometer. Figure 2 shows the relevant potential energy curves of CO. In one measurement, the CO^+ ion intensity is measured as a function of wavelength, yielding the rotational structure of the intermediate resonant state (Figure 3). In a second measurement, the laser frequency is set at the v = 2 bandhead, and the kinetic energy spectrum of the ejected electrons is measured (Figure 4). The observed vibrational branching ratios in these photoelectron spectra do not follow the pattern predicted by the Franck-Condon overlap between the intermediate A $^1\Pi$ state and the ionization continua. Several possible causes for this (not unexpected) deviation from ranck-Condon behavior are discussed.[6] Similar experiments involving multiphoton ionization of H_2 via the B $^1\Sigma_u^+$ state have also been performed,[7] and experiments with a two-color laser probe have begun.

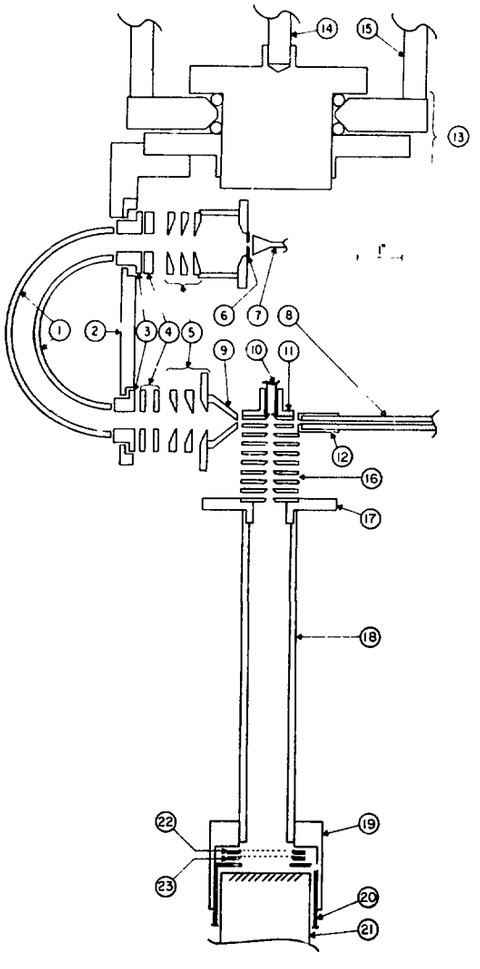

Fig. 1. Schematic diagram of the experimental apparatus. The main components are: (1) concentric hemispheres; (2) mounting plate for hemispheres and entrance and exit lenses; (3) Herzog lenses; (4) deflector plates, (5) three-aperture "zoom" lenses; (6) exit aperture; (7) channeltron detector; (8) 2 mm (i.d.) capillary leading to lamp (not shown); (9) entrance aperture; (10) gas jet; (11) gas-jet holder; (12) shield and holder for capillary tube; (13) sapphire ball bearing; (14) drive shaft; (15) mounting rods; (16) ion acceleration stack plates; (18) drift tube; (19) drift tube/detector mounting bracket; (20) detector housing; (21) electron multiplier; (22) drift tube potential grid; and (23) retarding grid.

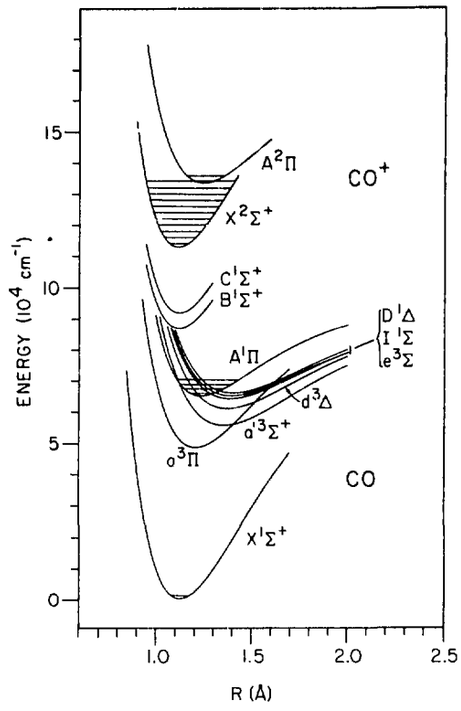

Fig. 2. Potential energy curves for states of CO and CO^+.

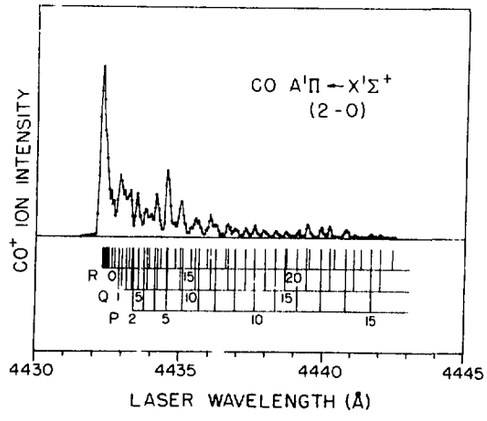

Fig. 3. Total cross section for multiphoton ionization of CO via the A $^1\Pi$, v=2 level.

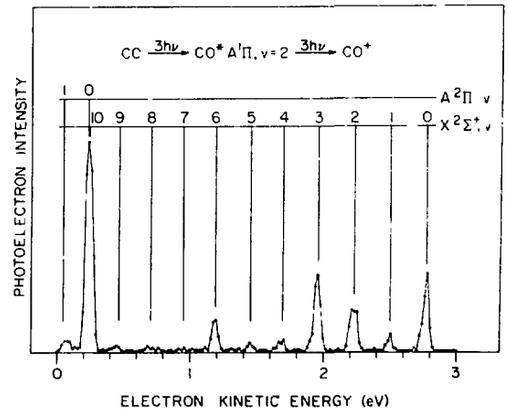

Fig. 4. Photoelectron spectrum of CO determined at the wavelength of the three-photon resonance to the R bandhead of the A $^1\Pi$, v=2 level (4432.5 Å).

References

1. J. L. Dehmer, D. Dill, and A. C. Parr, Proceedings of the NATO Advanced Study Institute on Photophysics and Photochemistry in the Vacuum Ultraviolet, Lake Geneva, WI, 16-27 August 1982 (D. Reidel Publishing Co., Dordrecht, Holland, 1983), in press.
2. J. C. Miller and R. N. Compton, J. Chem. Phys. 75, 22 (1981).
3. J. Kimman, P. Kruit, and M. J. van der Wiel, Chem. Phys. Lett. 88, 576 (1982).
4. M. G. White, M. Seaver, W. A. Chupka, and S. D. Colson, Phys. Rev. Lett. 49, 28 (1982).
5. J. C. Miller and R. N. Compton, Chem. Phys. Lett. (in press).
6. S. T. Pratt, E. D. Poliakoff, P. M. Dehmer, and J. L. Dehmer, J. Chem. Phys. 78, 65 (1983).
7. S. T. Pratt, P. M. Dehmer, and J. L. Dehmer, J. Chem. Phys. 78, 4315 (1983).

20. TWO-PHOTON RESONANT, FOUR-PHOTON IONIZATION OF CO VIA THE A $^1\Pi$ STATE WITH PHOTOELECTRON ENERGY ANALYSIS*

S. T. Pratt, P. M. Dehmer, and J. L. Dehmer

In a recent study,[1] we determined the photoelectron spectra resulting from the process:

$$CO\ X\ ^1\Sigma^+,\ v = 0 \xrightarrow{3h\nu} CO^*\ A\ ^1\Pi,\ v = 1\text{-}3 \xrightarrow{2h\nu\ or\ 3h\nu} CO^+\ X\ ^2\Sigma^+,\ v = 0\text{-}10 \text{ and } A\ ^2\Pi,\ v = 0,1 \qquad (1)$$

at wavelengths corresponding to the R-branch heads of the A $^1\Pi$, v = 1-3 ← X $^1\Sigma^+$, v = 0 bands. In the simplest approximation, one might expect the vibrational branching ratios to reflect the Franck-Condon overlap between the resonant intermediate level and the ionization continua; however, the observed branching ratios bear little resemblance to predictions based on this model. Explanations for this observation include perturbations of the resonant intermediate level, accidental resonances at higher energies, and autoionization phenomena.

We have now determined the photoelectron spectra for the simpler process:

$$CO\ X\ ^1\Sigma^+,\ v = 0 \xrightarrow{2h\nu} CO^*\ A\ ^1\Pi,\ v = 1\text{-}3 \xrightarrow{2h\nu} CO^+\ X\ ^2\Sigma^+,\ v = 0\text{-}12 \text{ and } A\ ^2\Pi,\ v = 0\text{-}3 \qquad (2)$$

at the wavelengths of the R-branch heads of the A $^1\Pi$, v = 1-3 ← X $^1\Sigma^+$, v = 0 bands. The resulting photoelectron spectra still do not exhibit branching ratios that reflect the Franck-Condon overlap between the intermediate A $^1\Pi$ state and the ionization continua. In most cases, however, interpretations of the observed spectra are possible in terms of accidental resonances with known states at the three-photon energy. The smaller number of photons necessary to ionize the intermediate level in the present study removes many of the ambiguities of the previous work.

---

*Summary of a paper to appear in J. Chem. Phys.

As an example, the photoelectron spectrum obtained at the wavelength of the two-photon transitions to the R-branch head of the A $^1\Pi \leftarrow X\ ^1\Sigma^+$ (2,0) band is shown in Figure 1. An intense peak is observed at the energy corresponding to the production of $CO^+\ X\ ^2\Sigma^+$, v = 0, and very little intensity is observed in the other vibrational bands. This strongly suggests an accidental resonance at the three-photon energy with an electronic state having an $X\ ^2\Sigma^+$, v = 0 ion core. The absorption spectrum of Ogawa and Ogawa[2] displays a band at 101456 cm^{-1}, which the authors assign to the $J\ ^1\Sigma^+$, v = 0 (4sσ) state. Using the reported rotational constants, we find that at the energies of the two-photon transitions to the R-branch head of the A $^1\Pi \leftarrow X\ ^1\Sigma^+$ (2,0) band, the photon wavelength is always within 50 cm^{-1} of an allowed rotational transition of the $J\ ^1\Sigma^+ \leftarrow A\ ^1\Pi$ (0,2) band. Thus, the $J\ ^1\Sigma^+$, v = 0 state almost certainly accounts for the intense peak at v = 0 in the photoelectron spectrum.

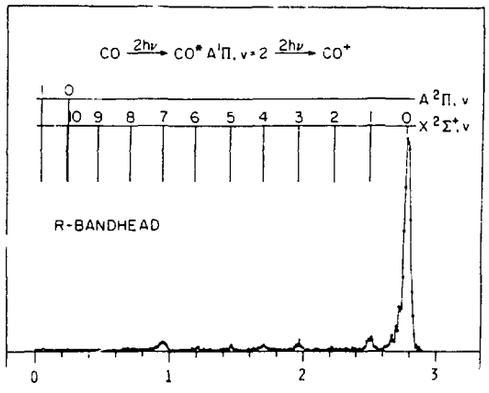

Fig. 1. Photoelectron spectrum of CO determined at the wavelength of the two photon resonance to the R-branch head of the A $^1\Pi \leftarrow X\ ^1\Sigma^+$ (2,0) band.

We calculated the Franck-Condon factors from the $J\ ^1\Sigma^+$, v = 0 level to the $CO^+\ X\ ^2\Sigma^+$, v = 0 - 12 levels by assuming Morse potentials for the $J\ ^1\Sigma^+$ and $X\ ^2\Sigma^+$ states. The Franck-Condon distribution is strongly peaked at the (0,0) transition, as is expected, and is in good agreement with the data shown in Figure 1. The weaker structure in the photoelectron spectrum does not reflect the Franck-Condon distribution for the ionizing transition from either the $J\ ^1\Sigma^+$, v = 0 level or the $A\ ^1\Pi$, v = 2 level. Because the $J\ ^1\Sigma^+$, v = 0 level is predissociated,[2] it is possible that the predissociating state also influences the vibrational branching ratios. The analysis of such effects must await more detailed studies, but it is clear that the dominant factor determining the branching ratios is the accidental resonance with the $J\ ^1\Sigma^+$, v = 0 level.

References

1. S. T. Pratt, P. M. Dehmer, and J. L. Dehmer, J. Chem. Phys. 78, 4315 (1983).
2. S. Ogawa and M. Ogawa, J. Mol. Spectrosc. 49, 454 (1974).

21. RESONANT MULTIPHOTON IONIZATION OF H_2 VIA THE B $^1\Sigma_u^+$, v = 7, J = 2 AND 4 LEVELS WITH PHOTOELECTRON ENERGY ANALYSIS*

S. T. Pratt, P. M. Dehmer, and J. L. Dehmer

Resonantly enhanced multiphoton ionization of molecules has been used to obtain detailed spectroscopic information on neutral intermediate states[1] and, when coupled with mass analysis of the product ions, to study the fragmentation mechanisms of the excited neutral and ionic species produced.[2-5] With the addition of kinetic energy analysis of the ejected electron, it is possible to determine the branching ratios into different vibrational levels of the product ion and to focus more directly on both the dynamics of multiphoton ionization and the photoionization of excited-state species.[3-13]

In this paper we present photoelectron spectra of H_2 obtained by three-photon absorption from the ground electronic state to specific rotational levels of the B $^1\Sigma_u^+$, v = 7 level, followed by the absorption of a single photon to the ionization continuum. Using a time-of-flight mass spectrometer, we recorded the photoion spectrum by monitoring the H_2^+-ion signal as the wavelength of the dye laser was scanned. The laser was then tuned to the wavelength of a specific rovibronic transition, as determined by the photoion measurements, and the photoelectron spectrum was recorded.

The photoion spectrum in the wavelength region containing the R(3) and P(3) transitions of the B $^1\Sigma_u^+$, v' = 7 ← X $^1\Sigma_g^+$, v" = 0 band is shown in Figure 1, and the photoelectron spectra obtained by pumping these rotational transitions are shown in Figure 2. The positions of the rotational levels of the H_2^+ ion are also indicated in Figure 2. The most dramatic feature of Figure 2 is that the observed rotational structure changes qualitatively with the intermediate rotational level of the B $^1\Sigma_u^+$ state, thus directly reflecting the selection rules for the ionizing transition. The photoelectron spectrum obtained by pumping the R(3) transition exhibits partially resolved rotational structure and clearly shows that no even rotational levels of the H_2^+ ion are produced.

---

*Summary of an article published in J. Chem. Phys. 78, 4315 (1983).

By considering the various selection rules for the ionizing transition ($a \not\leftrightarrow s$, $+ \leftrightarrow -$, $\Delta J = 0, \pm 1$), one can derive the allowed final rotational levels of the H_2^+ $X\ ^2\Sigma_g^+$ ion. The ionizing transitions must obey the selection rule $N(X\ ^2\Sigma_g^+) - J(B\ ^1\Sigma_u^+) = \pm 1, \pm 3$; therefore, for a given intermediate rotational level, the H_2^+ ion will be left in only odd or only even rotational states. Because the range of allowed H_2^+ rotational values differs for s and d waves, a rotationally resolved photoelectron spectrum can give detailed information on the relative importance of the different partial waves. From an analysis of the present results, we conclude that either the ejection of a d-wave electron or a j_t value[14,15] of 3 is highly unfavored.

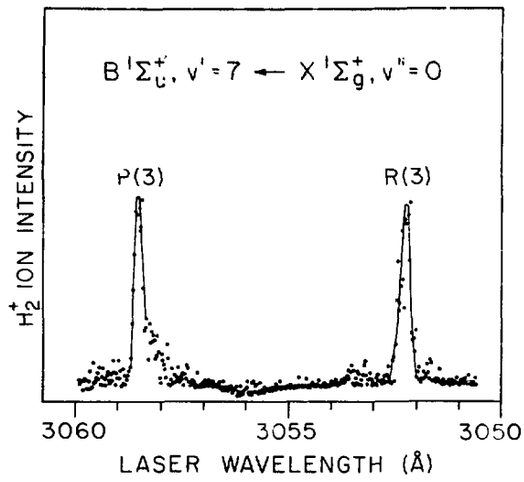

Fig. 1. Relative multiphoton ionization cross section for the production of H_2^+ from H_2 via the B $^1\Sigma_u^+$, v=7 level.

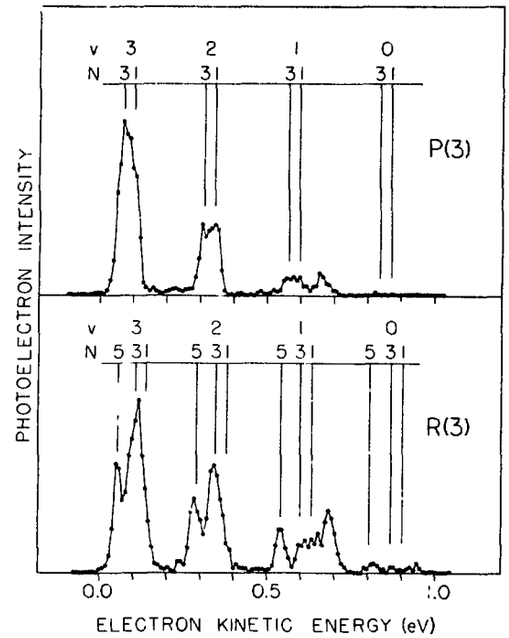

Fig. 2. Photoelectron spectra of H_2 determined at the wavelengths of the three-photon resonances to the J = 2[P(3)] and J = 4[R(3)] levels of the B $^1\Sigma_u^+$, v=7 level.

References

1. P. M. Johnson and C. E. Otis, Annu. Rev. Phys. Chem. 32, 139 (1981).
2. L. Zandee and R. B. Bernstein, J. Chem. Phys. 70, 2574 (1979).
3. U. Boesl, H. J. Neusser, and E. W. Schlag, J. Chem. Phys. 72, 4327 (1980).
4. D. Proch, D. M. Rider, and R. N. Zare, Chem. Phys. Lett. 81, 430 (1981).
5. T. E. Carney and T. Baer, J. Chem. Phys. 76, 5968 (1982).
6. J. H. Glownia, S. J. Riley, S. D. Colson, J. C. Miller, and R. N.

Compton, J. Chem. Phys. 77, 68 (1982).
7. J. C. Miller, R. N. Compton, T. E. Carney, and T. Baer, J. Chem. Phys. 76, 5648 (1982).
8. J. C. Miller and R. N. Compton, J. Chem. Phys. 75, 2020 (1981).
9. J. T. Meek, R. K. Jones, and J. P. Reilly, J. Chem. Phys. 73, 3503 (1980).
10. J. C. Miller and R. N. Compton, J. Chem. Phys. 75, 22 (1981).
11. J. Kimman, P. Kruit, and M. J. van der Wiel, Chem. Phys. Lett. 88, 576 (1982).
12. M. G. White, M. Seaver, W. A. Chupka, and S. D. Colson, Phys. Rev. Lett. 49, 28 (1982).
13. S. T. Pratt, E. D. Poliakoff, P. M. Dehmer, and J. L. Dehmer, J. Chem. Phys. 78, 65 (1983).
14. U. Fano and D. Dill, Phys. Rev. A 6, 185 (1972).
15. D. Dill, Phys. Rev. A 6, 160 (1972).

22. HIGH-RESOLUTION TOTAL ELECTRON-IMPACT EXCITATION OF INDIVIDUAL He 2^3S, 2^1S, 2^3P AND 2^1P STATES

David Spence, Dorothy Stuit, M. A. Dillon, R.-G. Wang,[†] and Z.-W. Wang[‡]

We have reinstated studies of the total electron-impact excitation of the He $2^{1,3}S$ and $^{1,3}P$ states at electron energies up to 4 eV above their thresholds. The only previous measurements of individual cross sections performed with sufficient resolution to be meaningfully compared with modern theories in this energy region were those of Brongersma et al.,[1] which were restricted to $^{1,3}S$ states.

The technique used by Brongersma et al.[1] was the double retarding potential difference (DRPD) trapped electron technique, which has the ability to energy-select the scattered electrons. We have used a similar apparatus but have replaced the RPD electron gun with a trochoidal monochromator (TM) so that a single modulation technique can be used.[2] As with all electron analyzers, there are two possible modes of operation with this technique for obtaining cross sections.

1. The first mode is to set the analyzer to accept electrons of a fixed energy loss at some threshold and to sweep the incident and analyzer energy to plot out an excitation function. Use of this mode of operation with the DRPD technique has three potentially serious defects: (a) "slipping out of tune" due to potential well end-effects at high energies, which produces an underestimate of the cross section;[3] (b) degradation of resolution at higher analysis energy, resulting in an additional underestimate of the cross section; and (c) because of (b) above, contributions from neighboring states may be included in the signal. To some degree, effects (a) and (b) are offset by effect (c), although by an unknown amount. There appear to be no criteria for producing unique excitation functions in this mode.

[†]Visiting Foreign Scholar. Permanent address: Department of Physics, Chengdu University of Science and Technology, Chengdu, People's Republic of China.
[‡]Visiting Foreign Scholar. Permanent address: Institute of Atomic and Molecular Physics, Jilin University, Changchun, People's Republic of China.

2. Alternatively, the analyzer is set to accept a fixed final energy of the scattered electrons for variable incident energy. This method produces energy loss spectra (see Figure 1) whose peak areas are proportional to the respective cross sections at a fixed energy ($W = E_R$) above threshold. From a series of such spectra, one can then measure peak areas and determine a cross section. Although more tedious than mode 1, mode 2 avoids all three defects, and therefore, we used this in the present work.

In an earlier report,[4] we presented individual cross sections of the ^3S and ^1S states in which the spectra of Figure 1 were deconvoluted by "eyeball". In the present work, the energy-loss spectra have been machine-digitized and computer-deconvoluted. The apparatus function, different for each value of E_R (due to rounding of the edges of the well) is obtained from the first, relatively isolated peak (i.e., the ^3S). Each spectrum is then deconvoluted using its appropriate apparatus function, into its four individual components. A computer-generated spectrum (dashed curve) then is matched against the raw data as a check.

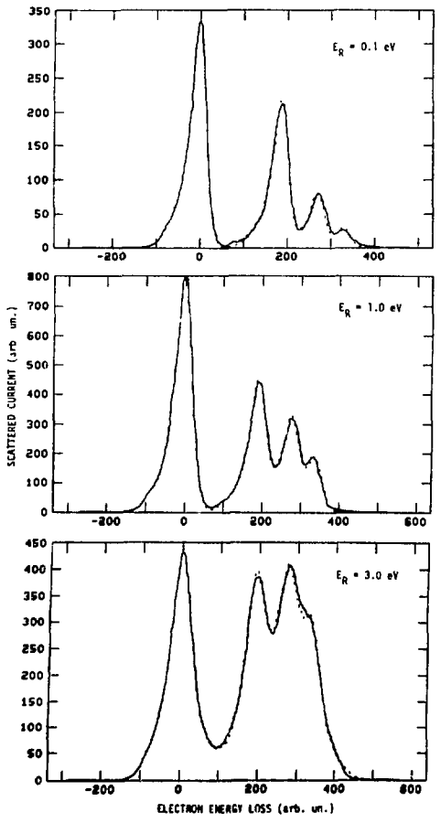

Fig. 1. Three examples of "total" (with respect to angle) energy-loss spectra obtained in the present experiments at different energies ($=E_R$) above thresholds. The solid curve represents the experimental data, and the dashed curve is a computer fit using instrument functions obtained from the first (^3S) peak. The instrument function is different for each of 102 spectra obtained.

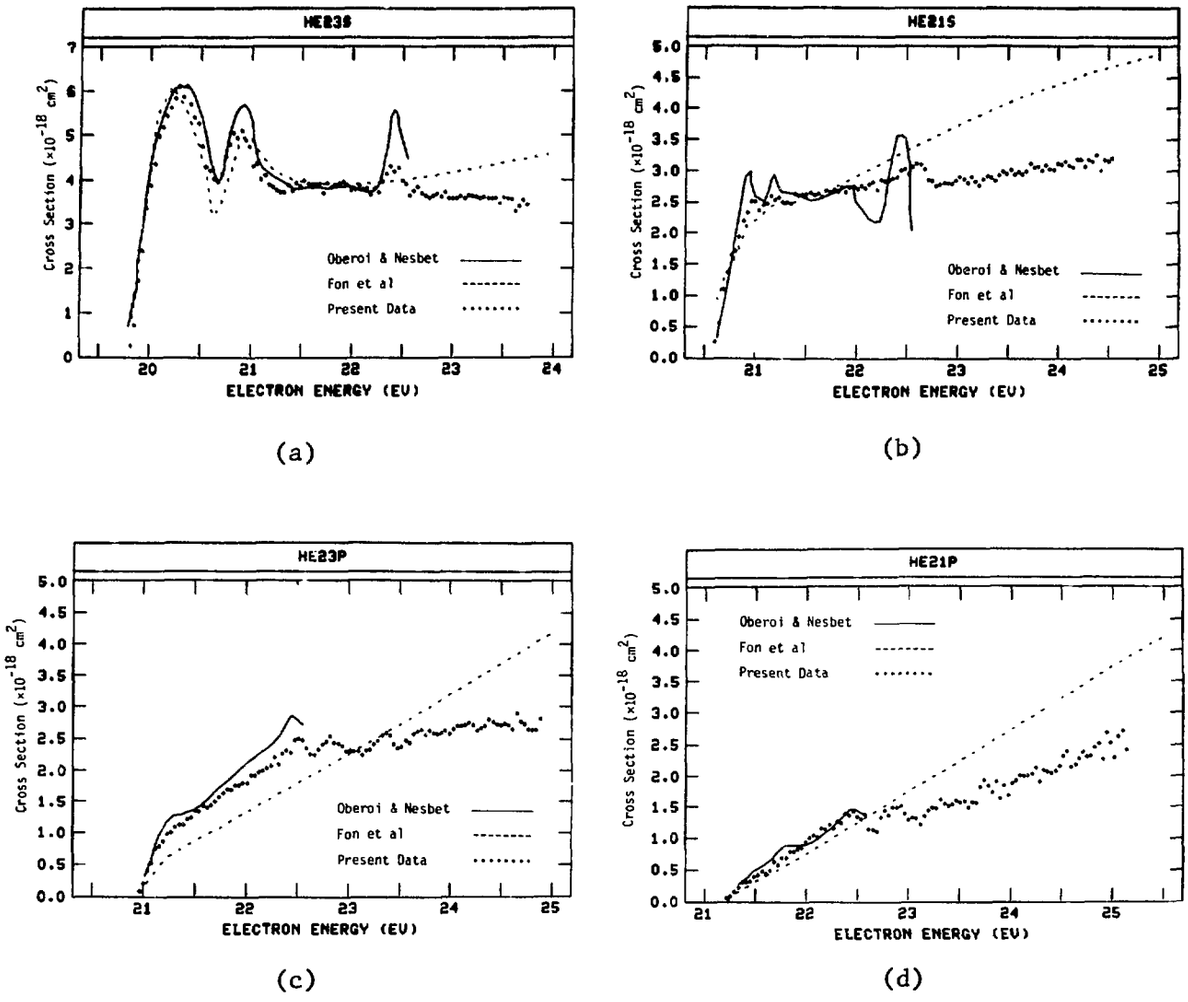

Fig. 2. Total cross sections compared with results of Oberoi and Nesbet[5] and Fon et al.[6] for: (a) He 2^3S; (b) He 2^1S; (c) He 2^3P; and (d) He 2^1P.

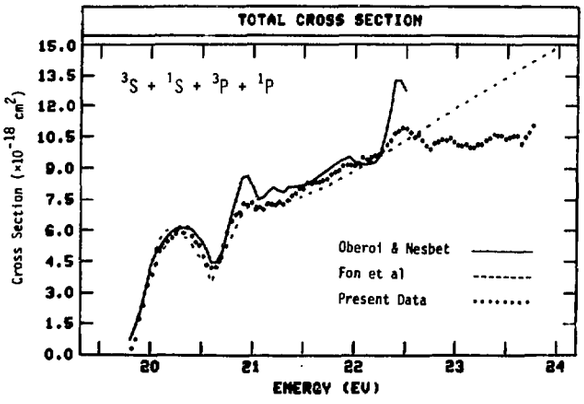

Fig. 3. "Total cross section ($^3S + {}^1S + {}^3P + {}^1P$) compared with results of Oberoi and Nesbet[5] and Fon et al.[6]

Each spectrum (102 in all) contributes one point on the individual cross sections shown in Figures 2a-d. Each figure shows a comparison with theoretical results of Oberoi and Nesbet[5] and of Fon et al.[6] The data of Figures 2a-d are normalized at one point, i.e., to 6.1×10^{-18} cm^2 at the first ^3S peak. This fixes the relative magnitudes of the $^{1,3}S$ and $^{1,3}P$ states both theoretically and experimentally. Note that the individual cross sections are not normalized independently. The scatter of the data points increases somewhat at higher energy due to loss of resolution at high W (= E_R) and the concomitant difficulty in deconvolution. However, the small structures in all cross sections are clearly in good agreement with those of Oberoi and Nesbet.[5]

Most previous measurements of the He cross sections have yielded only the sum of the individual cross section shown in Figures 2-5. In Figure 3 we compare the sums of our cross sections with theoretical values. Note that each point of Fig. 6 is not proportional to the total area of a single spectrum of Figure 1, but rather the sum of four different components taken from each of four different spectra. (Peaks occur in each spectrum at values of W (=E_R) above each threshold, whereas the total ($^{1,3}S$ + $^{1,3}P$) cross section requires the sum at the same energy.) Thus, the total cross section shown in Figure 3 is the true sum of the individual cross sections. Using our technique, we cannot measure this total directly, which is the reverse situation of most previous measurements using the trapped-electron technique.[7] However, our sum is in much closer agreement with both theories[5,6] than all previous direct measurements.[7] The cross sections are again normalized to 6.1×10^{-18} cm^2 at the first peak.

References

1. H. H. Brongersma, F. W. E. Knoop, and C. Backx, Chem. Phys. Lett. 13, 16 (1972).
2. D. Spence, Phys. Rev. A 12, 2353 (1975).
3. F. W. E. Knoop, H. H. Brongersma, and A. J. Boerboom, Chem. Phys. Lett. 5, 450 (1970).
4. D. Spence and D. Stuit, Argonne National Laboratory Radiological and Environmental Research Division Annual Report, ANL-78-63, Part I, October 1977 - September 1978, p. 133.
5. R. S. Oberoi and R. K. Nesbet, Phys. Rev. A 8, 2969 (1973).
6. W. C. Fon, K. A. Berrington, P. G. Burke, and A. E. Kingston, J. Phys. B 14, 2921 (1981).
7. A. R. Johnston and P. D. Burrow, J. Phys. B 16, 613 (1983).

23. ELECTRON SPECTROSCOPY OF HYDROGEN CHLORIDE FROM 5 TO 19 eV*

R.-G. Wang,† M. A. Dillon, and David Spence

Using an electron energy-loss spectrometer, we have measured the spectra of electrons inelastically scattered from HCl for an incident electron energy of 200 eV, energy losses between 5 and 19 eV, and scattering angles of 0° to 19°. The low-angle scattering spectra (presented in an earlier report[1]), correspond to photoabsorption. They confirm many optically allowed energy levels in HCl and locate many others, including six levels of the $\sigma^2\,\pi^3\,ns\sigma\ ^1\Pi$ Rydberg series. Series analysis yields an HCl ionization potential of 12.790 eV, midway between the known $HCl^+\ ^2\Pi_{3/2,1/2}$ energies of 12.750 and 12.830 eV. Spectra we have obtained at larger scattering angles are shown in Figure 1. Many structures show relatively large increases as a function of angle compared with structure 2, the $\sigma^2\pi^3\ 4s\sigma\ ^1\Pi$ state. The change in peak height as a function of θ provides information aiding in the identification of these structures via angular scattering prosperity rules. In the ionization continuum, we have located a new vibrational progression (Figure 2) associated with previously observed (negative ion) Feshbach resonances.[2] The new series has the configuration $3p\sigma 3p\pi^4\ 4s\sigma$ and is the lowest Rydberg state associated with the first excited ionic state $A^2\Sigma^+$. The relationship between the Rydberg states shown in Figure 2 and the previously observed Feshbach resonances is shown in Figure 3.

References

1. R.-G. Wang, M. A. Dillon, and D. Spence, Argonne National Laboratory Radiological and Environmental Research Division Annual Report, ANL 81-85, Part I, October 1980 - September 1981, p. 93.
2. D. Spence and T. Noguchi, J. Chem. Phys. 63, 505 (1975).

*Expanded abstract of a paper submitted to J. Chem. Phys.

†Visiting Foreign Scholar. Permanent address: Department of Physics, Chengdu University of Science and Technology, Chengdu, People's Republic of China.

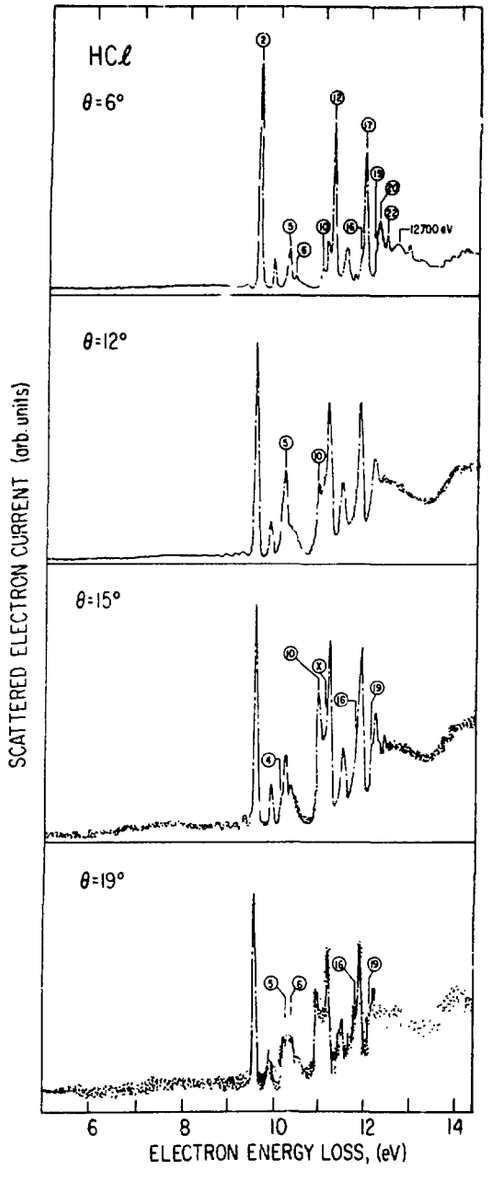

Fig. 1. Electron-energy loss spectra of HCl for an incident electron energy of 200 eV and various scattering angles (θ). The spectra demonstrate the large increase in relative intensity of some peaks as a function of scattering angle. The small structures between 8.5 and 9.2 eV for θ = 12° and 15° are N_2 Lyman-Birge-Hopfield impurity lines.

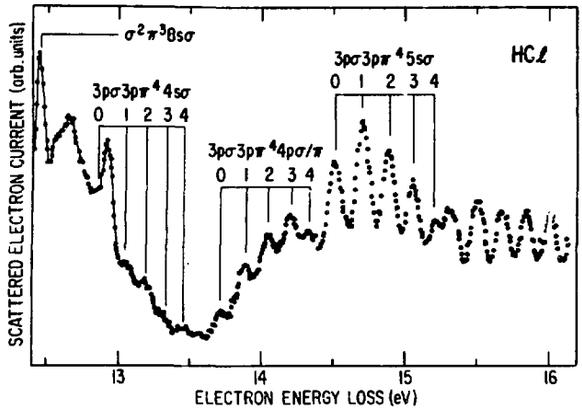

Fig. 2. Detailed electron energy-loss spectrum in HCl between 12.5 and 16 eV, showing structures arising from autoionizing Rydberg states in the continuum and converging to the lowest excited ionic state, $A^2\Sigma^+$. A new series, labelled $3p\sigma 3p\pi^4 4s\sigma$, is shown. The large structure at 12.9 eV is an N_2 impurity line.

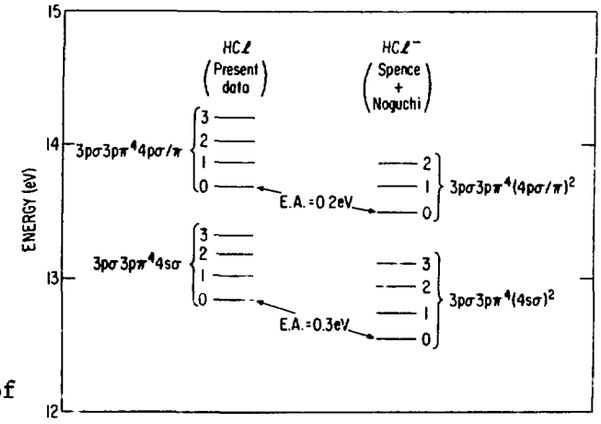

Fig. 3. Energy level diagram showing the relationship between Rydberg series observed in the present experiments in the ionization continuum of HCl and Feshbach resonances previously observed by Spence and Noguchi.

24. ELECTRON ENERGY-LOSS SPECTROSCOPY OF SILANE, SiH_4*

R.-G. Wang,† M. A. Dillon, D. Spence, and Z.-W. Wang‡

Electron impact spectra of silane were obtained as a function of scattering angle in the energy-loss mode using incident electrons of 200 eV and in the residual energy mode with electrons of 40 to 50 eV incidence.

The 200-eV results are summarized in Figure 1. The energy loss spectrum recorded at a scattering angle of 2° (top panel of Figure 1) closely resembles the optical spectrum reported by Roberge et al.[1] Assignment of the various features in the spectrum is largely speculative[1,2] because of the lack of sharp structure and awaits accurate CI calculations for clarification. The spectrum shown in the bottom panel of Figure 2 (obtained under conditions which favored symmetry-forbidden transitions) reveals two vibrational progressions in the energy-loss range of 16 to 18 eV. Reexamination of the electron impact spectrum of CH_4 at a scattering angle of 15° uncovered a similar vibrational structure at somewhat higher energies. In both cases, the vibrational bands are broadened considerably by autoionization. Work is proceeding with CD_4 in an effort to shed some light on the vibrational modes involved in the electronic excitation.

---

*Summary of a paper under preparation.

†Visiting Foreign Scholar. Permanent address: Department of Physics, Chengdu University of Science & Technology, Chengdu, People's Republic of China.

‡Visiting Foreign Scholar. Permanent address: Institute of Atomic and Molecular Physics, Jilin University, Changchun, People's Republic of China.

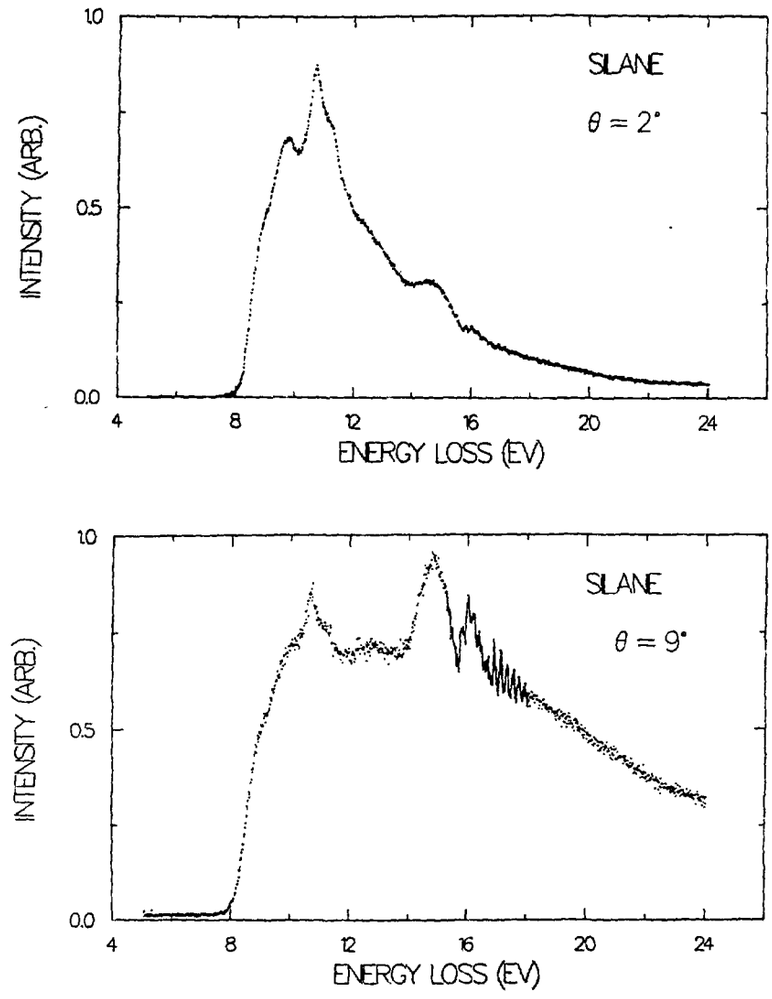

Fig. 1. Electron impact spectra of silane at scattering angles of 2° (top) and 9° (bottom).

References

1. R. Roberge, C. Sandorfy, J. I. Mathews, and O. P. Stravs, J. Chem. Phys. 69, 4955 (1978).
2. M. B. Robin, Higher Excited States of Polyatomic Molecules, (Academic, New York, 1974), Vol. 1, Chapter 3; Vol. 2, pp. 297-301.

25. STUDIES OF FORBIDDEN TRANSITIONS IN SATURATED HYDROCARBONS BY ELECTRON IMPACT SPECTROSCOPY*

R.-G. Wang,† M. A. Dillon, David Spence, and Z.-W. Wang‡

Electron impact spectra for CH_4, C_2H_6, $n\text{-}C_4H_{10}$ and C_5H_{12} (neopentane) were recorded as a function of scattering angle using incident electron energies of 30 to 40 eV in the constant residual energy mode. Examples of results are shown in Figures 1 and 2.

Spectra of methane recorded at scattering angles of 4° to 18° for 50-eV residual energy and at 84° for 30-eV residual energy are shown in Figure 1. The 4° to 18° spectra reveal an onset of electron scattering, for excitation energies of 8 to 9 eV, somewhat below the first optical threshold. This effect is greatly enhanced in the 84° spectrum, indicating the presence of the lowest triplet state of methane. This result is in agreement with the observations of Johnson[1] and others.[2] The spectra for ethane (Figure 2) are similar to those for methane. In addition to the lowest triplet of ethane in the 7.5 to 8 eV range, a shoulder at 8.5 eV emerges with increasing scattering angle. Since this feature persists to relatively high incident-electron energies,[2] it has been suggested that the transition is optically forbidden but quadrupole allowed.[1]

References

1. K. E. Johnson, K. Kim, D. B. Johnston and S. Lipsky, J. Chem. Phys. 70, 2189 (1979).
2. M. B. Robin, Higher Excited States of Polyatomic Molecules, (Academic, New York, 1974), Vol. 1, Chapter 3; Vol. 2, pp. 297-301.

*Summary of a paper in preparation.

†Visiting Foreign Scholar. Permanent adress: Department of Physics, Chengdu University of Science & Technology, Chengdu, People's Republic of China.
‡Visiting Foreign Scholar. Permanent address: Institute of Atomic and Molecular Physics, Jilin University, Changchun, People's Republic of China.

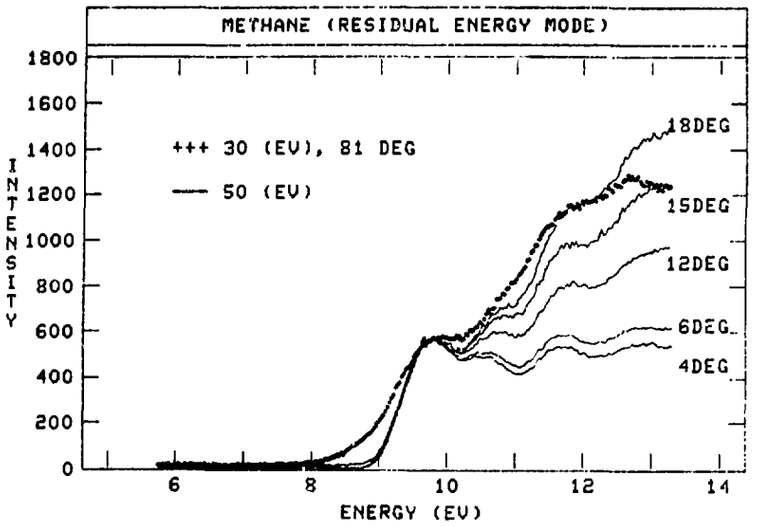

Fig. 1. Electron impact spectra methane:

——— as a function of scattering angle at 50 eV residual energy;
•••• at a scattering angle of 81° and a residual energy of 30 eV.

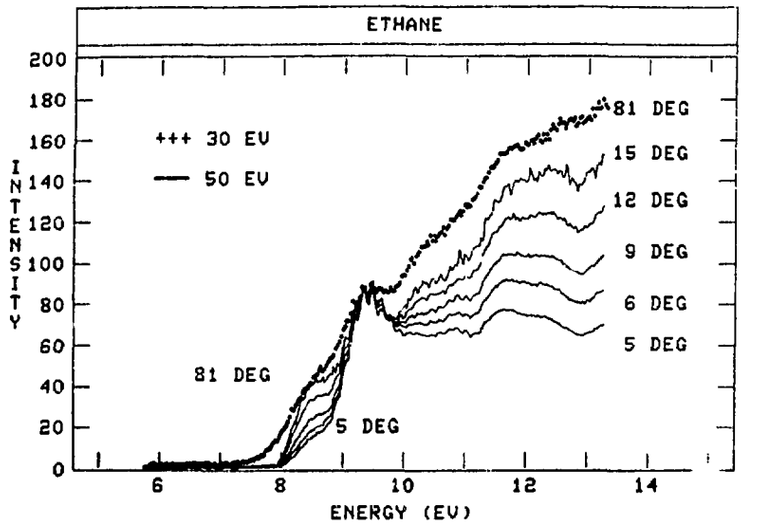

Fig. 2. Electron impact spectra ethane:

——— as a function of scattering angle at 50 eV residual energy;
•••• at a scattering angle of 81° and a residual energy of 30 eV.

26. PHENOMENOLOGICAL STUDY OF HETEROGENEOUS CHEMICAL REACTIONS OF MERCURIC CHLORIDE ON HEATED STAINLESS-STEEL SURFACES*

R.-G. Wang,† M. A. Dillon, and David Spence

We have made the first measurements of the products of surface chemical reactions of mercuric chloride on heated stainless steel using the technique of electron-energy-loss spectroscopy as an analytic tool. We find that $HgCl_2$ reacts with hydrogen in the stainless steel to form hydrochloric acid (HCl). Under our experimental conditions, HCl becomes the dominant species observed in our spectra at surface temperatures greater than about 150°C. The possible consequences of our observation on the efficiency of mercuric halide lasers is discussed.

---

*Abstract of a paper published in J. Chem. Phys. 79, 1100 (1983).

†Visiting Foreign Scholar. Permanent address: Department of Physics, Chengdu University of Science and Technology, Chengdu, People's Republic of China.

27. CROSS SECTIONS FOR INELASTIC SCATTERING OF ELECTRONS BY ATOMS - SELECTED TOPICS RELATED TO ELECTRON MICROSCOPY*

Mitio Inokuti and S. T. Manson†

We begin with a resumé of the Bethe theory, which provides a general framework for discussing the inelastic scattering of fast electrons and leads to powerful criteria for judging the reliability of cross-section data. The central notion of the theory is that the generalized oscillator strength is a function of both the energy transfer and the momentum transfer and is the only non-trivial factor in the inelastic-scattering cross section. Although the Bethe theory was initially conceived for free atoms, its basic ideas apply to solids, with suitable generalizations. In this respect, the notion of the dielectric response function is the most fundamental. Topics discussed include the generalized oscillator strengths for the K-shell and L-shell ionization for all atoms with $Z \leq 30$, evaluated by use of the Hartree-Slater potential. As a function of energy transfer, the generalized oscillator strength most often shows a non-monotonic structure near the K-shell and L-shell thresholds. This has been interpreted as a manifestation of electron-wave propagation through atomic fields. For molecules and solids, there are additional structures caused by the scattering of ejected electrons by the fields of other atoms.

*Abstract of an article to appear in the Proceedings of the First Pfefferkorn Conference on Electron Beam Interactions with Solids for Microscopy, Microanalysis, and Microlithography, Asilomar, Pacific Grove, California, 18-23 April 1982, (Scanning Electron Microscopy, Inc., in press).

†Department of Physics and Astronomy, Georgia State University, Atlanta, Georgia 30303.

28. ANGULAR AND ENERGY DISTRIBUTION OF SLOW ELECTRONS EJECTED FROM He BY ELECTRON IMPACT*

Y.-K. Kim

Suggested angular and energy distributions of slow electrons ($\leq$ 40 eV) ejected from He by electron impact have been deduced. The results are presented in a compact table of coefficients A_n for Legendre polynomials:

$$\frac{d^2\sigma(T)}{dW d\Omega_s} = \sum_{n=0}^{6} A_n(T,W)\, P_n(\cos\theta),$$

where $d\Omega_s$ is the solid angle element of the slow-electron direction, W and T are the kinetic energies of the ejected and incident electron, respectively, P_n is the nth order Legendre polynomial, and θ is the angle of the ejected electron measured from the incident beam direction.

Various theoretical and experimental results were used in deducing the suggested cross sections. The cross sections have proper asymptotic behavior and are consistent with known single differential and total ionization cross sections.

The suggested cross sections not only fill missing gaps in experimental data (e.g., for $W < 5$ eV, $\theta < 30°$, $\theta > 150°$) but also provide a convenient basis for interpolation within the given ranges of electron variables ($0° \leq \theta \leq 180°$, 0 eV $\leq W \leq$ 40 eV, 100 eV $\leq T \leq$ 2 keV).

These cross sections should be reliable in the angular range $30° \leq \theta \leq 120°$, so that they can serve as normalization standards for relative measurements. In Figure 1, the suggested angular distribution for the case of T = 200 eV, W = 20 eV is compared with available theoretical and experimental data.

---

*Abstract of an article published in the Phys. Rev. A 28, 656 (1983).

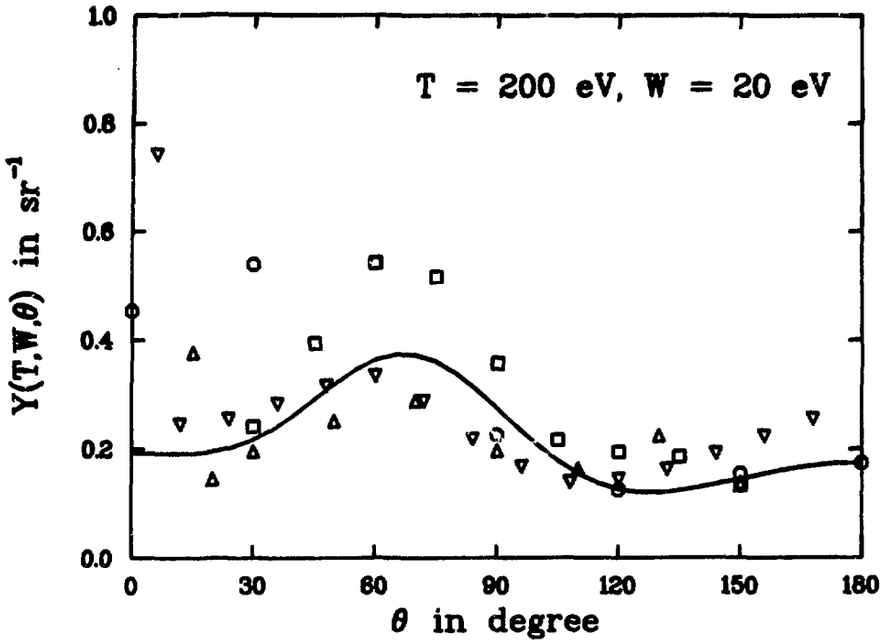

Fig. 1. Comparison of angular distributions for T = 200 eV and W = 20 eV. The ordinate is the double differential cross section in units of free electron (Rutherford) cross sections, hence representing effective number of free electrons ejected into $d\Omega_s$. The solid curve is the suggested cross section, and the circles are plane-wave Born cross sections. Other symbols represent experimental data. The sharp peaks at $\theta < 20°$ in the experimental data are most likely experimental artifacts.

29. THEORETICAL TRIPLY DIFFERENTIAL CROSS SECTION OF ELECTRON-IMPACT IONIZATION OF ATOMS*†

K.-N. Huang

Impact ionization of atoms or ions by charged particles is important for diagnostics of high-temperature plasmas, as well as for fundamental understanding of atomic structure. In recent years, electron coincidence spectroscopy has become a powerful tool for testing dynamical theories of final states with two outgoing electrons.[1-4] To the author's knowledge, no theoretical kinematic analysis of the electron-impact ionization of atoms has been given. A complete kinematic analysis can provide an overall symmetry of the impact-ionization processes and facilitate the comparison between theory and experiment.

In this paper, we describe the triply differential cross section in terms of angle-independent dynamical parameters. For low-energy ionization, where only the first few partial waves contribute significantly, a small number of dynamical parameters are adequate to describe the full angular correlation between the incoming and outgoing electrons. The kinematic analysis which we present can apply to collision processes of the general type

$$a + A \longrightarrow B + b + c, \tag{1}$$

where A and B are assumed to be sufficiently heavy that they are stationary in the center-of-momentum frame. For definiteness, however, we shall consider specifically the electron-impact ionization of atoms. Application of the present formulation is demonstrated. Merits of coplanar measurements are discussed. It is also shown that the coplanar up-down asymmetry of the ejected electron is linear in the scattering angle, or the momentum transfer, of the incident electron for small momentum transfers.

---

*Summary of a Rapid Communication published in Phys. Rev. A 28, 1869 (1983).
†The author would like to express deep gratitude to Professor R. H. Pratt for his hospitality at the University of Pittsburgh, where part of this research was performed. This research was also supported in part by the U.S. Department of Energy.

To apply the present formulation to analyze coplanar coincidence, we write coplanar distribution as:

$$\sigma(\theta_1,\theta_2) = \sum_{\ell=0}^{L} \beta_1(\theta_1) d_{00}^{\ell}(\theta_2) + \sum_{\ell=1}^{L} \gamma_1(\theta_1) d_{01}^{\ell}(\theta_2) , \qquad (2)$$

where β_1 and γ_1 can be written as expansions in terms of dynamical parameters. The summation over a large number of partial waves for the scattered fast electron is implied in the definition of β_1 and γ_1. The maximum L of the explicit summation in Eq. (2) is determined only by the ejected slow electron. The first term on the right-hand side of Eq. (2) is even both in θ_1 and in θ_2, and the second term is odd. Coplanar measurements can determine all (2L + 1) functions, $\beta_1(\theta_1)$ and $\gamma_1(\theta_1)$. In contrast, a complete triply differential measurement would yield (L + 1)(L + 2)/2 independent functions of θ_1.

As a demonstration, we fit the functional form Eq. (2) to the experimental data of electron-impact ionization of helium presented in Figure 1 of Ehrhardt et al.[4] The incident electron has an energy E_i = 500 eV and is scattered at $\theta_1 = 3.5°$. The ejected slow electron has an energy E_2 = 5 eV. We therefore include up to, say, *d* waves of the ejected slow electron; i.e., we consider L = 4. The semiempirical parameters obtained at $\theta_1 = 3.5°$ are β_0 = 2.288, β_1 = 0.306, β_2 = -0.943, β_3 = -0.906, β_4 = 0.095, γ_1 = -0.806, γ_2 = -2.530, γ_3 = 0.360, and γ_4 = 0.133. The coplanar cross section constructed from these parameters is presented in Figure 1, along with the experimental data of Ehrhardt et al.[4] Also presented in the figure are the semiempirical fittings with L = 2 and L = 3. The fitting with L = 2 is apparently inadequate. The dependence of these parameters on θ_1 can be obtained by fitting experimental data at different angles θ_1. Because these parameters can also be calculated theoretically by using formulas presented here, summarizing experimental data in terms of these parameters can facilitate the comparison between experiment and theory, as well as between experiments with different scattering angles θ_1.

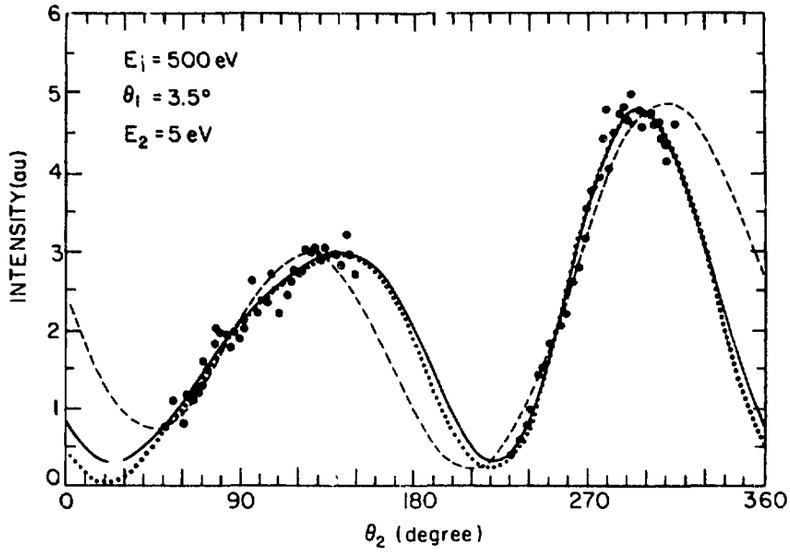

Fig. 1. Triply differential cross section (in a.u.) for the ionization of helium by electron impact. The dots are experimental data of Ehrhardt et al.[4] The solid curve is obtained semi-empirically with the functional form (1) for L=4; the dotted curve is that for L=3; the dashed curve is that for L=2.

References

1. H. Ehrhardt, K. H. Hesselbacher, K. Jung, and K. Willmann, in Case Studies in Atomic Physics, edited by E. W. McDaniel and M. R. C. McDowell (North-Holland, Amsterdam, 1972), Vol. 2, Chap. 3.
2. I. E. McCarthy and E. Weigold, Phys. Rev. 27C, 275 (1976), and references therein.
3. F. W. Byron, Jr., C. J. Joachain, and B. Piraux, J. Phys. B 15, L293 (1982).
4. H. Ehrhardt, M. Fischer, K. Jung, F. W. Byron, Jr., C. J. Joachain, and B. Piraux, Phys. Rev. Lett. 48, 1807 (1982).

30. ANGULAR AND POLARIZATION CORRELATION IN INELASTIC ELECTRON-ATOM SCATTERINGS*

K.-N. Huang

A relativistic theory of elecron-atom scattering is developed for polarized incident electrons on unpolarized atoms. The projectile and the target are treated as a composite system; therefore, the exchange effect can be incorporated by antisymmetrization of the total wave function. The general case of inelastic scattering is considered, with elastic scattering treated as a special case. Formulas for angular distribution and spin polarization of the scattered electron are presented in terms of angle-independent dynamical parameters. These dynamical parameters are given as linear sums of radial integrals, suitable for numerical computations. The connection with well-known formulas for elastic scattering is demonstrated. The analyzing power and polarizing power of the target are given generally for the electron-impact excitation of atoms. Spin polarization of total scattered electrons with a definite energy is also presented.

I. INTRODUCTION

Particle scattering on a many-particle target has been one of the most fruitful probes of elementary interactions and of the target structure. Electron-atom and electron-molecule scatterings, in particular, have important applications in astrophysics, plasma physics, and radiation physics. A review of earlier studies of electron-impact excitation of atoms was given by Moiseiwitsch and Smith.[1] Inelastic collisions of fast charged particles with atoms and molecules were reviewed by Inokuti,[2,3] with emphases on properties of generalized oscillator strength and the integrated cross section at the high-velocity limit. Summaries of experimental measurements of total electron-atom scattering cross sections were given by Bederson and Kieffer,[4] by Andrick,[5] and by de Heer.[6] Resonance effects in atomic and molecular scattering processes were reviewed by Taylor,[7] by Schulz,[8] and by Golden.[9] Specific dynamical theories were reviewed by Burke and Robb[10] on the R-matrix method and by Callaway[11] and by Drachman and Temkin[12] on the polarized orbital method. A more recent review on close-coupling theory was given by Seaton.[13] Nesbet[14] surveyed the theory of low-energy electron scattering by

complex atoms and discussed resonances and threshold effects and inelastic processes. Theory and its application to low-energy electron-molecule collisions were reviewed by Lane,[15] with emphases on elastic scattering and vibrational and rotational excitation of small molecules. Extensive data on theoretical and experimental cross sections for electron-impact excitation of positive ions have been compiled by Merts et al.[16] These works[1-16] and the references therein can be consulted for recent developments in this fertile field of electron scattering.

Most previous studies on electron scatterings have dealt with the total cross section. However, angular distribution and spin polarization of the scattered electron can reveal a wealth of information about the interaction and the target structure. In addition, as was pointed out by Bederson[17] and by Kleinpoppen,[18] valuable new information about electron-atom scattering processes can be obtained from experiments with polarized particle beams. A notable recent application is the observation of parity nonconservation in inelastic scattering of longitudinally polarized electrons from unpolarized targets.[19,20] An excellent discussion of the scattering of polarized electrons was given by Kessler.[21] The application of polarized beams to the study of interference phenomena in electron-hydrogen collisions was reviewed by Lubell.[22]

The angular dependence of spin polarization of electrons elastically scattered by noble gas atomic beams was first measured at incident electron energies between 40 and 150 eV by Schackert.[23] Kessler et al.[24] presented their experimental results for incident energies between 150 and 300 eV. More recently, Klewer et al.[25] have reported the spin polarization of electrons elastically scattered from xenon at energies between 5 and 300 eV and from cesium at between 13 and 25 eV. Coulthard[26] has calculated polarization curves at 50 and 100 eV using relativistic Hartree potential. Fink and Yates[27] have reported polarization data for energies over the range of 25 to 800 eV using relativistic Hartree-Fock-Slater potentials. Exchange of the incident electron with the atomic electrons, however, was not taken into account in those two calculations. Theoretical calculations of elastic electron scatterings were also carried out for various atoms by Walker[28,29] in the relativistic distorted-wave approximation including exchange. McCarthy et al.[30] computed elastic scattering results for electrons incident on rare gases

at energies from 20 to 3000 eV employing a local optical potential. The agreement between theory and experiment is generally good for incident energies above 150 eV, where the calculation of Walker[28,29] was favored. At energies below 150 eV, all calculatioins fail to predict the correct polarization.

All the relativistic calculations mentioned above were carried out for elastic scatterings, while the inelastic scatterings do constitute a substantial portion of the exit channels at low incident energies. Formulas for angular distribution and spin polarization of elastically scattered electrons are well known[21,28,29,31] and depend only on the incident energy and the phase shifts of partial waves. On the other hand, for inelastically scattered electrons, the angular distribution and spin polarization depend on the energies of the incident and outgoing electrons, on the phase shifts, and on the transition amplitudes involving both the projectile and the target. To the author's knowledge, the kinematics of the inelastic scattering of a spin-1/2 particle on a many-particle system has never been fully reported. A full exposition of the kinematics can help to focus on specific dynamical effects and can provide a convenient reference for future works in the same field.

In the present paper, we treat the projectile and the target as a single system; therefore, the exchange effect can be introduced by antisymmetrization of the total wave function. We also consider the general case of inelastic scattering, with elastic scattering treated as a special case. A relativistic approach is used from the outset; the spin polarization of the electron and fine structures of the atom are built in. Although we have in mind the application to electron-atom scatterings, the present formulation is applicable to any spin-1/2 particle inelastically scattered on a many-particle system. Symbolically, we consider the general processes:

$$a + A \rightarrow b + B, \tag{I-1}$$

where a and b are both spin-1/2 particles (with the possibility of being different kinds), and A and B are the initial and final states of the target before and after the collision, provided that A and B are much heavier than a and b. The angular distribution and spin polarization of the scattered particle are presented in concise parameterized expressions. For low-energy

electron scatterings, where only a few partial waves suffice, these angle-independent parameters can provide simple comparisons between theory and experiment. Even when large numbers of partial waves become important, these dynamical parameters provide a convenient classification of contributions and facilitate comparisons between different calculations. In addition, the present approach is formulated in such a way that any single-channel or multichannel dynamical theory can be used to calculate pertinent parameters.

In Section II, we derive the density matrix of the scattered electron and express it in terms of radial integrals. In Section III, we evaluate the angular distribution and spin polarization of the scattered electron. All measurable quantities are presented in terms of angle-independent dynamical parameters. The special case of potential scattering is also discussed. Analyzing power and polarization power of the target are given in Section IV, while spin polarization of the total scattered electron flux is calculated in Section V. Matrix elements of various potential functions are summarized in Appendix A. The relativistic orbital and its phase convention used in this paper are given in Appendix B. In Appendix C, electron helicity states are presented, and in Appendix D, explicit formulas for the transformation of the spin-polarization vector between different coordinate systems are given.

II. DENSITY MATRIX OF THE SCATTERED ELECTRON

The scattering amplitude of electron scattering can be written in atomic units as:

$$f_{fi} = \frac{4\pi^2}{c^2}\sqrt{\frac{E_i E_\alpha k_\alpha}{k_i}} < \Psi_f | H_I | \Psi_i >, \qquad \text{(II-1)}$$

where c is the speed of light, and the incident electron has a momentum $k_i = |\vec{k}_i|$ and an energy $E_i = (k_i^2 + c^2)^{1/2}$; the scattered electron is similarly specified by k_α and E_α. Although the scattered electron can be either the scattered incident electron or the exchanged electron from the target, for convenience we shall refer to either of them as the scattered electron. In (II-1),

Ψ_i and Ψ_f are the initial and final states, respectively, of the combined projectile and target system, and H_I is the interaction between electrons, having the two-particle operator form:

$$H_I = \sum_{i<j}^{N} v(ij). \qquad \text{(II-2)}$$

In the lowest approximation, v(ij) is given by the Coulomb interaction $1/r_{ij}$. This and high-order corrections are discussed in Appendix A.

Now we consider the experimental situation where the electron $|\vec{k}_i \mu_i>$, having a linear momentum $\vec{k}_i$ and helicity μ_i, incidents upon the target atom in the total angular momentum eigenstate $|J_o M_o>$. After the collision, an electron is detected at a macroscopic distance in the direction (θ,ϕ) with respect to the incident electron direction $\hat{k}_i$. The scattered electron has a linear momentum $\vec{k}_\alpha$ and helicity μ, where the subscript α is the channel index making the provision for different exit channels. The target atom is, in general, left in an excited angular momentum eigenstate $|J_\alpha M_\alpha>$. This collision process is illustrated in Figure 1.

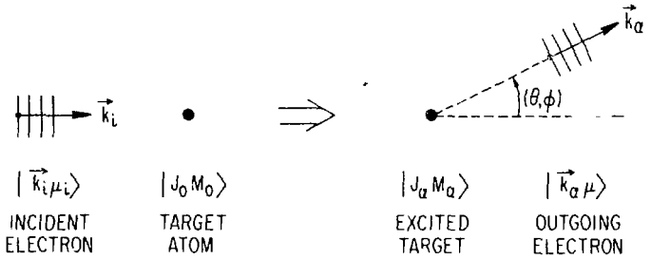

Fig. 1. Schematic diagram of electron-impact excitation of atoms.

The initial state of the combined projectile and target system can be expressed in terms of the composite helicity eigenstates[32] as:

$$|\Psi_i> = (4\pi)^{-1/2} \sum_J [J] |\, k_i \mu_i - M_o;\ J\lambda >, \qquad \text{(II-3)}$$

where $\lambda = \mu_i + M_o$, and we have used the notation $[J] \equiv (2J+1)^{1/2}$. The helicity eigenstate is defined in Appendix C. The final state can also be expressed in terms of helicity eigenstates as:

$$|\Psi_f\rangle = (4\pi)^{-1/2} \sum_{J'\nu'} D^{(J')}_{\nu'\nu}(\hat{k}_\alpha)[J']\,|k_\alpha^- \mu - M_\alpha;\ J'\nu'\rangle, \qquad \text{(II-4)}$$

where $\nu = \mu + M_\alpha$. The rotation matrices $D^{(J')}_{\nu'\nu}(\hat{k}_\alpha)$ in Eq. (II-4) effect the rotation of the helicity states to align with the direction $\hat{k}_i$ of the incident electron, and is given explicitly as:

$$D^{(J')}_{\nu'\nu}(\hat{k}_\alpha) = e^{-i\nu'\phi}\, d^{J'}_{\nu'\nu}(\theta), \qquad \text{(II-5)}$$

where $d^{J'}_{\nu'\nu}$ are the standard d-functions.[33] The final helicity states must satisfy the incoming-wave boundary condition, and this is denoted symbolically by the superscript "-" on k_α^- in Eq. (II-4).

By substituting Eqs. (II-3) and (II-4) into Eq. (II-1) we can rewrite the scattering amplitude as

$$f(\mu_i J_o M_o;\ \mu J_\alpha M_\alpha) = \frac{\pi}{k_i} \sum_{\kappa_i \kappa_\alpha J} D^{(J)*}_{\lambda\nu}(\hat{k}_\alpha)\, \frac{[\ell_i \ell_\alpha]}{[J]}$$

$$\times \langle j_i \mu_i | \ell_i 0 s \mu_i\rangle \langle J\lambda | J_o M_o j_i \mu_i\rangle$$

$$\times \langle \ell_\alpha o\ s\mu | j_\alpha \mu\rangle \langle J_\alpha M_\alpha j_\alpha \mu | J\nu\rangle\, D_\alpha, \qquad \text{(II-6)}$$

where the quantum number $\kappa \equiv (\ell j)$ specifies both the parity and the total angular momentum of a given relativistic orbital. In arriving at Eq. (II-6), we have used the explicit expressions for the helicity states and applied the Wigner-Eckart theorem:

$$\langle \alpha^- JM | H_I | JM\rangle = \frac{1}{[J]} \langle \alpha^- J \| H_I \| J\rangle, \qquad \text{(II-7)}$$

where the state $|\alpha^- JM\rangle$ is called the open-channel state and has the asymptotic behavior of containing an outgoing Coulomb spherical wave only in channel α. We emphasize here that both the initial state $|JM\rangle$ and the final state $|\alpha^- JM\rangle$ of the combined projectile-target system are antisymmetrized for electron-atom collisions, while only the target is antisymmetrized if the incident particle is not an electron. The reduced matrix element D_α in Eq. (II-6) is defined as:

$$D_\alpha = i^{(\ell_i - \ell_\alpha)} \exp(i\sigma_{\kappa_\alpha}) \langle \alpha^- J \| H_I \| J\rangle, \qquad \text{(II-8)}$$

where the term σ_{κ_α} is the Coulomb phase shift of the continuum state in the particular channel α. For computational purpose, we define a real amplitude d_α such that

$$D_\alpha = e^{i\phi_\alpha} d_\alpha, \tag{II-9}$$

where the phase ϕ_α is:

$$\phi_\alpha = \sigma_\alpha + \ell_i \pi/2 \tag{II-10}$$

with σ_α being the total channel phase shift. Evaluation of d_α in terms of radial integrals is discussed in Appendix A.

By considering the general scattering amplitude (II-6), we can analyze the coincidence measurements of the excited target and the scattered electron, and study the de-excitation processes (fluorescence or Auger transitions). We will report these separately. For the present purpose, we assume that the target is unpolarized and has a well-defined angular momentum J_o, and that the polarization of the excited target is not observed. We therefore define the appropriate interaction matrix as:

$$I(\mu_i' \mu_i; \mu'\mu) = \frac{1}{[J_o]^2} \sum_{M_o M_\alpha} f(\mu_i' J_o M_o; \mu' J_\alpha M_\alpha) \; f^*(\mu_i J_o M_o; \mu J_\alpha M_\alpha). \tag{II-11}$$

If the incident electron beam is, in general, polarized and specified by the density matrix $\rho_{\mu_i'\mu_i}$, the outgoing electrons can be specified through the relation:

$$\rho_{\mu'\mu} = \sum_{\mu_i'\mu_i} \rho_{\mu_i'\mu_i} I(\mu_i'\mu_i; \mu'\mu). \tag{II-12}$$

III. ANGULAR DISTRIBUTION AND SPIN POLARIZATION OF SCATTERED ELECTRONS

It is more convenient to define the spin polarization of the scattered electron in the coordinate system of the detector as follows. We define a fixed (at the target) coordinate system XYZ such that the Z axis is in the direction $\vec{k}_i$

of the incident electron. The X axis can be chosen in any convenient direction because the spin polarization P_X, P_Y, and P_Z of the incident electron are determined accordingly. We may, of course, choose the X axis such that $P_Y = 0$; however, we will consider the more general case. We also define a coordinate system xyz associated with the detector, where the z axis, making an angle θ with the Z axis, is in the direction $\vec{k}_\alpha$ of the scattered electron, and the y axis is perpendicular to the scattering plane, i.e., $\hat{y} = \hat{Z} \times \hat{z}/|\hat{Z} \times \hat{z}|$. The spin polarization of the scattered electron is defined in the xyz coordinate system as $P_x(\theta,\phi)$, $P_y(\theta,\phi)$, and $P_z(\theta,\phi)$, where (θ,ϕ) defines the orientation of $\vec{k}_\alpha$ with respect to the fixed XYZ coordinate system. The relative orientation of these two coordinate systems is shown in Figure 2.

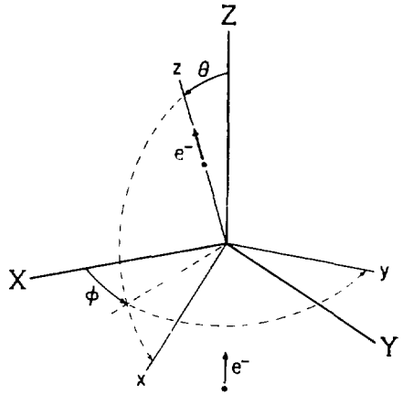

Fig. 2. Geometrical relationships used in angular distribution and spin-polarization formulas. The incident electron is along the Z-axis and is scattered along the z-axis.

The angular distribution and spin polarization of the scattered electron can be expressed in terms of the spin density matrix $\rho = (\rho_{\mu',\mu})$ as:

$$\frac{d\sigma(\theta,\phi)}{d\Omega} = \mathrm{Tr}\{\rho\}, \qquad \text{(III-1)}$$

$$\vec{P}(\theta,\phi) \equiv \langle\vec{\Sigma}\rangle = \mathrm{Tr}\{\vec{\sigma}\rho\}/\mathrm{Tr}\{\rho\}. \qquad \text{(III-2)}$$

Here $\mathrm{Tr}\{\}$ denotes the trace of a matrix, and the electron spin operator $\vec{\Sigma}$ is:

$$\vec{\Sigma} = \begin{pmatrix} \vec{\sigma} & 0 \\ 0 & \vec{\sigma} \end{pmatrix}. \qquad \text{(III-3)}$$

Evaluation of Eqs. (III-1) and (III-2) gives the explicit expressions:

$$\frac{d\sigma(\theta,\phi)}{d\Omega} = \rho_{1/2\,1/2} + \rho_{-1/2\,-1/2}, \qquad \text{(III-4)}$$

$$P_x(\theta,\phi) = (\rho_{1/2,-1/2} + \rho_{-1/2,1/2})/\frac{d\sigma}{d\Omega}, \quad \text{(III-5)}$$

$$P_y(\theta,\phi) = i(\rho_{1/2,-1/2} - \rho_{-1/2,1/2})/\frac{d\sigma}{d\Omega}, \quad \text{(III-6)}$$

$$P_z(\theta,\phi) = (\rho_{1/2,1/2} - \rho_{-1/2,-1/2})/\frac{d\sigma}{d\Omega}. \quad \text{(III-7)}$$

The spin polarization of the incident electron is similarly related to its density matrix $\rho = (\rho_{\mu_i',\mu_i})$ as:

$$P_X = \rho_{1/2,-1/2} + \rho_{-1/2,1/2}, \quad \text{(III-8)}$$

$$P_Y = i(\rho_{1/2,-1/2} - \rho_{-1/2,1/2}), \quad \text{(III-9)}$$

$$P_Z = \rho_{1/2,1/2} - \rho_{-1/2,-1/2}, \quad \text{(III-10)}$$

with

$$\rho_{1/2,1/2} + \rho_{-1/2,-1/2} = 1. \quad \text{(III-11)}$$

After some reduction, the angular distribution of the scattered electron is given as:

$$\frac{d\sigma(\theta,\phi)}{d\Omega} = \frac{\sigma}{4\pi} F(\theta,\phi), \quad \text{(III-12)}$$

where the angular distribution function is:

$$F(\theta,\phi) = 1 + a + b(p_Y\cos\phi - p_X\sin\phi), \quad \text{(III-13)}$$

and the spin polarization is:

$$P_x(\theta,\phi)F(\theta,\phi) = c\,p_Z + d(p_X\cos\phi + p_Y\sin\phi), \quad \text{(III-14)}$$

$$P_y(\theta,\phi)F(\theta,\phi) = e + f(p_Y\cos\phi - p_X\sin\phi), \quad \text{(III-15)}$$

$$P_z(\theta,\phi)F(\theta,\phi) = g\,p_Z + h(p_X\cos\phi + p_Y\sin\phi). \quad \text{(III-16)}$$

In Eqs. (III-13) through (III-16), the symbols a, b, c, d, e, f, g, and h are angular functions defined as:

$$a = \sum_{\ell \geq 1} \beta_{0\ell} \, d^{\ell}_{00}, \tag{III-17}$$

$$b = \sum_{\ell \geq 1} \beta_{1\ell} \, d^{\ell}_{10}, \tag{III-18}$$

$$c = \sum_{\ell \geq 1} \xi_{3\ell} \, d^{\ell}_{10}, \tag{III-19}$$

$$d = \sum_{\ell \geq 1} (\xi_{2\ell} d^{\ell}_{11} + \eta_{2\ell} d^{\ell}_{1-1}), \tag{III-20}$$

$$e = \sum_{\ell \geq 1} \eta_{0\ell} d^{\ell}_{10}, \tag{III-21}$$

$$f = \sum_{\ell \geq 1} (\xi_{2\ell} d^{\ell}_{11} - \eta_{2\ell} d^{\ell}_{1-1}), \tag{III-22}$$

$$g = \sum_{\ell = 0} \zeta_{3\ell} d^{\ell}_{00}, \tag{III-23}$$

$$h = \sum_{\ell \geq 1} \zeta_{2\ell} d^{\ell}_{10}, \tag{III-24}$$

where d^{ℓ}_{mn} are the standard d-functions of the polar angle θ in Eq. (II-5). The total cross section σ in Eq. (III-12) has the explicit expression:

$$\sigma = \frac{2\pi^3}{k_i^2 \, [J_o]^2} \, \bar{\sigma}, \tag{III-25}$$

where

$$\bar{\sigma} = \sum_{\alpha} |D_{\alpha}|^2 = \sum_{\alpha} d_{\alpha\alpha}. \tag{III-26}$$

Here for brevity, we have defined

$$\sum_{\alpha} \equiv \sum_{\kappa_i \kappa_{\alpha} J}, \tag{III-27}$$

$$d_{\alpha'\alpha} \equiv d_{\alpha'} d_{\alpha}, \tag{III-28}$$

where d_{α} was defined in Eq. (II-9). The dynamical parameters in Eqs. (III-17) through (III-24) are given as:

$$\beta_{0\ell} = \sum_{\alpha'\alpha}^{(+)} K_\ell(00)\cos\phi_{\alpha'\alpha} , \tag{III-29}$$

$$\beta_{1\ell} = \sum_{\alpha'\alpha}^{(+)} K_\ell(10)\sin\phi_{\alpha'\alpha} , \tag{III-30}$$

$$\xi_{2\ell} = \frac{1}{2} \sum_{\alpha'\alpha} K_\ell(11)\cos\phi_{\alpha'\alpha} , \tag{III-31}$$

$$\xi_{3\ell} = \sum_{\alpha'\alpha}^{(-)} K_\ell(01)\cos\phi_{\alpha'\alpha} , \tag{III-32}$$

$$\eta_{0\ell} = \sum_{\alpha'\alpha}^{(+)} K_\ell(01)\sin\phi_{\alpha'\alpha} , \tag{III-33}$$

$$\eta_{2\ell} = \frac{1}{2} \sum_{\alpha'\alpha} (-)^{\ell_{\alpha'}+\ell_\alpha+\ell} K_\ell(11)\cos\phi_{\alpha'\alpha} , \tag{III-34}$$

$$\zeta_{2\ell} = -\sum_{\alpha'\alpha}^{(-)} K_\ell(10)\cos\phi_{\alpha'\alpha} , \tag{III-35}$$

$$\zeta_{3\ell} = \sum_{\alpha'\alpha}^{(-)} K_\ell(00)\cos\phi_{\alpha'\alpha} , \tag{III-36}$$

where the superscripts (±) denote the parity selection rule:

$$(\pm) \equiv \begin{cases} (\ell_i' + \ell_i), \text{ even}, \\ (\ell_i' + \ell_i), \text{ odd}. \end{cases} \tag{III-37}$$

Here we have used the notation $\phi_{\alpha'\alpha} = \phi_{\alpha'} - \phi_\alpha$ with ϕ_α defined in Eq. (II-9), and the coupling coefficients are:

$$K_\ell(00) = C_\ell \begin{pmatrix} j_i' & j_i & \ell \\ \frac{1}{2} & -\frac{1}{2} & 0 \end{pmatrix} \begin{pmatrix} j_\alpha' & j_\alpha & \ell \\ \frac{1}{2} & -\frac{1}{2} & 0 \end{pmatrix} , \tag{III-38}$$

$$K_\ell(10) = C_\ell(-)^{j_i'+\ell_i'+1/2} \begin{pmatrix} j_i' & j_i & \ell \\ -\frac{1}{2} & -\frac{1}{2} & 1 \end{pmatrix} \begin{pmatrix} j_\alpha' & j_\alpha & \ell \\ \frac{1}{2} & -\frac{1}{2} & 0 \end{pmatrix}, \tag{III-39}$$

$$K_\ell(01) = C_\ell(-)^{j_\alpha'+\ell_\alpha'+1/2} \begin{pmatrix} j_i' & j_i & \ell \\ \frac{1}{2} & -\frac{1}{2} & 0 \end{pmatrix} \begin{pmatrix} j_\alpha' & j_\alpha & \ell \\ -\frac{1}{2} & -\frac{1}{2} & 1 \end{pmatrix}, \tag{III-40}$$

$$K_\ell(11) = C_\ell(-)^{j_i'+\ell_i'+j_\alpha'+\ell_\alpha'} \begin{pmatrix} j_i' & j_i & \ell \\ -\frac{1}{2} & -\frac{1}{2} & 1 \end{pmatrix} \begin{pmatrix} j_\alpha' & j_\alpha & \ell \\ -\frac{1}{2} & -\frac{1}{2} & 1 \end{pmatrix}, \quad \text{(III-41)}$$

where

$$C_\ell = \bar{\sigma}^{-1} d_{\alpha'\alpha}(-)^{J_\alpha - J_0}[j_i'j_\alpha'J'][j_ij_\alpha J][\ell]^2 \begin{Bmatrix} J' & J & \ell \\ j_i & j_i' & J_0 \end{Bmatrix} \begin{Bmatrix} J' & J & \ell \\ j_\alpha & j_\alpha' & J_\alpha \end{Bmatrix}. \quad \text{(III-42)}$$

We emphasize that in obtaining Eqs. (III-29) through (III-36) we assumed parity-conserved interaction. Spin polarization in different coordinate systems can be obtained easily. For convenience, the transformation matrix is given in Appendix D.

The angular distribution and spin polarization of the scattered electron in Eqs. (III-13) through (III-16) can also be written in vector forms. We define three orthogonal unit vectors ($\hat{t}$, $\hat{n}$, $\hat{k}_i$) as:

$$\hat{k}_i = \vec{k}_i / |\vec{k}_i|, \quad \text{(III-43)}$$

$$\hat{n} = \vec{k}_i \times \vec{k}_\alpha / |\vec{k}_i \times \vec{k}_\alpha|, \quad \text{(III-44)}$$

$$\hat{t} = \hat{n} \times \vec{k}_i / |\hat{n} \times \vec{k}_i|, \quad \text{(III-45)}$$

where $\hat{k}_i$ is along the direction of the incident electron, $\hat{n}$ is normal to the scattering plane, and $\hat{t}$ is on the scattering plane and perpendicular to $\hat{k}_i$. We can therefore rewrite Eqs. (III-13) through (III-16) as:

$$F(\theta,\phi) = 1 + a + b(\vec{p}\cdot\hat{n}), \quad \text{(III-46)}$$

$$P_x(\theta,\phi)F(\theta,\phi) = c(\vec{p}\cdot\hat{k}_i) + d(\vec{p}\cdot\hat{t}), \quad \text{(III-47)}$$

$$P_y(\theta,\phi)F(\theta,\phi) = e + f(\vec{p}\cdot\hat{n}), \quad \text{(III-48)}$$

$$P_z(\theta,\phi)F(\theta,\phi) = g(\vec{p}\cdot\hat{k}_i) + h(\vec{p}\cdot\hat{t}). \quad \text{(III-49)}$$

Or we can combine Eqs. (III-47) through (III-49) as:

$$\vec{P}(\theta,\phi)F(\theta,\phi) = [c(\vec{p}\cdot\hat{k}_i) + d(\vec{p}\cdot\hat{t})](\hat{t}\cos\theta - \hat{k}_i \sin\theta)$$

$$+ [e + f(\vec{p}\cdot\hat{n})]\ \hat{n}$$

$$+ [g(\vec{p}\cdot\hat{k}_i) + h(\vec{p}\cdot\hat{t})](\hat{t}\sin\theta + \hat{k}_i \cos\theta). \qquad \text{(III-50)}$$

We can see from Eqs. (III-12) through (III-16) or (III-46) through (III-49) that there are in general eight independent functions of the polar angle θ, that characterize the scattering of a spin-1/2 particle on an unpolarized target. These eight functions can, in turn, be expressed in terms of d-functions of the rotation matrices with certain dynamical parameters as the expansion coefficients. These dynamical parameters, $\beta_{0\ell}$, $\beta_{1\ell}$, $\xi_{2\ell}$, $\xi_{3\ell}$, $\eta_{0\ell}$, $\eta_{2\ell}$, $\zeta_{2\ell}$, and $\zeta_{3\ell}$, are characteristics of the projectile and the target and the interaction involved. In the case of potential scattering or scatterings which can be approximated by it, there are only four independent functions of the polar angle θ, and we can prove, for potential scatterings,

$$a = f - 1, \qquad \text{(III-51)}$$

$$b = e, \qquad \text{(III-52)}$$

$$c = -h, \qquad \text{(III-53)}$$

$$d = g. \qquad \text{(III-54)}$$

Consequently, we can write the angular distribution and spin polarization of the scattered electron for potential scatterings as:

$$F(\theta,\phi) = 1 + a + b(\vec{p}\cdot\hat{n}), \qquad \text{(III-55)}$$

$$\vec{P}(\theta,\phi)F(\theta,\phi) = b\,\hat{n} + (1 + a)\vec{p}$$

$$+(c\cos\theta - d\sin\theta)\vec{p} \times \hat{n}$$

$$+ (1 + a - c\sin\theta - d\cos\theta)(\vec{p} \times \hat{n}) \times \hat{n}. \qquad \text{(III-56)}$$

We can easily prove that this agrees formally with the well-known result.[21,28,29]

IV. ANALYZING POWER AND POLARIZING POWER OF THE TARGET

The analyzing power $\vec{A}(\theta,\phi)$ of the target can be obtained from Eqs. (III-13) or (III-46) as:

$$\vec{A}(\theta,\phi) = \left(\frac{b}{1+a}\right) \hat{n}. \tag{IV-1}$$

The polarizing power $\vec{P}(\theta,\phi)$ of the target is defined as the polarization of the scattered electron when the incident electron is unpolarized. By setting $\vec{p}=0$ in Eq. (III-50), we get:

$$\vec{P}(\theta,\phi) = \left(\frac{e}{1+a}\right) \hat{n}. \tag{IV-2}$$

It is clear from Eqs. (IV-1) and (IV-2) that the analyzing power does not, in general, equals the polarizing power even when the interaction involved in the scattering conserves parity. Only when the scattering can be approximated by a potential scattering can we equate the analyzing power to the polarizing power, as indicated by Eq. (III-52).

V. POLARIZATION OF TOTAL SCATTERED ELECTRONS WITH A DEFINITE ENERGY

The polarization (P_X, P_Y, P_Z) of total scattered electron flux with a definite energy can be obtained by integrating Eq. (III-50) over all angles. the result is given as:

$$P_X = p_X \delta_\perp, \tag{V-1}$$

$$P_Y = p_Y \delta_\perp, \tag{V-2}$$

$$P_Z = p_Z \delta_\parallel, \tag{V-3}$$

or simply as:

$$\vec{P} = \vec{p}_\perp \delta_\perp + \vec{p}_\parallel \delta_\parallel, \tag{V-4}$$

where the dynamical parameter $\delta_\perp$ is for the polarization components perpen-

dicular to the incident direction $\hat{k}_i$, and $\delta_\parallel$ is for the polarization component parallel to the incident direction. They have the explicit forms:

$$\delta_\perp = \frac{1}{3}\left(\xi_{21} - \eta_{21} - \frac{1}{\sqrt{2}}\,\zeta_{21}\right), \tag{V-5}$$

$$\delta_\parallel = \frac{1}{3}\left(-\sqrt{2}\,\xi_{31} + \zeta_{31}\right), \tag{V-6}$$

where ξ_{21}, ξ_{31}, η_{21}, ζ_{21}, and ζ_{31} are given in Eqs. (III-31), (III-31), and (III-34) through (III-36), respectively. It is of interest to note that $\delta_\perp$ and $\delta_\parallel$ depend only on dynamical parameters with $\ell=1$, i.e., interferences between partial waves with $j' - j \geq 2$ do not contribute.

APPENDIX A: POTENTIAL FUNCTIONS AND THEIR MATRIX ELEMENTS

Various forms of the lowest-order interaction between electrons in quantum field theory have been reviewed.[34] A step-by-step graphical procedure has been given for evaluating matrix elements of these interactions between many-electron configurations.[35] The essential results are summarized in this appendix.

Matrix elements of an arbitrary two-particle operator v(ij) between many-electron configurations can always be expressed as linear combinations of jm-scheme matrix elements in corresponding two-electron configurations. This can be accomplished, for example, by a graphical procedure.[35] The jm-scheme matrix element of the two-particle operator v(ij) is defined as:

$$\langle ab|v(12)|cd\rangle = \int d^3r_1 \int d^3r_2 \; U_a^\dagger(1) U_b^\dagger(2) v(12) U_c(1) U_d(2) \;, \qquad \text{(A-1)}$$

where a, b, c, and d denote generally different Dirac orbitals. The definition and phase convention of the Dirac orbital used here is given in Appendix B. The matrix element (A-1) can always be written in the form:

$$\langle ab|v(12)|cd\rangle = \sum_j G_j(ab;cd) X_j(ab;cd). \qquad \text{(A-2)}$$

Here G_j is called the interaction diagram,

$$G_j(ab;cd) = \begin{pmatrix} j_a & j & m_c \\ m_a & m_c - m_a & j_c \end{pmatrix} \begin{pmatrix} j_b & m_d & m_c - m_a \\ m_b & j_d & j \end{pmatrix}$$

$$= \qquad , \qquad \text{(A-3)}$$

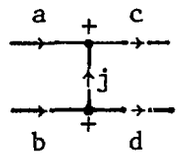

where we have used the covariant Wigner 3-j symbols and their graphical representations.[35,36] The interaction strength X_j is defined as:

$$X_j(ab;cd) = C_j(ab;cd) I_j(ab;cd) \;, \qquad \text{(A-4)}$$

where

$$C_j(ab;cd) = (-)^{j_a + j_d}[j_a j_b j_c j_d] \begin{pmatrix} j_a & j & j_c \\ 1/2 & 0 & -1/2 \end{pmatrix} \begin{pmatrix} j_b & j & j_d \\ 1/2 & 0 & -1/2 \end{pmatrix} \quad \text{(A-5)}$$

and $I_j(ab;cd)$ is given in terms of radial integrals, depending on the specific form of $v(12)$.

Expressions of $I_j(ab;cd)$ for commonly used potential functions are summarized as follows:

(i) Coulomb potential: $1/r_{12}$.

$$I_j(ab;cd) = \langle W_{ac} R_j W_{bd} \rangle^{\text{even}},$$

which has the explicit form:

$$\langle W_{ac} R_j W_{bd} \rangle^{\text{even}} = \int_0^\infty dr_1 \int_0^\infty dr_2 \; W_{ac}(r_1) \; R_j(r_1 r_2) W_{bd}(r_2) \; , \quad \text{(A-6)}$$

with

$$W_{ac}(r) = G_a(r)G_c(r) + F_a(r)F_c(r), \quad \text{(A-7)}$$

$$R_j(r_1 r_2) = r_<^j / r_>^{j+1}, \quad \text{(A-8)}$$

where the radial functions G_a and F_a are the large and small components, respectively, of orbital a, defined in Appendix B. The notation $\langle\rangle^{\text{even(odd)}}$ in Eq. (A-6) denotes that the integral is to be replaced by zero unless both $(\ell_a+j+\ell_c)$ and $(\ell_b+j+\ell_d)$ are even (odd).

(ii) Covariant photon interaction: $(1-\vec{\alpha}_1 \cdot \vec{\alpha}_2)(e^{i\omega r_{12}}/r_{12})$.

$$I_j(ab;cd) = (2j+1)\langle W_{ac} g_j W_{bd} \rangle^{\text{even}}$$

$$- (1-\delta_{jo})(\kappa_a + \kappa_c)(\kappa_b + \kappa_d) \frac{2j+1}{j(j+1)} \langle V_{ac} g_j V_{bd} \rangle^{\text{odd}}$$

$$+ j\langle P_{ac} g_{j-1} P_{bd} \rangle^{\text{even}} + (j+1)\langle Q_{ac} g_{j+1} Q_{bd} \rangle^{\text{even}}, \quad \text{(A-9)}$$

where

$$g_j(r_1r_2) = i\omega j_j(\omega r_<)h_j(\omega r_>) \ , \qquad \text{(A-10)}$$

with j_j and h_j being the spherical Bessel and Hankel functions, respectively. In Eq. (A-9) the different combinations of radial functions are defined as:

$$V_{ac}(r) = -G_aF_c - F_aG_c,$$

$$P_{ac}(r) = -G_aF_c + F_aG_c + V_{ac}(\kappa_c - \kappa_a)/j,$$

$$Q_{ac}(r) = G_aF_c - F_aG_c + V_{ac}(\kappa_c - \kappa_a)/(j + 1). \qquad \text{(A-11)}$$

(iii) Transverse photon interaction:

$$-(\alpha_1\cdot\alpha_2)\frac{e^{i\omega r_{12}}}{r_{12}} + (\vec{\alpha}_1\cdot\vec{\nabla}_1)(\vec{\alpha}_2\cdot\vec{\nabla}_2)\ [\frac{e^{i\omega r_{12}-1}}{\omega^2 r_{12}}].$$

$$I_j(ab;cd) = -(1-\delta_{jo})(\kappa_a + \kappa_c)(\kappa_b + \kappa_d)$$

$$\times\ [(2j + 1)/j(j + 1)]\langle V_{ac}g_jV_{bd}\rangle^{odd}$$

$$+ (\kappa_c - \kappa_a)[\langle V_{ac}g_{j-1}P_{bd}\rangle^{even} + \langle V_{ac}g_{j+1}Q_{bd}\rangle^{even}]$$

$$+ j(j + 1)[\langle P_{ac}s_jQ_{bd}\rangle^{even} + \langle Q_{ac}t_jP_{bd}\rangle^{even}], \qquad \text{(A-12)}$$

where

$$s_j = \begin{cases} -(i/r_1)j_{j+1}(\omega r_2)h_j(\omega r_1), & r_1>r_2 \\ r_1^{j-1}/\omega^2 r_2^{j+2} - (i/r_1)j_j(\omega r_1)h_{j+1}(\omega r_2), & r_1<r_2 \end{cases} , \qquad \text{(A-13)}$$

$$t_j = \begin{cases} r_2^{j-1}/\omega^2 r_1^{j+2} - (i/r_1)j_{j-1}(\omega r_2)h_j(\omega r_1), & r_1>r_2 \\ -(i/r_1)j_j(\omega r_1)h_{j-1}(\omega r_2), & r_1<r_2 \end{cases} . \qquad \text{(A-14)}$$

(iv) Breit interaction:

$$-\frac{1}{2r_{12}}\ [(\vec{\alpha}_1\cdot\vec{\alpha}_2) + \frac{(\vec{\alpha}_1\cdot\vec{r}_{12})(\vec{\alpha}_2\cdot\vec{r}_{12})}{r_{12}^2}],$$

which represents the transverse photon interaction in the limit $\omega \to 0$.

$$I_j(ab;cd) = -(1-\delta_{jo})(\kappa_a+\kappa_c)(\kappa_b+\kappa_d)\frac{1}{j(j+1)}\langle V_{ac}R_jV_{bd}\rangle^{odd}$$

$$+\frac{j(j+1)}{2j+1}\left[\frac{1}{2j-1}\langle P_{ac}R_{j-1}P_{bd}\rangle^{even}\right.$$

$$+\frac{1}{2j+3}\langle Q_{ac}R_{j+1}Q_{bd}\rangle^{even}$$

$$\left.+\frac{1}{2}\langle Q_{ac}v_j(12)P_{bd}\rangle^{even}+\frac{1}{2}\langle P_{ac}v_j(21)Q_{bd}\rangle^{even}\right], \qquad \text{(A-15)}$$

where

$$v_j(12) = \varepsilon(r_1-r_2)(R_{j+1}-R_{j-1}), \qquad \text{(A-16)}$$

with $\varepsilon(r_1-r_2)$ being the step function

$$\varepsilon(x) = \begin{cases}1, & x>0,\\ 0, & x<0.\end{cases}$$

APPENDIX B: DIRAC ORBITALS

We review briefly the Dirac orbital and its phase convention used here. Dirac orbitals in central field can be completely specified by the quantum numbers n, κ, and m. For a definite κ, the total-angular-momentum quantum number j and the orbital-angular-momentum quantum number ℓ of the large component, which determines the parity of the Dirac orbital, are given as:

$$j = |\kappa| - \frac{1}{2}, \quad \ell = \begin{cases} \kappa, & \kappa>0 \\ -\kappa-1, & \kappa<0. \end{cases} \tag{B-1}$$

For example, the values κ = -1, 1, -2, and 2 correspond to $s_{1/2}$, $p_{1/2}$, $p_{3/2}$, and $d_{3/2}$ orbitals, respectively. The magnetic quantum number m is associted with the z component J_z of the total angular momentum. Dirac orbitals with definite nκm have the explicit form:

$$U_{n\kappa m} = \frac{1}{r}\begin{pmatrix} G_{n\kappa}\,\Omega_{\kappa m} \\ iF_{n\kappa}\,\Omega_{-\kappa m} \end{pmatrix}. \tag{B-2}$$

Here the radial functions $G_{n\kappa}$ and $F_{n\kappa}$ are the large and small components, respectively, and satisfy the orthonormality condition:

$$\int_0^\infty dr(G_{n\kappa}G_{n'\kappa} + F_{n\kappa}F_{n'\kappa}) = \delta_{nn'}. \tag{B-3}$$

The angular functions $\Omega_{\kappa m}$ in Eq. (B-2) are normalized spherical spinors defined as:

$$\Omega_{\kappa m} \equiv \Omega_{j\ell m} = \sum_{M\mu} \langle \ell M \tfrac{1}{2}\mu | jm\rangle Y_{\ell M}(\hat{r})\,\chi_\mu \tag{B-4}$$

where $Y_{\ell M}$ is the spherical harmonics, and χ_μ is the spin eigenfunction with $s = \frac{1}{2}$ and $s_z = \mu$, given, for example, by the two-component Pauli spinor.

Note that the phase convention (B-2) used here is different from that of Reference 35, namely,

$$U_{n\kappa m} = \frac{1}{r}\begin{pmatrix} iG_{n\kappa}\,\Omega_{\kappa m} \\ F_{n\kappa}\,\Omega_{-\kappa m} \end{pmatrix}. \tag{B-5}$$

Therefore to use formulas presented in Reference 35, where the convention (B-5) is used, we have to make the following substitution:

$$G_{n\kappa} \to -G_{n\kappa}, \text{ or } F_{n\kappa} \to -F_{n\kappa}. \tag{B-6}$$

APPENDIX C: HELICITY STATES

Angular-momentum helicity states (or spherical helicity states) $|k\lambda;jm\rangle$ with helicity λ can be constructed from linear-momentum helicity states (or linear helicity state) $|\vec{k}\lambda\rangle$, and vice versa. They are related by the following:

$$|k\lambda;jm\rangle = (\frac{2j+1}{4\pi})^{1/2} \int d\hat{k}\ D^{(j)}_{m\lambda}(\hat{k})^*\ |\vec{k}\lambda\rangle \tag{C-1}$$

and

$$|\vec{k}\lambda\rangle = \sum_{jm} (\frac{2j+1}{4\pi})^{1/2}\ D^{(j)}_{m\lambda}\ (\hat{k})\ |k\lambda;jm\rangle, \tag{C-2}$$

where $D^{(j)}_{m\lambda}(k)$ are rotation matrices. Here the helicity states are normalized such that:

$$\langle\vec{k}\lambda|\vec{k}'\lambda'\rangle = \delta^3(\vec{k} - \vec{k}')\delta_{\lambda\lambda'}, \tag{C-3}$$

$$\langle k\lambda;jm|k'\lambda';j'm'\rangle = \frac{1}{k^2}\ \delta(k-k')\ \delta_{\lambda\lambda'}\delta_{jj'}\delta_{mm'}. \tag{C-4}$$

The linear-momentum helicity state is given by:

$$\langle\vec{r}|\vec{k}\mu\rangle = (2\pi)^{-3/2}[(E + c^2)/2E]^{1/2} \begin{pmatrix} 1 \\ \frac{c\vec{\sigma}\cdot\vec{k}}{E+c^2} \end{pmatrix} \chi_\mu e^{i\vec{k}\cdot\vec{r}}, \tag{C-9}$$

where χ_μ is the spin eigenfunction, with the quantization axis chosen in the $\vec{k}$ direction, $s_{\hat{k}} = \mu$. The angular-momentum helicity state can be obtained by:

$$\begin{aligned}\langle\vec{r}|k\mu;jm\rangle &= (\frac{2j+1}{4\pi})^{1/2}\ \int d\hat{k}\ D^{(j)}_{m\mu}(\hat{k})^*\langle\vec{r}|\vec{k}\mu\rangle \\ &= \sum_{\ell}\ i^{\ell}[\frac{(2\ell+1)c^2}{kE(2j+1)}]^{1/2}\langle\ell 0 s\mu|j\mu\rangle\langle\vec{r}|\kappa m\rangle,\end{aligned} \tag{C-10}$$

where $\langle\vec{r}|\kappa m\rangle$ is the usual angular-momentum eigenstate and is normalized on the energy scale:

$$\langle\vec{r}|\kappa m\rangle \equiv \psi_{\kappa m}(\vec{r}) \equiv \frac{1}{r} \begin{pmatrix} G_{\kappa m}\ \Omega_{\kappa m} \\ iF_{\kappa m}\ \Omega_{-\kappa m} \end{pmatrix}. \tag{C-11}$$

In the Pauli approximation, we have:

$$\langle \vec{r} | \kappa m \rangle \equiv \langle r | (\ell s) j m \rangle$$

$$= \sum_{m\nu} \langle \ell m s \nu | j m \rangle \langle \vec{r} | \ell m \rangle \chi_\nu, \qquad \text{(C-12)}$$

where χ_ν is the spin eigenfunction with $s_z = \nu$.

APPENDIX D: TRANSFORMATION OF THE POLARIZATION VECTOR $\vec{P}$

The polarization vector $\vec{P} = (P_X\ P_Y\ P_Z)$ in a coordinate system XYZ can be expressed in terms of components $(P_x\ P_y\ P_z)$ along axes of a rotated coordinate system xyz. Assume that the coordinate system xyz is obtained from the coordinate system XYZ by a rotation with Euler angles $(\phi,\theta,0)$ as illus-trated in Figure 2. The components of the same polarization vector $\vec{P}$ in these two coordinate systems are related by:

$$\begin{pmatrix} P_X \\ P_Y \\ P_Z \end{pmatrix} = \begin{pmatrix} \cos\phi\cos\theta & -\sin\phi & \cos\phi\sin\theta \\ \sin\phi\cos\theta & \cos\phi & \sin\phi\sin\theta \\ \sin\theta & 0 & \cos\theta \end{pmatrix} \begin{pmatrix} P_x \\ P_y \\ P_z \end{pmatrix} . \qquad \text{(D-4)}$$

References

1. B. L. Moiseiwitsch and S. J. Smith, Rev. Mod. Phys. 40, 238 (1968).
2. M. Inokuti, Rev. Mod. Phys. 43, 297 (1971).
3. M. Inokuti, Y. Itikawa, and J. E. Turner, Rev. Mod. Phys. 50, 23 (1978).
4. B. Bederson and L. J. Kieffer, Rev. Mod. Phys. 43, 601 (1971).
5. D. Andrick, Adv. At. Mol. Phys. 9, 207 (1973).
6. F. J. de Heer, in The Physics of Electronic and Atomic Collisions, edited by J. S. Risley and R. Geballe (Univ. of Washington, Seattle, 1976), p. 79.
7. H. S. Taylor, Adv. Chem. Phys. 18, 91 (1970).
8. G. J. Schulz, Rev. Mod. Phys. 45, 378 (1973).
9. D. E. Golden, Adv. At. Mol. Phys. 14, 1 (1978).
10. P. G Burke and W. D. Robb, Adv. At. Mol. Phys. 11, 143 (1975).
11. J. Callaway, Comp. Phys. Commun. 6, 265 (1973).
12. R. J. Drachman and A. Temkin, in Case Studies in Atomic collision Physics, edited by E. W. McDaniel and M. R. C. McDowell (North-Holland, Amsterdam, 1972), Vol. 2, p. 399.
13. M. J. Seaton, Adv. At. Mol. Phys. 11, 83 (1975).
14. R. K. Nesbet, Adv. At. Mol. Phys. 13, 315 (1978).
15. N. F. Lane, Rev. Mod. Phys. 52, 29 (1980).
16. A. L. Merts, J. B. Mann, W. D. Robb, and N. H. Magee, Jr., Los Alamos Scientific Laboratory Report LA-8267-MS (1980).
17. B. Bederson, Comments At. Mol. Phys. 1, 41; 65 (1969).
18. H. Kleinpoppen, Phys. Rev. A 3, 2015 (1971).
19. W. B. Atwood et al., Phys. Rev. D 18, 2223 (1978).
20. C. Y. Prescott et al., Phys. Lett. 77 B, 347 (1978).
21. J. Kessler, Polarized Electrons (Springer, Berlin, 1976).
22. M. S. Lubell, in Coherence and Correlation in Atomic Collisions, edited by H. Kleinpoppen and J. F. Williams (Plenum, New York, 1980), p. 663.
23. K. Schackert, Z. Phys. 213, 316 (1968).
24. J. Kessler, C. B. Lucas, and L. Vušković, J. Phys. B10, 847 (1979).
25. M. Klewer, M. J. M. Beerlage, and M. J. van der Wiel, J. Phys. B12, 3935; L525 (1979).
26. M. A. Coulthard, as cited in Ref. 22.
27. M. Fink and A. C. Yates, Electronic Research Center, University of Texas, Austin, Technical Report No. 88 (1970).
28. D. W. Walker, Adv. Phys. 20, 257 (1971).
29. D. W. Walker, J. Phys. B7, L489 (1974).
30. I. E. McCarthy, C. J. Noble, B. A. Phillips, and A. D. Turnbull, Phys. Rev. A15, 2173 (1977).
31. N. F. Mott, Proc. Roy. Soc. A124, 425 (1929).
32. K.-N. Huang, Phys. Rev. A22, 223 (1980).
33. M. E. Rose, Elementary Theory of Angular Momentum (Wiley, New York, 1957).
34. K.-N. Huang, Phys. Rev. A18, 1119 (1978).
35. K.-N. Huang, Rev. Mod. Phys. 51, 215 (1979).
36. E. P. Wigner, Group Theory (Academic, New York, 1959), p. 295.

31. SUMMARY OF THE WORKSHOP ON THE INTERFACE BETWEEN RADIATION CHEMISTRY AND RADIATION PHYSICS HELD AT ARGONNE NATIONAL LABORATORY, 9-10 SEPTEMBER 1982*

M. A. Dillon, R. J. Hanrahan,† R. Holroyd,‡ Y.-K. Kim, M. C. Sauer, Jr.,¶ and L. H. Toburen§

At many conferences, including a succession of the U.S. Department of Energy contractors' meetings, numerous papers have been presented by radiation chemists and also by physicists who model systems closely related to those treated by chemists. An observer unfamiliar with the topic might have believed that physicists and chemists were talking about two entirely different branches of radiation research.

At a recent DOE contractors' meeting in Gettysburg,[1] there evolved the idea of holding a conference devoted to areas of interest common to both radiation chemistry and radiation physics. The proposed conference became the Workshop on the Interface Between Radiation Chemistry and Radiation Physics, held at Argonne National Laboratory on 9-10 September 1982. We are grateful to Dr. Robert W. Wood and Dr. Frank P. Hudson of the Office of Health and Environmental Research of DOE for providing us with funds on short notice.

The workshop proved to be both timely and enlightening. It demonstrated that except for a difference in emphasis, physicists and chemists share a fairly common view of gas- and liquid-phase radiolysis. Chemists tend to operate in a time domain where chemical reactions can be observed and to deduce therefrom initial G values. Meanwhile, physicists naturally focus considerable attention on initial energy deposition events and perform calculations that should predict the same initial yields.

Formal presentations at the workshop were kept to a minimum so as to allow sufficient time for short, informal presentations and subsequent discussions. All participants were encouraged to submit written contributions, comments, and even afterthoughts. The topics of interest to the workshop

---

*From Argonne National Laboratory Report ANL-82-88, (March, 1983).
†Dept. of Chemistry, University of Florida, Gainesville, FL.
‡Dept. of Chemistry, Brookhaven National Laboratory, Upton, NY.
¶Chemistry Division, Argonne National Laboratory.
§Pacific Northwest Laboratory, Richland, WA.

participants are diverse, reflecting the nature of radiation research. Yet, there is a unifying theme; we are all trying to understand the interaction of radiation with matter in terms of basic physical and chemical processes.

The workshop answered some questions, raised more, and pointed to future possibilities. We will attempt to enumerate some of these here.

I. Main Issues and Accomplishments of Workshop

a. Theorists and experimentalists became more aware of each other's accomplishments. The instances available for comparison of theory with experiment in aqueous systems became clear. The need to identify adjustable parameters in the theory and test the effects of variations in such was also suggested. Also, the ability to simulate energy deposition events brought up the question as to whether the older, more intuitive concepts of spurs are still valuable in guiding our thinking. Discussions at the workshop and some contributions clearly indicate that, in track structure modeling, the quality of input cross-section data is a more crucial problem than the bookkeeping of the energy transport processes. Further effort is needed, however, to develop theory to predict more diverse, experimentally verifiable results.

b. There were presentations to indicate that the gas-liquid difference is becoming better understood, particularly with respect to the initial energy deposition. At present, however, no general theoretical methods exist to correlate gas-phase data with liquid-phase data and vice versa. Although primary events that involve large energy transfers, such as the production (but not the fate) of delta rays, should be independent of target phase, more study is desirable on the utility of gas-phase data in simulating condensed-phase events.

c. Many comments were directed to the lack of knowledge concerning events occurring in the time range 10^{-16} to 10^{-12} sec. The study of physico-chemical events during this time range should get more attention, particularly in the radiation chemistry of condensed media.

II. Suggestions for Future Efforts

Discussions both formal and informal converged to the following suggestions:

a. Choose some molecule (other than water) and measure yields and kinetics over a large pressure range for the gas (including the critical region, if possible) and also for the liquid. Both the validity of various modeling codes and the use of gas-phase data can then be properly assessed.

b. Although the energy deposition events are calculable given the necessary cross sections, the exact nature of the primary chemical species and how they change at early times is still unknown. Workshop participants were undecided as to whether new experimental techniques in the near future (ten years) will allow time resolution in the 10^{-16} - 10^{-12} sec. range to see, for example, how the solvated electron in water forms.

c. Can theory be useful in this time range? For example, in the case of condensed media there is a need to know about the motion and reactivity of collective excitations. Initial yields and spatial distributions of reactants derived from such knowledge can then be used as initial input for calculating time-dependent kinetics.

d. The degradation of slow electrons (< 10 eV) undoubtedly depends on the phase of the target medium as well as the shape of target molecules, because slow electrons have long de Broglie wavelengths extending over many molecules. For instance, the formation of transient negative ion states may substantially alter the diffusion and localization characteristics of these electrons. Most of the modeling codes currently available do not treat the degradation of slow electrons in sufficient detail. More theoretical studies on the fate of slow electrons may lead to a better understanding of the transition from the physical to the chemical stage.

e. More attention should be paid to nonpolar solvents, particularly with respect to the process of geminate ion-recombination and its relationship to the energy-deposition events.

f. Some theoretical and experimental effort should be invested in the radiation chemistry of mixtures. Investigations of this sort provide an opportunity to observe reactions between radiolytically produced transients of mixture components. Also, important questions about the partition of initial energy deposition in liquid mixtures have yet to be answered. For example, how valid is it to assume that energy deposited in a mixture component is proportional to its electron fraction?

g. Complete sets of energy-loss cross sections (for elastic and inelastic scattering of projectiles and secondary electrons generated by them) should be measured and compiled for a few selected substances. These should be used initially to calculate track structure to determine if such detailed knowledge is required in predicting important consequences in radiation chemistry. A secondary objective would be to utilize the systematics of the measurements to interpolate for molecular systems where complete data are not available.

h. In general, cross sections for the interaction of photons with media are better known than those for the interactions of charged particles such as electrons and heavy ions. Under certain conditions, the two types of interactions are related. Yet no systematic method has been developed to correlate cross sections for charged particle interactions with those for photon interactions except for the cases where the first Born approximation is applicable. Further exploration of this possibility is desirable to make use of more abundant, and often more reliable photoionization, and photoexcitation data. Success in this direction, coupled with success in relating gas-phase data to liquid-phase data described earlier, will open new horizons in radiation physics and chemistry.

i. Photoionization of liquids should be further investigated to elucidate the mechanism of ion-pair formation and separation. In this area, development of high-repetition rate picosecond lasers with photon energies of 5 eV and higher should allow substantial progress to be made in the area of photoionization in liquids. The observation of ions and their reactions on shorter time scales than was generally possible previously will be feasible.

Reference

1. The Biological Effects of Ionizing Radiation: 15th Meeting of the Radiological Physics Contractors, Office of Health and Environmental Research, Office of Energy Research, U.S. Department of Energy. 4-6 May 1982, Gettysburg, PA.

32. ELECTRONIC RELAXATION IN RARE-GAS SOLIDS: EJECTION OF ATOMS BY FAST CHARGED PARTICLES*

R. E. Johnson† and Mitio Inokuti

Recent experiments show that the sputtering yields for condensed-gas solids bombarded by fast ions are large, even after allowance for the small surface binding energies. These yields are related to the electronic excitation produced by the incident ions, in contrast to yields for metals and semiconductors. To understand the measured yields for condensed rare-gas solids we examine the conversion of electronic energy to lattice, nuclear motion. Thermal-spike models indicate that about 10-20% of the electronic energy deposited must be converted to nuclear motion in the vicinity of the ion track within 10^{-11} sec to account for the observed yields. In this article we point out that results and data from recent spectroscopic and luminescence studies show that this is indeed the case. On electronic excitation of these closed-shell, van der Waals solids, new covalent bonds form. These bonds cause significant lattice displacements and thus provide a mechanism for the electronic recombination. Relaxation to low-lying electronic states then occurs via repulsive potentials, by which means sufficient electronic energy is converted to nuclear motion to account for the observed ejection (sputtering) from these solids by fast light ions.

---

*Abstract of a paper published in Nucl. Instrum. Methods 206, 289 (1983).
†Faculty Research Participant, Division of Educational Programs, Argonne National Laboratory, April-June 1982. Permanent address: Department of Nuclear Engineering and Engineering Physics, University of Virginia, Charlottesville, VA 22901.

33. THE LOCAL-PLASMA APPROXIMATION TO THE OSCILLATOR-STRENGTH SPECTRUM: HOW GOOD IS IT AND WHY?*

R. E. Johnson† and Mitio Inokuti

A procedure introduced by Lindhard and Scharff three decades ago permits evaluation of the oscillator-strength spectrum solely from the ground-state charge distribution of any atom or molecule. In this procedure, one regards an atom or molecule as consisting of small volumes that independently respond to an external uniform electric field in the same way as a free-electron gas. Some of the results of this procedure, called the local-plasma approximation, are remarkably realistic; an example is the mean excitation energy for stopping power in the Bethe theory. However, other results of the local-plasma approximation, most notably the oscillator-strength spectrum itself, are unrealistic in many respects, as we show. The present article discusses various consequences of the local-plasma approximation and points out its limitations. We also explain how difficult it is to derive the local-plasma approximation from first principles, i.e., starting with the standard definition of the oscillator strength in terms of the dipole matrix element and carrying out systematic mathematical operations.

---

*Abstract of an article publishedr in Comments Atom. Molec. Phys. 14, 19 (1983).

†Faculty Research Participant, Division of Educational Programs, Argonne National Laboratory, April-June 1982. Permanent address: Department of Nuclear Engineering and Engineering Physics, University of Virginia, Charlottesville, VA 22901.

34. CORRELATION AND RELATIVISTIC EFFECTS IN SPIN-ORBIT SPLITTING*

K.-N. Huang, Y.-K. Kim, K. T. Cheng,† and J. P. Desclaux‡

A large discrepancy between Dirac-Fock calculations and experimental data for spin-orbit splitting, $^2P_{1/2} - {}^2P_{3/2}$, in the ground states of boron- and fluorine-like ions is resolved. The discrepancy arises from spurious terms inherent in the relativistic self-consistent field procedure. These terms can be evaluated by setting the speed of light very large in the relativistic wavefunction code. After appropriate corrections for these terms, systematic Z-dependence of the difference between theory and experiment can be determined and hence reliable predictions for the spin-orbit splitting for high-Z ions can be made. The Dirac-Fock results with the above-mentioned correction on boron- and fluorine-like ions are compared with experimental data in Figure 1.

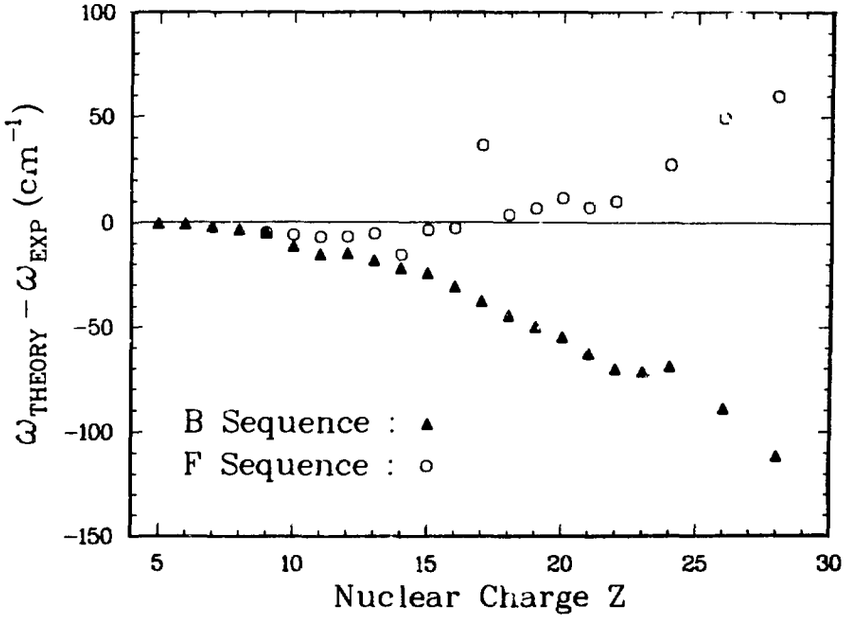

Fig. 1. Comparison between theoretical calculations and experimental data for the spin-orbit splitting, $^2P_{1/2} - {}^2P_{3/2}$, in the ground states of B- and F-like ions. [Reprinted from Phys. Rev. Lett. 48, 1245 (1982)].

---

*Abstract of an article that appeared in Phys. Rev. Lett. 48, 1245 (1982).

†Physics Division, Argonne National Laboratory.
‡Centre d'Études Nucléaires de Grenoble, 38041 Grenoble Cedex, France.

35. SPIN-ORBIT INTERVAL IN THE GROUND STATE OF F-LIKE IONS*

Y.-K. Kim and K.-N. Huang

Using the procedure outlined in the preceding abstract [K.-N. Huang et al.], we have determined suggested spin-orbit interval, $2p^5\ ^2P_{3/2} - {}^2P_{1/2}$, in the ground state of highly-stripped fluorine-like ions. The suggested values are based on Dirac-Fock calculations with corrections deduced from known experimental values in the low-Z side of the isoelectronic sequence. Sample data are presented in Table 1.

Table I. Suggested values of $2p^5\ ^2P_{3/2} - {}^2P_{1/2}$ splitting (cm^{-1}).

Ion	Dirac-Fock Theory	Correction	Suggested Values
Mo^{33+}	887003	-590	886413 ± 150
Cd^{39+}	1603582	-1110	1602472 ± 250
Xe^{45+}	2705507	-1980	2703527 ± 500
Ba^{47+}	3181278	-2350	3178928 ± 600

*Abstract of an article published in the Phys. Rev. A 26, 1984 (1982).

36. ENERGY-LEVEL SCHEME AND TRANSITION PROBABILITIES OF Cl-LIKE IONS*

K.-N. Huang, Y.-K. Kim, and K. T. Cheng†

Theoretical energy levels and transition probabilities are presented for 31 low-lying levels of chlorine-like ions. The multiconfiguration Dirac-Fock technique is used to calculate energy levels and wave functions. The Breit-interaction and Lamb-shift contributions are calculated perturbatively as corrections to the Dirac-Fock energy. The E1 transitions between excited and ground levels and the M1 and E2 transitions between the two levels of the ground-state configuration are presented, In Figure 1 we present the Grotrian diagram for FeX to demonstrate the general feature of the low-lying levels of chlorine-like ions.

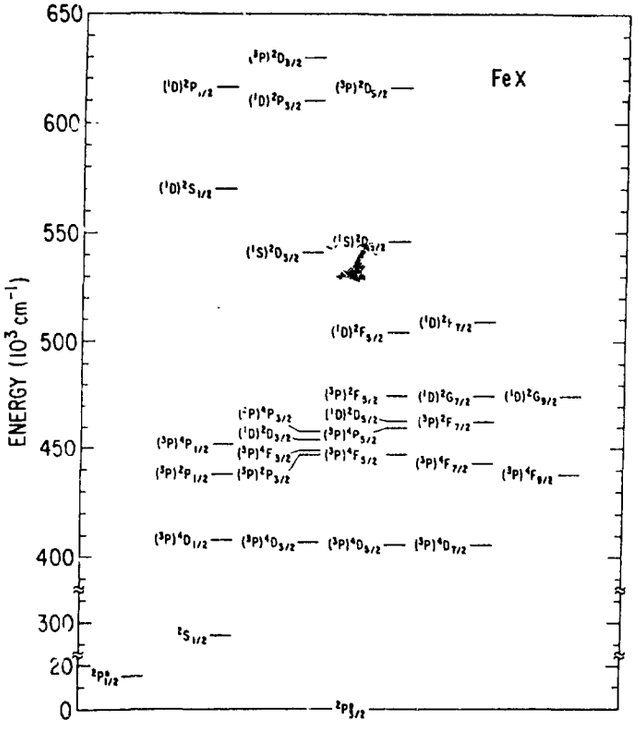

Fig. 1. Grotrian diagram of low-lying levels of chlorine-like FeX.

*Summary of a paper published in Atomic Data and Nuclear Data Tables 28, 355 (1983).

†Physics Division, Argonne National Laboratory.
‡Centre d'Etudes Nucléaires de Grenoble, 38041 Grenoble, France.

37. ELECTRIC-DIPOLE, QUADRUPOLE, AND MAGNETIC-DIPOLE SUSCEPTIBILITIES AND SHIELDING FACTORS FOR CLOSED-SHELL IONS OF THE He, Ne, Ar, Ni(Cu^+), Kr, Pb, AND Xe ISOELECTRONIC SEQUENCES*

W. R. Johnson,† Dietmar Kolb,† and K.-N. Huang

Theoretical values of electric and magnetic susceptibilities (α_1, α_2, χ_1) and shielding factors (γ_1, γ_2, σ_1) calculated in the relativistic random-phase approximation are presented in tabular form for ions with closed 1s, 2p, 3p, 3d, 4p, 4d, and 5p shells. The table includes all ions in these sequences with nuclear charge up to Z = 56 and a representative selection of ions with $56 < Z < 92$.

In Table 1 we present sample results of theoretical studies of susceptibilities and shielding factors for various closed-shell ions. These studies are based on the relativistic random-phase approximation (RRPA), which, in the present context, is a relativistic generalization of the coupled Hartree-Fock (CHF) theory well suited to the calculation of static properties of highly charged, closed-shell ions.

---

*Summary of a paper published in Atomic Data and Nuclear Data Tables 28, 334 (1983).

†Department of Physics, University of Notre Dame, Notre Dame, IN 46556.

Table 1. Susceptibilities and Shielding Factors for Ions of Closed-Shell Isoelectronic Sequences.

Ion	Z	Z_i	α_1	γ_1	α_2	γ_2	$10^6\chi_1$	$10^2\sigma_1$
Palladium Isoelectron Sequence								
Pd	46	0	21.17	1	268.8	-85.29	-381.3	.5339
Ag	47	1	8.829	.9789	49.9	-45.7	-305.1	.5527
Cd	48	2	4.971	.9536	17.86	-33.92	-258.4	.572
In	49	3	3.22	.9389	8.386	-27.78	-225.2	.5917
Sn	50	4	2.264	.9201	4.583	-23.84	-199.7	.6116
Sb	51	5	1.68	.9021	2.76	-21.02	-179.2	.6319
Te	52	6	1.295	.8838	1.779	-18.87	-162.3	.6526
I	53	7	1.028	.868	1.205	-17.15	-148	.6737
Xe	54	8	.8345	.8519	.8482	-15.75	-135.8	.6956
Cs	55	9	.6894	.8365	.6156	-14.58	-125.2	.7174
Ba	56	10	.578	.8215	.458	-13.59	-116	.74
Tb	65	19	.1753	.7078	.06192	-8.631	-65.86	.9687
W	74	28	.07655	.6217	.01534	-6.403	-42.78	1.265
Pt	78	32	.0564	.5899	.009125	-5.986	-36.25	1.429
Au	79	33	.05248	.5824	.008075	-5.868	-34.85	1.473
Hg	80	34	.04892	.5751	.007166	-5.758	-33.52	1.52
Pb	82	36	.04268	.5611	.005685	-5.559	-31.09	1.618
Rn	86	40	.03302	.5351	.003674	-5.235	-26.92	1.841
U	92	46	.02323	.5002	.002018	-4.894	-22.03	2.258
Xenon Isoelectronic Sequence								
Xe	54	0	26.97	.9999	204.3	-168.5	-542.8	.704
Cs	55	1	15.81	.9819	86.4	-114.3	-454.4	.7267
Ba	56	2	10.61	.9644	45.96	-87.83	-393	.7503
La	57	3	7.673	.9475	27.85	-71.82	-346.7	.7748
Ce	58	4	5.826	.9306	18.48	-60.95	-310.2	.7991
Nd	60	6	3.69	.9	11.16	-45.59	-255.4	.8487

38. RESONANCE TRANSITIONS OF Be-LIKE IONS FROM MULTICONFIGURATION RELATIVISTIC RANDOM-PHASE APPROXIMATION*

W. R. Johnson† and K.-N. Huang

Relativistic excitation energies and transition rates from the $^1S_0$ ground states to the first $^3P_1$ and $^1P_1$ excited states of beryllium-like ions are determined by using the newly developed multiconfiguration relativistic random-phase approximation (MCRRPA). Results from the MCRRPA theory are compared with those from other theories, in particular the relativistic random-phase approximation (RRPA), and with experimental results. The errors in RRPA and MCRRPA excitation energies, as determined by comparison with precise experimental measurements, are plotted against nuclear charges in Figure 1.

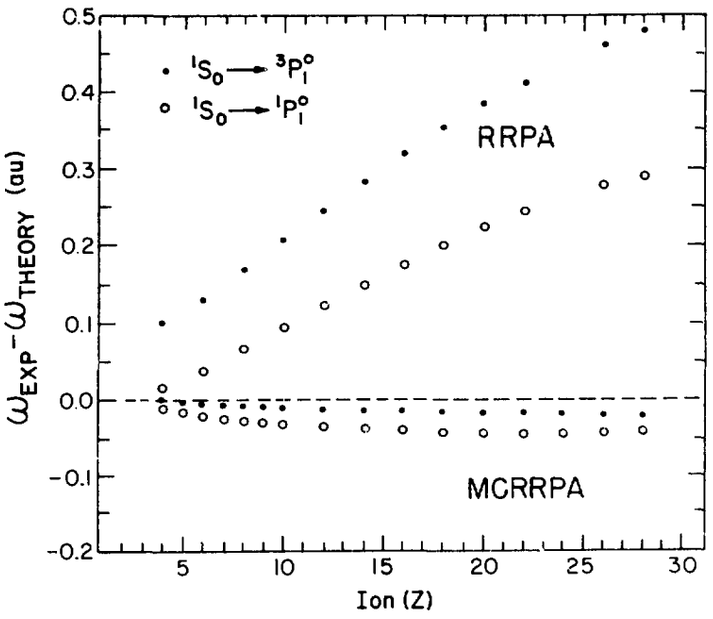

Fig. 1. Comparison of RRPA and MCRRPA excitation energies with experimental data.

*Summary of a letter published in Phys. Rev. Lett. 48, 315 (1982).

†Physics Department, University of Notre Dame, Notre Dame, IN 46556.

39. MULTICONFIGURATION RELATIVISTIC RANDOM-PHASE APPROXIMATION. THEORY*

K.-N. Huang and W. R. Johnson†

The relativistic random-phase approximation is generalized to describe excitations of an atomic system having a multiconfiguration ground state. The response of such an atom to an imposed harmonic perturbation is determined by applying the time-dependent variational principle to a multiconfiguration wave function constructed from Dirac orbitals. Terms in the wave function independent of the external field lead to the multiconfiguration Dirac-Fock description of the ground state. Terms proportional to the external field lead to a multiconfiguration generalization of the relativistic random-phase approximation. For the special case of an atom having a ground state with two electrons coupled to J = 0 outside of closed shells, we provided detailed equations for the configuration weights and for the electronic orbitals. These equations are expanded in a suitable basis to give expressions for the excitation probabilities. An angular-momentum analysis is carried out, leading to a set of coupled algebraic equations for the configuration weights and a set of radial differential equations for the electronic orbitals.

*Summary of a paper published in Phys. Rev. A 25, 634 (1982).
†Physics Department, University of Notre Dame, Notre Dame, IN 46556.

40. RELATIVISTIC MANY-BODY THEORY OF ATOMIC TRANSITIONS. THE RELATIVISTIC EQUATION-OF-MOTION APPROACH*

K.-N. Huang

An equation-of-motion approach is used to develop the relativistic many-body theory of atomic transitions. The relativistic equations of motion for transition matrices are formulated with the use of techniques of quantum-field theory. To reduce the equations of motion to a tractable form that is appropriate for numerical calculations, a graphical method to resolve the complication arising from the antisymmetrization and angular-momentum coupling. The relativistic equation-of-motion method allows an *ab initio* treatment of correlation and relativistic effects in both closed- and open-shell many-body systems. A special case of the present formulation reduces to the relativistic random-phase approximation.

*Summary of a paper published in Phys. Rev. A 26, 734 (1982).

FUNDAMENTAL MOLECULAR PHYSICS AND CHEMISTRY SECTION

PAPERS AND ABSTRACTS
1 October 1981 - 31 December 1982

Journal Articles

M. H. Chen, B. Crasemann, M. Aoyagi, K.-N. Huang, and H. Mark, Theoretical Atomic Inner-Shell Energy Levels, $70 \leq Z \leq 106$, At. Data Nucl. Data Tables 26, 561-574 (1981).

K. T. Cheng, C. Froese-Fischer, and Y.-K. Kim, Intershell Correlation Corrections to the Energy Levels of the n = 2 States of Li-Like to F-Like Ions, J. Phys. B: At. Mol. Phys. 15, 181-189 (1982).

J. L. Dehmer, A. C. Parr, S. Wallace, and D. Dill, Photoelectron Branching Ratios and Angular Distributions for the Valence Levels of SF_6 in the Range 16 eV $< h\nu <$ 30 eV, Phys. Rev. A 26, 3283-3292 (1982).

P. M. Dehmer and J. L. Dehmer, Observation of Bending Modes in the X $^2\Pi_u$ State of the Acetylene Ion Using HeI Photoelectron Spectroscopy, J. Electron Spectrosc. Relat. Phenom. 28, 145 (1982).

P. M. Dehmer and S. T. Pratt, Systematics of Rydberg Structure in the Spectra of the Rare Gas Dimers Between the Atomic $^2P^\circ_{3/2}$ and $^2P^\circ_{1/2}$ Fine-Structure Thresholds, J. Chem. Phys. 75, 5265-5270 (1981).

P. M. Dehmer and S. T. Pratt, Photoionization of ArKr, ArXe, and KrXe and Bond Dissociation Energies of the Rare Gas Dimer Ions, J. Chem. Phys. 77, 4804 (1982).

P. M. Dehmer and S. T. Pratt, Photoionization of Argon Clusters, J. Chem. Phys. 76, 843-853 (1982).

P. M. Dehmer, APS Reviews Refereeing Procedures, Physics Today 35(2), 9 and 95-97 (1982).

P. M. Dehmer, Photoionization of Ar_2 at High Resolution, J. Chem. Phys. 76, 1263-1272 (1982).

M. A. Dillon and M. Inokuti, Precise Test of the Coulomb-Projected Born Approximation for the 2^1S and 3^1S Excitation of Helium by Electron Impact, J. Chem. Phys. 76, 5887-5892 (1982).

P. M. Dittman, D. Dill, and J. L. Dehmer, Shape-Resonance-Induced Non-Franck-Condon Effects in the Valence-Shell Photoionization of O_2, J. Chem. Phys., 76, 5703-5709 (1982).

D. L. Ederer, A. C. Parr, B. E. Cole, R. Stockbauer, J. L. Dehmer, J. B. West, and K. Codling, Vibrational-State Dependence of Partial Cross Sections and Photoelectron Angular Distributions through Autoionizing Resonances: The n = 3 Rydberg State Converging to the $B^2\ \Sigma^+$ State of CO^+, Proc. R. Soc. Lond. A 378, 423-435 (1981).

D. L. Ederer, A. C. Parr, J. B. West, D. Holland, and J. L. Dehmer, Measurement of the Spin-Orbit Branching Ratios and the Angular Asymmetry Parameter in the Region of the $4s4p^6 5p$ Resonances in Krypton and the $5s5p^6 6p$ Resonances in Xenon, Phys. Rev. A 25, 2006-2011 (1982).

D. M. P. Holland, A. C. Parr, D. L. Ederer, J. L. Dehmer, and J. B. West, The Angular Distribution Parameters of Argon, Krypton and Xenon for Use in Calibration of Electron Spectrometers, Nucl. Instrum. Methods, 195, 331-337 (1982).

K.-N. Huang, Angular Distribution and Spin Polarization of Auger Electrons Following Photoionization and Photoexcitation, Phys. Rev. A 26, 2274-2276 (1982).

K.-N. Huang, Addendum to "Theory of Angular Distribution and Spin Polarization of Photoelectrons," Phys. Rev. A 26, 3676-3678 (1982).

K.-N. Huang and V. W. Hughes, Theoretical Hyperfine Structure of the Muonic Helium-3 and Helium-4 Atoms, Phys. Rev. A 26, 3676-3678 (1982).

K.-N. Huang and W. R. Johnson, The Multiconfiguration Relativistic Random-Phase Approximation: I. Theory, Phys. Rev. A 25, 634-649 (1982).

K.-N. Huang, Y.-K. Kim, K. T. Cheng, and J. P. Desclaux, Correlation and Relativistic Effects in Spin-Orbit Splitting, Phys. Rev. Lett. 48, 1245-1248 (1982).

K.-N. Huang, Coherent Fluorescence Radiation Following Photoexcitation and Photoionization, Phys. Rev. A 25, 3438-3441 (1982).

K.-N. Huang, Kinematic Analysis of Photoelectrons from Polarized Targets with J=1/2, Phys. Rev. Lett. 26, 1811 (1982).

K.-N. Huang, Relativistic Many-Body Theory of Atomic Transitions. The Relativistic Equation-of-Motion Approach, Phys. Rev. A 26, 734-739 (1982).

M. Inokuti, Distribution of the Oscillator Strength Over the Entire Range of Excitation Energy, Bunkyo Kenkyu (J. Spectrosc. Soc. Japan) 30, 393-405 (1981). (in Japanese)

M. Inokuti and D. Y. Smith, Fermi Density Effect on the Stopping Power of Metallic Aluminum, Phys. Rev. B 25, 61-66 (1982).

M. Inokuti, Radiation Doses to the Survivors of the Atomic Bombs in Hiroshima and Nagasaki, Butsuri (Proc. Phys. Soc. Japan) 37, 192-194 (1982). (in Japanese)

W. R. Johnson and K.-N. Huang, Resonance Transitions of Be-Like Ions from Multiconfiguration Relativistic Randon-Phase Approximation, Phys. Rev. Lett. 48, 315-318 (1982).

Y.-K. Kim and K.-N. Huang, Spin-Orbit Interval in the Ground State of F-like Ions, Phys. Rev. A 26, 1984-1987 (1982).

Yong-Ki Kim, Book Review: R. D. Cowan, The Theory of Atomic Structure and Spectra, Physics Today 35(6), 57 (1982).

D. Loomba, S. Wallace, D. Dill, and J. L. Dehmer, Pictures of Unbound Molecular Electrons, Including Shape-Resonant States. Eigenchannel Countour Maps. J. Chem. Phys. 75, 4546-4552 (1981).

A. C. Parr, D. L. Ederer, J. B. West, D. M. P. Holland, and J. L. Dehmer, Triply Differential Photoelectron Studies of Non-Franck-Condon Behavior in the Photoionization of Acetylene, J. Chem. Phys. 76, 4349-4355 (1982).

A. C. Parr, D. L. Ederer, J. L. Dehmer, and D. M. P. Holland, Characterization of Some Autoionization Resonances in CO_2 Using Triply Differential Photoelectron Spectroscopy, J. Chem. Phys. 77, 111-117 (1982).

E. D. Poliakoff, J. L. Dehmer, A. C. Parr, and G. E. Leroi, Fluorescence Polarization as a Probe of Molecular Autoionization, J. Chem. Phys. 77, 5243 (1982).

E. D. Poliakoff, P. M. Dehmer, J. L. Dehmer, and R. Stockbauer, Photoelectron-Photoion Coincidence Spectroscopy of Gas-Phase Clusters, J. Chem. Phys. 76, 5214-5224 (1982).

S. T. Pratt and P. M. Dehmer, Photoionization of the Neon-Rare Gas Dimers NeAr, NeKr, and NeXe, J. Chem. Phys. 76, 3433-3439 (1982).

S. T. Pratt and P. M. Dehmer, Photoionization of the Neon-Rare Gas Dimers near the Neon 3s Resonance Transitions: Associative Ionization Half-Reactions, J. Chem. Phys. 76, 4865-4871 (1982).

S. T. Pratt and P. M. Dehmer, Photoionization of the Kr_2 Dimer, Chem. Phys. Lett. 87, 533-538 (1982).

D. S. Soh, B. H. Cho, and Y.-K. Kim, Relativistic Born Cross Sections for Li-Like C and W Ions, Phys. Rev. A 26, 1357-1368 (1982).

David Spence, W. A. Chupka and C. M. Stevens, Mass Spectrometric Observation of the Stable Negative Molecular Ions HI^- and H_2I^-, J. Chem. Phys. 76, 2759-2761 (1982).

David Spence, W. A. Chupka and C. M. Stevens, Search for Long-Lived Doubly Charged Atomic Negative Ions, Phys. Rev. A. 26, 654-657 (1982).

D. Spence, R.-G. Wang, and M. A. Dillon, Pseudo-Optical Absorbtion Spectra in $HgCl_2$ and $HgBr_2$ from 4 to 14 eV, Appl. Phys. Lett. 41, 1021-1023 (1982).

J. A. Stephens, D. Dill, and J. L. Dehmer, Vibrational Branching Ratios and Photoelectron Angular Distributions in 5σ Photoionization of CO, J. Phys. B: At. Mol. Phys. 14, 3911-3918 (1981).

S. Wallace, D. Dill, and J. L. Dehmer, Shape Resonant Features in the Photoionization Spectra of NO, J. Chem. Phys. 76, 1217-1222 (1982).

H. F. Winters and M. Inokuti, Dissociation of CF_4 and Other Fluoro-Alkanes by Electron Impact, Phys. Rev. A 25, 1420-1430 (1982).

Abstracts

J. L. Dehmer, E. D. Poliakoff, and P. M. Dehmer, Photoelectron Angular Distributions from Multiphoton Ionization. Seven-Photon Ionization of Kr at 532 nm, Bull. Am. Phys. Soc. 26, 1322 (1981).

J. L. Dehmer, P. M. Dehmer, and S. T. Pratt, Multiphoton Ionization as a Probe of Molecular Photoionization Dynamics, First U.S.-Japan Seminar on Electron-Molecule Collisions and Photoionization Processes, California Institute of Technology, Pasadena, CA, 26-29 October 1982, Book of Extended Abstracts, p. 18.

P. M. Dehmer and S. T. Pratt, Systematics of Binding in the Rydberg States of the Homonuclear and Heteronuclear Rare Gas Dimers, Bull. Am. Phys. Soc. 26, 1318 (1981).

P. M. Dehmer, VUV Spectroscopy of Van Der Waals Dimers and Heavier Clusters, Proceedings of the 2nd European Workshop on Molecular Spectroscopy and Photon-Induced Dynamics, Flevopolder, The Netherlands, September 27-30, 1982, AMOLF-Report 83-3, p. 11.

K.-N. Huang, Polarization of Residual Ions from Photoionization, Bull. Am. Phys. Soc. 26, 1301 (1981).

K.-N. Huang, Spin Polarization, Orientation, and Coherence Effects in Photoionization Processes, Bull. Am. Phys. Soc. 27, 40 (1982).

Y.-K. Kim and K.-N. Huang, Dirac-Fock Term Values for the ^3P Levels of Oxygen, Bull. Am. Phys. Soc., 27, 515 (1982).

Y.-K. Kim and K.-N. Huang, Spin-Orbit Splitting in the Ground State of Oxygen-Like Ions, Abstracts, Eighth International Conference on Atomic Physics, 2-6 August 1982, Göteborg, Sweden, Edited by I. Lindgren, A. Rosén, and S. Svanberg, Paper A20.

A. C. Parr, D. L. Ederer, R. Stockbauer, J. B. West, D.M.P. Holland, K. Codling, and J. L. Dehmer, Triply Differential Photoelectron Studies of Autoionization and Shape-Resonance Effects in Molecular Photoionization, Bull. Am. Phys. Soc. 26, 1322 (1981).

E. D. Poliakoff, P. M. Dehmer, J. L. Dehmer, and R. Stockbauer, Photoelectron-Photoion Coincidence Spectroscopy of Gas-Phase Clusters, Bull. Am. Phys. Soc. 26, 1322 (1981).

S. T. Pratt and P. M. Dehmer, Photoionization of NeAr, NeKr, and NeXe in the Region of the Neon 3s and 3s′ Resonance Transitions, Bull. Am. Phys. Soc. 26, 1299 (1981).

D. Spence, R.-G. Wang, and M. A. Dillon, Pseudo-Optical Absorption Spectra in $HgCl_2$ and $HgBr_2$ from 4 to 14 eV, In: Program and Abstracts. Thirty-fifth Annual Gaseous Electronics Conference, Dallas, TX, 19-22 October 1982.

D. Spence, R.-G. Wang, and M. A. Dillon, Excitation and Dissociation Mechanisms in Molecules with Application to Mercuric Halide Lasers, In: Symposium on Electron Molecule and Photoionization Processes: Invited papers. Cal Tech., Calif., eds., V. McKoy, H. Suzuki, K. Takayanagi, and S. Trajmar, 170-173 (1982).

Distribution for ANL-82-65 Part I

Internal:

C. C. Baker
F. S. Beckjord
J. Berkowitz
H. G. Berry
K-T. Cheng
J. L. Dehmer
P. M. Dehmer
J. D. DePue
M. A. Dillon
H. Drucker
T. H. Dunning
A. J. Dvorak
P. Frenzen
B. R. T. Frost
D. S. Gemmell
S. Gordon
S. L. Gotlund
W. J. Hallett
G. J. Hamilton
K-N. Huang
E. Huberman
R. H. Huebner
M. Inokuti
K. L. Kliewer
A. B. Krisciunas (15)
K-T. Lu
P. Messina
A. Pagnamenta
E. G. Pewitt
S. T. Pratt
J. Rundo
M. C. Sauer
J. P. Schiffer
R. A. Schlenker
D. Y. Smith
D. Spence
R. W. Springer
A. F. Stehney
E. P. Steinberg
C. M. Stevens
P. A. Tyrolt (5)
S. Wexler
ER Division (70)
ANL Patent Dept.
ANL Contract File
ANL Libraries (2)
TIS Files (6)

External:

DOE-TIC, for distribution per UC-48 (146)
Manager, Chicago Operations Office, DOE
A. W. Trivelpiece, Office of Energy Research, DOE
Radiological and Environmental Research Division Review Committee:
- A. K. Blackadar, Pennsylvania State U.
- A. W. Castleman, Jr., Pennsylvania State U.
- R. E. Gordon, U. Notre Dame
- R. A. Hites, Indiana U.
- D. Kleppner, Massachusetts Inst. Technology
- G. M. Matanoski, Johns Hopkins U.
- R. A. Reck, General Motors Research Lab.
- L. A. Sagan, Electric Power Research Inst.
- R. E. Wildung, Battelle Pacific Northwest Lab.

W. J. Argersinger, Jr., U. Kansas
Arkansas, U. of, Library for Medical Sciences, Little Rock
L. Armstrong, Jr., Johns Hopkins U.
J. C. Ashley, Oak Ridge National Lab.
P. Ausloos, National Bureau of Standards, Washington
J. A. Auxier, Oak Ridge National Lab.
P. S. Bagus, IBM Research Labs., San Jose
J. N. Bardsley, U. Pittsburgh
N. F. Barr, Office of Health and Environmental Research, USDOE
J. W. Baum, Brookhaven National Lab.
B. Bederson, New York U.
M. J. Berger, National Bureau of Standards, Washington
R. S. Berry, U. Chicago
C. C. Bhalla, Kansas State U.
H. Bichsel, Seattle
R. D. Birkhoff, Oak Ridge National Lab.
W. H. Blahd, Veterans Administration Center, Los Angeles
M. J. W. Boness, Avco Everett Research Corp., Everett, Mass.
R. A. Bonham, Indiana U.

J. W. Boring, U. Virginia
D. J. Brenner, Columbia U.
A. B. Brill, Brookhaven National Lab.
B. H. Bruckner, National Center for Radiological Health, USHEW, Rockville, Md.
S. R. Bull, U. Missouri
R. A. Burnstein, Illinois Inst. Technology
P. D. Burrow, U. Nebraska
L. K. Bustad, Washington State U.
T. A. Carlson, Oak Ridge National Lab.
W. S. Caswell, National Bureau of Standards, Washington
R. J. Celotta, National Bureau of Standards, Washington
H. Cember, Northwestern U.
E. S. Chang, U. Massachusetts
T-N. Chang, U. Southern California
C. Y. Chen, U. California, San Diego
J. E. Christian, Purdue U.
L. G. Christophorou, Oak Ridge National Lab.
W. A. Chupka, Yale U.
C. W. Clark, National Bureau of Standards, Washington
R. G. Cochran, Texas A&M U.
S. H. Cohn, Brookhaven National Lab.
Colorado, U. of, Joint Inst. for Laboratory Astrophysics
R. N. Compton, Oak Ridge National Lab.
J. W. Cooper, National Bureau of Standards, Washington
Cornell University, Library, Geneva, N. Y.
D. H. Crandall, Oak Ridge National Lab.
B. Crasemann, U. Oregon
J. A. Cummings, Wisconsin State U.
A. Dalgarno, Harvard College Observatory and Smithsonian Astrophysical Observatory
S. Datz, Oak Ridge National Lab.
R. D. Deslattes, Jr., National Bureau of Standards, Washington
D. Dill, Boston U.
D. A. Douthat, U. Alaska
G. H. Dunn, U. Colorado
M. P. Durso, Environmental Measurements Lab., USDOE, New York
D. L. Ederer, National Bureau of Standards, Washington
C. W. Edington, Office of Health and Environmental Research, USDOE
C. E. Edmund, Milwaukee, Wis.
R. D. Evans, Scottsdale, Ariz.
U. Fano, U. Chicago
M. R. Flannery, Georgia Inst. Technology
A. C. Gallagher, U. Colorado
W. R. Garrett, Oak Ridge National Lab.
R. Geballe, U. Washington
S. Geltman, U. Colorado
G. H. Gillespie, Physical Dynamics, Inc., La Jolla
W. A. Glass, Battelle Northwest Lab.
M. Goldman, U. California, Davis
A. E. S. Green, U. Florida
T. A. Green, Sandia National Labs., Albuquerque
C. H. Greene, Louisiana State U.
R. Grunewald, U. Wisconsin, Milwaukee
A. J. Haverfield, Battelle Northwest Lab.

R. J. W. Henry, Louisiana State U.
G. R. Holeman, Yale U.
Houston, U. of, Libraries
G. S. Hurst, Oak Ridge National Lab.
Illinois, U. of, Library, Chicago
R. A. Isaacson, National Science Foundation
K. H. Johnson, Massachusetts Inst. Technology
R. E. Johnson, U. Virginia
W. R. Johnson, U. Notre Dame
B. R. Junker, Office of Naval Research, Arlington, Va.
R. J. Kandel, Office of Basic Energy Sciences, USDOE
H. P. Kelly, U. Virginia
W. V. Kessler, Purdue U.
Y-K. Kim, National Bureau of Standards, Washington
J. W. Klappenbach, U.S. Environmental Protection Agency, Chicago
W. M. Kosman, Valparaiso U.
M. O. Krause, Oak Ridge National Lab.
A. Kuppermann, California Inst. Technology
C. E. Kuyatt, National Bureau of Standards, Washington
P. Lambropoulos, U. Southern California
N. F. Lane, Rice U.
E. N. Lassettre, Carnegie-Mellon U.
Y. T. Lee, U. California, Berkeley
S. H. Levine, Pennsylvania State U.
J. C. Light, U. Chicago
W. C. Lineberger, U. Colorado
S. Lipsky, U. Minnesota
L. Lohr, Jr., U. Michigan
D. C. Lorents, SRI International, Menlo Park
H. Maccabee, Lawrence Berkeley National Lab.
J. H. Macek, U. Nebraska
R. P. Madden, National Bureau of Standards, Washington
J. L. Magee, Lawrence Berkeley National Lab.
C. J. Maletskos, Gloucester, Mass.
S. T. Manson, Georgia State U.
E. A. Martell, National Center for Atmospheric Research, Boulder
J. V. Martinez, Office of Basic Energy Sciences, USDOE
Mayo Clinic Library, Rochester
S. P. McGlynn, Louisiana State U.
D. H. McKelvie, U. Arizona
V. McKoy, California Inst. Technology
J. E. McLaughlin, Environmental Measurements Lab., USDOE, New York
R. Meer, Massachusetts General Hospital
G. G. Meisels, U. Nebraska
J. Mentall, NASA Goddard Space Flight Center
A. L. Mertz, Los Alamos National Lab.
E. Merzbacher, U. North Carolina at Chapel Hill
Michigan Technological U. Library, Houghton
D. W. Moeller, Kresge Center for Environmental Health, Boston
R. D. Moseley, Jr., U. New Mexico Medical School
G. Murphy, Iowa State U.
W. G. Myers, Ohio State U. Hospital
D. P. Naismith, U. North Dakota
R. K. Nesbet, IBM Research Labs., San Jose

W. R. Ney National Council on Radiation Protection and Measurements, Bethesda
G. Nichols, Jr., Boston, Mass.
D. W. Norcross, U. Colorado
O. F. Nygaard, Case Western Reserve U.
M. J. Ohanian, U. Florida
A. L. Orvis, Mayo Clinic
J. Ovadia, Michael Reese Hospital, Chicago
L. R. Painter, U. Tennessee
J. Pan, Purdue U., Calumet Campus
A. C. Parr, National Bureau of Standards, Washington
J. M. Peek, Sandia National Labs., Albuquerque
A. V. Phelps, U. Colorado
R. T. Poe, U. California, Riverside
E. D. Poliakoff, Boston U.
M. L. Pool, Western Illinois U.
M. Pope, New York U.
C. Powell, National Bureau of Standards, Washington
R. H. Pratt, U. Pittsburgh
A. R. P. Rau, Louisiana State U.
W. P. Reinhardt, U. Colorado
J. S. Risley, North Carolina State U. at Raleigh
R. H. Ritchie, Oak Ridge National Lab.
J. S. Robertson, Mayo Clinic
W. C. Roesch, Battelle Northwest Lab.
C. C. J. Roothaan, U. Chicago
H. H. Rossi, Columbia U.
M. E. Rudd, U. Nebraska
J. H. Rust, U. Chicago
E. L. Saenger, Cincinnati General Hospital
E. Salmon, McLean, Va.
J. A. R. Samson, U. Nebraska
R. P. Saxon, SRI International, Inc., Menlo Park
R. H. Schuler, U. Notre Dame
D. A. Shirley, U. California, Berkeley
T. W. Shyn, U. Michigan
Siemens Gammasonics, Inc., Des Plaines, Ill.
R. M. Sinclair, National Science Foundation
W. K. Sinclair, National Council on Radiation Protection and Measurements, Bethesda
J. B. Smathers, Texas A&M U.
F. T. Smith, SRI International, Inc., Menlo Park
L. V. Spencer, National Bureau of Standards, Washington
A. F. Starace, U. Nebraska
R. F. Stebbings, Rice U.
R. L. Stockbauer, National Bureau of Standards, Washington
P. M. Stone, Office of Fusion Energy, USDOE
S. Tani, Marquette U.
H. S. Taylor, U. Southern California
L. S. Taylor, Bethesda, Md.
A. Temkin, Goddard Space Flight Center
C. E. Theodosiou, U. Toledo
J. K. Thomas, U. Notre Dame
C. A. Tobias, U. California, Berkeley
L. H. Toburen, Battelle Northwest Lab.

S. Trajmer, Jet Propulsion Lab.
J. E. Turner, Oak Ridge National Lab.
A. C. Upton, New York U. Medical Center
D. Varney, Eastern Kentucky U.
S. D. Vesselinovitch, U. Chicago
S. Wallace, Massachusetts Inst. Technology
W. L. Wiese, National Bureau of Standards, Washington
R. H. Williams, U. Michigan
W. E. Wilson, Battelle Northwest Lab.
H. F. Winters, IBM Research Labs., San Jose
W. F. Witzig, Pennsylvania State U.
R. W. Wood, Office of Health and Environmental Research, USDOE
H. O. Wyckoff, International Commission on Radiation Units and Measurements, Bethesda
K. F. Wylie, U. Mississippi
M. A. Zaider, Columbia U.
R. N. Zare, Stanford U.
Comision Nacional de Energia Atomica, Library, Buenos Aires, Argentina
Cancer Institute Library, Melbourne, Australia
Ian E. McCarthy, Flinders U. of South Australia, Adelaide, Australia
J. F. Wil ams, U. of Western Australia, Perth, Australia
K. A. Dudley, IAEA, Vienna, Austria
J. M. Debois, St. Norbertus Hospital, Duffel, Belgium
A. Heyndrickx, U. Ghent, Belgium
N. Brearley, U. British Columbia, Vancouver, Canada
C. E. Brion, U. British Columbia, Vancouver, Canada
Canadian Forces Base, Halifax, Canada
J. D. Carette, Universite Laval, Quebec, Canada
D. Charlton, Concordia U., Montreal, Canada
G. Cowper, Atomic Energy of Canada Ltd., Chalk River
Defence Research Establishment Library, Ottawa, Canada
G. R. Freeman, U. Alberta, Edmonton, Canada
Health and Welfare Canada, Radiation Protection Bu., Ottawa
J. W. McConkey, U. Windsor, Canada
J. W. McGowan, U. Western Ontario, London, Canada
C. Pomroy, Dept. National Health and Welfare, Ottawa, Canada
L. Sanche, U. Sherbrooke, Sherbrooke, Canada
A. G. Szabo, National Research Council of Canada, Ottawa
Toronto, U. of, Library, Canada
C. Willis, National Research Council of Canada, Ottawa
D-J. Fu, Chinese Academy of Sciences, Shanghai, People's Republic of China
Q-Q. Gou, Chengdu U. of Science and Technology, People's Republic of China
J-M. Li, Chinese Academy of Sciences, Beijing, People's Republic of China
R-G. Wang, Chengdu U. of Science and Technology, People's Republic of China
C-H. Cheng, National Tsing Hua U., Republic of China
Czechoslovak Atomic Energy Commission, Zbraslav nad Vltavou
H. H. Andersen, H. C. Ørsted Inst., Copenhagen, Denmark
N. Andersen, H. C. Ørsted Inst., Copenhagen, Denmark
M. Faber, Finsen Inst. Copenhagen, Denmark
P. Hvelplund, Aarhus U., Denmark
J. Lindhard, Aarhus U., Denmark
P. Sigmund, Odense U., Denmark
G. E. Adams, MRC Radiobiology Unit, Harwell, England
J. W. Boag, Sutton, Surrey, England

P. R. J. Burch, U. Leeds, England
Y. Cocking, MRC Radiobiology Unit, Harwell, England
K. Codling, U. Reading, England
J. A. Dennis, National Radiological Protection Board, Harwell, England
K. T. Dolder, The University, Newcastle-upon-Tyne, England
J. A. Edgington, Queen Mary College, London, England
J. F. Fowler, Mt. Vernon Hospital, Northwood, England
D. T. Goodhead, MRC Radiobiology Unit, Harwell, England
S. J. Harris, U. Surrey, Guildford, England
M. T. Herbert, National Radiological Protection Board, Chilton, England
C. R. Hill, Inst. of Cancer Research, Belmont, England
G. V. Marr, U. Reading, England
W. V. Mayneord, Tadworth, Surrey, England
M. R. C. McDowell, Royal Holloway College, Surrey, England
D. H. Peirson, U. K. AERE, Harwell, England
E. E. Pochin, National Radiological Protection Board, Harwell, England
F. H. Read, U. Manchester, England
K. J. Ross, U. Southampton, England
M. J. Seaton, U. College London, England
A. J. Swallow, Christie Hospital & Holt Radium Inst., Manchester, England
J. B. West, Daresbury Lab., Daresbury, England
T. Åberg, Helsinki U. of Technology, Otaniemi, Finland
Institute of Radiation Protection, Library, Helsinki, Finland
P. Pyykkö, Åbo Akademi, Turku, Finland
A. Allisy, Bu. International des Poids et Mesures, Sèvres, France
M. Barat, U. Paris, Orsay, France
J-P. Briand, Lab. de Physique Atomique et Nucleaire, Paris, France
J. Coursaget, CEA, Saclay, France
J. P. Desclaux, CEN/G DRF-CPN, Grenoble, France
J. Durup, U. Paris, Orsay, France
L. F. Ferreira, U. Paris, Orsay, France
P. M. Guyon, U. Paris, Orsay, France
R. I. Hall, U. Paris, Paris, France
V. K. Lan, Observatoire de Paris, Meudon, France
M. Tronc, Lab. de Collisions Electroniques, Orsay, France
R. Voltz, Centre de Recherches Nucleaires, Strasbourg-Cronenbourg, France
S. Watanabe, Observatoire de Paris, Meudon, France
F. Wuilleumier, U. Paris, Orsay, France
P. Armbruster, Gesellschaft für Schwerionenforschung, Darmstadt, Germany
J. Booz, Institut für Medizin, Jülich, Germany
J. S. Briggs, U. Freiburg, Germany
R. J. Buenker, U. Bonn, Germany
G. Drexler, Institute für Strahlenschutz, Munich, Germany
H. Ehrhardt, U. Kaiserslautern, Germany
J. Eichler, Hahn-Meitner-Institut, Berlin, Germany
J. Geiger, U. Kaiserslautern, Germany
Gesellschaft für Strahlenforschung m.b.H., Frankfurt, Germany
B. Grosswendt, Physikalisch-Technische Bundesanstalt, Braunschweig, Germany
R. Haensel, U. Kaiserslautern, Germany
D. Harder, U. Göttingen, Germany
I. V. Hertel, Freie U., Berlin, Germany
H. Hotop, U. Kaiserslautern, Germany
A. Kaul, Inst. für Strahlenhygiene, Neuherberg, Germany
J. Kessler, Physikalisches Inst. der Universität Münster, Germany

F. Linder, U. Kaiserslautern, Germany
W. Mehlhorn, U. Freiburg, Germany
H. Muth, U. Saarlandes, Homburg, Germany
E. Oberhausen, U. Saarlandes, Homburg, Germany
H. G. Paretzke, Institut für Strahlenschutz, Neuherberg, Germany
S. D. Peyerimhoff, U. Bonn, Germany
G. zu Putlitz, Gesellschaft für Schwerionenforschung, Darmstadt, Germany
H. Schmoranzer, U. Kaiserslautern, Germany
B. Sonntag, Deutsches Elektronen Synchrotron, Hamburg, Germany
G. Stöcklin, Kernforschungsanlage Jülich, Germany
N. Stolterfoht, Hahn-Meitner-Institut, Berlin, Germany
K. J. Vogt, Kernforschungsanlage, Jülich, Germany
R. K. Hukkoo, Bhabha Atomic Research Centre, Bombay, India
A. N. Tripathi, U. Roorke, India
I. B. Berlman, Hebrew U., Jerusalem, Israel
Y. Feige, Israel AEC, Yavne, Israel
A. Benco, Commission of the European Communities, Ispra, Italy
E. Casnati, CNEN, Rome, Italy
A. Cigna, CNEN, Rome, Italy
G. F. Clemente, CNEN, Rome, Italy
F. A. Gianturco, U. di Roma, Italy
V. Prodi, CNEN, Bologna, Italy
O. Rimondi, Istituto di Fisica, Ferrara, Italy
S. Arai, Inst. Physical and Chemical Research, Saitama-ken, Japan
Y. Hatano, Tokyo Inst. Tech., Tokyo, Japan
T. Higashimura, Kyoto U., Japan
H. Inokuchi, Inst. for Molecular Science, Okazaki, Japan
Y. Itikawa, Inst. Space and Astronautical Science, Tokyo, Japan
S. Iwata, Keio U., Yokohama, Japan
S. Kaneko, U. Tokyo, Japan
Y. Kaneko, Tokyo Metropolitan U., Japan
K. Kimura, Inst. for Molecular Science, Okazaki, Japan
I. Koyano, Inst. for Molecular Science, Okazaki, Japan
M. Matsuzawa, U. of Electro-Communications, Tokyo, Japan
H. Nakamura, Institute for Molecular Science, Okazaki, Japan
M. Nakamura, Tsukuba U., Ibaraki-ken, Japan
H. Nishimura, Niigata U., Japan
N. Oda, Tokyo Inst. of Technology, Tokyo, Japan
T. Sasaki, National Lab. for High Energy Physics, Ibaraki, Japan
S. Sato, Tokyo Inst. Technology, Japan
H. Suzuki, Sophia U., Tokyo, Japan
T. Takahashi, Inst. of Physical and Chemical Research, Saitama-ken, Japan
K. Takayanagi, Inst. of Space and Astronautical Science, Tokyo, Japan
H. Tanaka, Sophia U., Tokyo, Japan
K. Tanaka, Inst. for Molecular Science, Okazaki, Japan
T. Watanabe, Inst. Physical and Chemical Research, Saitama-ken, Japan
Korea Advanced Energy Research Inst., Seoul, Korea
Sang-Soo Lee, The Korea Advanced Inst. of Science, Seoul, Korea
H. H. Brongersma, Philips Research Laboratories, Eindhoven, The Netherlands
F. J. de Heer, FOM Inst. for Atomic and Molecular Physics, Amsterdam, The Netherlands
M. Gavrilla, FOM Inst. for Atomic and Molecular Physics, Amsterdam, The Netherlands

J. Kistemaker, FOM Inst. for Atomic and Molecular Physics, Amsterdam, The Netherlands
J. Los, FOM Inst. for Atomic and Molecular Physics, Amsterdam, The Netherlands
A. Niehaus, Utrecht U., The Netherlands
M. van der Wiel, FOM Inst. for Atomic and Molecular Physics, Amsterdam, The Netherlands
J. M. Warman, Interuniversity Reactor Inst., Delft, The Netherlands
P. G. Burke, Queen's U., Belfast, Northern Ireland
M. U. Shaikh, Pakistan Atomic Energy Commission, Rawalpindi
J. R. Greening, The Royal Infirmary, Edinburgh, Scotland
R. D. Cherry, U. Cape Town, South Africa
A. Brahme, Karolinska Inst., Stockholm, Sweden
O. Goscinski, Uppsala U., Sweden
I. Jansson, National Inst. of Radiation Protection, Stockholm, Sweden
K. Liden, Dept. of Radiation Physics--Lasarettet, Lund, Sweden
A. E. Nahum, U. Umeå, Sweden
G. Wendin, Inst. of Theoretical Physics, Göteborg, Sweden
A. Donath, Service Cantonal de Controle des Irradiations, Geneva, Switzerland
A. Gunther, CERN, Geneva, Switzerland
G. D. Alkhazov, Academy of Sciences of the U.S.S.R., Leningrad
M. Ya. Amusia, Academy of Sciences of the U.S.S.R., Leningrad
E. Komarov, Central Res. Inst. of Roentgenology and Radiology, Leningrad, U.S.S.R.
V. Tal'roze, Academy of Sciences of the U.S.S.R., Moscow
D. Srdoc, Rudjer Boskovic Inst., Zagreb, Yugoslavia
L. Vuskovic, Inst. of Physics, Belgrade, Yugoslavia